# Study of constrained minimal supersymmetry

G. L. Kane, Chris Kolda, Leszek Roszkowski, and James D. Wells
*Randall Physics Laboratory, University of Michigan, Ann Arbor, Michigan 48190*
(Received 1 December 1993)

Taking seriously the phenomenological indications for supersymmetry we have made a detailed study of unified minimal SUSY, including many effects at the few percent level in a consistent fashion. We report here a general analysis of what can be studied without choosing a particular gauge group at the unification scale. Firstly, we find that the encouraging SUSY unification results of recent years do survive the challenge of a more complete and accurate analysis. Taking into account effects at the 5–10% level leads to several improvements of previous results and allows us to sharpen our predictions for SUSY in the light of unification. We perform a thorough study of the parameter space and look for patterns to indicate SUSY predictions, so that they do not depend on arbitrary choices of some parameters or untested assumptions. Our results can be viewed as a fully constrained minimal SUSY standard model. The resulting model forms a well-defined basis for comparing the physics potential of different facilities. Very little of the acceptable parameter space has been excluded by CERN LEP or Fermilab so far, but a significant fraction can be covered when these accelerators are upgraded. A number of initial applications to the understanding of the values of $m_h$ and $m_t$, the SUSY spectrum, detectability of SUSY at LEP II or Fermilab, $B(b \to s\gamma)$, $\Gamma(Z \to b\bar{b})$, dark matter, etc., are included in a separate section that might be of more interest to some readers than the technical aspects of model building. We formulate an approach to extracting SUSY parameters from data when superpartners are detected. For small $\tan\beta$ or large $m_t$ both $m_{1/2}$ and $m_0$ are entirely bounded from above at $\sim$ 1 TeV without having to use a fine-tuning constraint.

PACS number(s): 12.60.Jv, 12.10.Dm, 14.80.Cp, 95.35.+d

## I. INTRODUCTION

There has recently been a significant amount of activity in the field of supersymmetric grand unified theories (SUSY GUT's) and its possible implications for the existence of low-energy SUSY and for future SUSY searches. This renewed interest was primarily caused by the observation [1] that measurements of the gauge coupling constants at the CERN $e^+e^-$ collider LEP seem to imply their (grand) unification in a supersymmetric theory with superpartners near the weak scale, reinforced by the awareness that several phenomenological outcomes were consistent with SUSY [2] although they need not have been. It was shown [1,3–5] that the couplings merge at the GUT energy scale $M_X$ even in the simplest supersymmetric extension of the standard model, the so-called minimal SUSY standard model (MSSM), while they badly fail to do so in the standard model (SM) alone. This remarkable fact has been interpreted by many as a strong hint for a SUSY GUT, especially since its main arch-rivals for expected physics beyond the SM, the composite and technicolor approaches, seem now even more disfavored by the precise measurements at LEP [6]. It has been argued that the unification of gauge couplings is also possible in some non-SUSY models [7]. These models are, however, exuberantly complicated and lack other virtues. In addition, one should not forget that ordinary GUT's suffer from the hierarchy and naturalness problems which SUSY automatically cures.

Certainly SUSY gauge coupling unification does not constitute a proof of SUSY, nor can it serve as a substitute for the direct discovery of a SUSY particle. On the other hand, it is clearly very encouraging and should not be ignored. In fact, initial simplified studies [4] claimed that it should be possible to put stringent limits on $M_X$ and the GUT value of the gauge coupling $\alpha_X$, as well as on the typical scale of supersymmetry breaking. Subsequently it was realized [3,5,8,9] that additional effects, both around the electroweak and the GUT scale, may introduce significant modifications to the early results without, however, destroying supersymmetric unification. Several authors thus focused on increasingly refined studies of the subtleties of gauge coupling unification [3,5,8,10–14]. Some [15–18] also considered the unification of the bottom and $\tau$ masses, which, in addition to the prediction of the correct value of $\sin^2\theta_W$, was regarded as a success of the early GUT's. In some of these studies it was argued that the $m_b - m_\tau$ unification almost invariably implies a very heavy top quark. Many studies mentioned above typically did not address other important issues of the MSSM. (Some, for example, did not require correct electroweak gauge symmetry breaking.) Finally, some studies have adopted a more comprehensive approach [8,19–27]. The goal is to generate, simultaneously with gauge coupling unification, realistic mass spectra of the Higgs and SUSY particles. This is usually done in the framework of the MSSM coupled to the minimal supergravity model which relates many unknown quantities of the MSSM in terms of a few basic parameters at the GUT scale. Next, various experimental and cosmological limits can be applied to the resulting couplings and mass spectra. One can then

 

examine whether all the constraints are consistent with each other and whether the SUSY partners have masses in the region of low-energy ($\lesssim$ 1 TeV) SUSY. This is the way we study the MSSM in this work. Similar approaches have been studied in the programs of Arnowitt and Nath in Refs. [19,28,29] and of Lopez and co-workers, in Refs. [21–23,30,31] among others.

We want to stress that only such a comprehensive study can be regarded as relatively self-consistent. Considering gauge coupling unification alone neglects the contribution (at two loops) from the Yukawa couplings. It usually also assumes grossly oversimplified supersymmetric mass spectra. More importantly, if one wants to include also the running of the Yukawa couplings, one is faced with the problem of whether or not one can at the same time generate electroweak symmetry breaking [32], where the magnitude of the top Yukawa coupling is of crucial importance. Furthermore, in general one must take into account the running of *all* the Yukawa coupling of the third generation, as we do in the present study. In order to impose electroweak symmetry breaking properly one needs to run not only the Higgs boson mass parameters but in fact all the relevant SUSY parameters which will be specified below. Deriving spectra that are compatible with the gauge coupling unification and electroweak symmetry breaking can only be achieved if the whole set of relevant parameters is simultaneously evaluated. Further, numerical effects from two loops, the full one-loop Higgs effective potential, etc. often significantly affect the results.

Only after implementing this comprehensive approach are we able to reject the ranges of parameters that are either unphysical or experimentally excluded, while maintaining consistency with gauge coupling unification. Many of the detailed effects we include have important consequences. For example, the two typical solutions presented as a result of such an analysis in Ref. [8] are no longer acceptable when the more complete analysis is done.

Once we derive a self-consistent SUSY spectrum that follows from grand unification, we can compare it with the present experimental limits. Furthermore, we can study its implications for cosmology and derive additional bounds. Finally, we may establish what ranges (and properties) of the parameter space are compatible with all limits. Such ranges should then be focused on in planning for experimental searches as the most "natural" — those expected in the constrained minimal supersymmetric standard model (CMSSM).

It should be emphasized that one reason it is worthwhile doing extensive work constructing SUSY models and analyzing their implications even though the full theory is not known, and the origin of SUSY breaking is not understood, is that the form of the Lagrangian at the GUT energy scale ($\sim 10^{16}$ GeV) is very general and quite insensitive to our ignorance. The kinetic energy terms are not completely unique, but corrections are likely to be of order $v_{\rm GUT}/m_{\rm Pl}$ and thus small [33]. Apart from these, given the $R$-parity conservation that we think is motivated by the stability of the proton and by cold dark matter, the superpotential we write is general, and so is the form of the soft terms [34]. Whether one arrives at the Lagrangian from supergravity or string theory, it has the same form [35] so long as quadratic divergences that would mix the high and low scales (i.e., terms which are not soft) are excluded. Thus anything one can learn about the Lagrangian by imposing physics constraints will be of general validity. Until superpartners are detected the information we have will not be sufficiently extensive to determine all parameters in it separately, of course, so one will have to make various simplifying assumptions. These assumptions can be tested in many ways as soon as superpartner masses and branching ratios are available.

Some aspects of SUSY GUT's, most notably the GUT-scale corrections [11,18,19,36] to the running of the gauge and Yukawa couplings and proton decay [19,30,37], can only be considered once a specific GUT model is selected. While we have no objections to most GUT gauge groups, for several reasons we would rather proceed by first learning what we can say without specifying a gauge group, and then by making a comparative study of GUT gauge groups. One reason is that there may be no unification group at all [38]. In fact in many string models the SM gauge group [perhaps enlarged by one or two U(1)'s] is obtainable directly from strings in which case one has gauge coupling unification without an underlying gauge group unification. Also we are concerned about SU(5) as a unification gauge group because we think it would be an astonishing accident if SUSY was otherwise successful and also provided just the amount and kind of cold dark matter needed by cosmology, but either nature did not use this dark matter or did not have it occur naturally [39] in the structure of the theory [as would have to be the case with SU(5) because $R$-parity conservation has to be imposed by hand there]. Further, while some groups [19,30] have shown that the proton decay constraint can be very important, others [37] have argued that the situation is not unambiguous. Thus we feel that it is important to maintain the distinction between the MSSM and the particular low-energy model one derives by choosing a specific GUT model. We will assume throughout this analysis only that the gauge couplings unify with $\sin^2\theta_W(M_X) = 3/8$ and that the theory remains $\mathrm{SU}(3)\times\mathrm{SU}(2)\times\mathrm{U}(1)_Y$ symmetric up to that unification scale. We are extending our approach to include a comparative study of implications of unification gauge groups (or no simple unification), and will report on this in a future publication.

In Sec. II A we briefly remind the reader of the basic assumptions underlying the MSSM. In Sec. II B we take an initial approach to the issue of gauge coupling unification and focus in particular on the effect of light mass thresholds. In Sec. III we digress on the issue of $m_b - m_\tau$ unification and discuss to what extent it requires a very heavy top quark. The dynamical radiative electroweak symmetry breaking and the resulting constraints are treated in Sec. IV. In Sec. V we briefly list supergravity-induced relations between the parameters of the model, and in the next section we use them to specify the list of independent parameters that we choose to perform our numerical studies. Also in this section we

describe the technical aspects of the procedure used in this analysis. In Sec. VII we discuss several experimental and cosmological limits which we use in Sec. VIII to constrain the remaining parameter space. In Sec. VIII we also survey a number of results of our analysis concerning the resulting patterns of SUSY spectra. From the phenomenological point of view we arrive at a constrained minimal parameters space (COMPASS) such that every choice of constrained parameters is guaranteed to have gauge coupling unification, electroweak symmetry breaking, and all experimental constraints and cosmological constraints satisfied. COMPASS will be our guide to what predictions could really occur and are not excluded by any known constraint.

COMPASS still does not uniquely determine each parameter ($m_{1/2}$, $m_0$, $m_t$, $\tan\beta$, $A_0$, $\mathrm{sgn}\,\mu_0$ as defined in Sec. VI). They can take a range of (highly correlated) values, though remarkably it typically implies mass spectra within the 1 TeV mass range. We want to avoid further assumptions about the parameters because no further theory or data are available to guide us, so we explore the general implications resulting from COMPASS by varying all relevant parameters over wide ranges of values. In future work we will explore in detail predictions for hadron [Fermilab, the CERN Large Hadron Collider (LHC)] and electron [LEP, LEP II, Next Linear Collider (NLC)] colliders, including to what extent SUSY is detectable at LEP II and Fermilab (with upgrades); in Sec. IX we give a first survey. We also study such issues as what gives the dominant contributions to $m_h$ and $m_t$, the spectrum of superpartners and predictions of SUSY for the cosmological abundance of the lightest supersymmetric particle (LSP), $B(b \to s\gamma)$, and $\Gamma(Z \to b\bar{b})$. In addition we briefly illustrate a new approach to extracting SUSY parameters from data. Solving the equations giving the parameters of the Lagrangian in terms of experimental observables can be difficult and misleading if approximations are introduced, but with our CMSSM the basic parameters can be easily extracted. Section IX can be read independently of the rest of the paper, and those more interested in the phenomenological implications rather than the technical aspects of model building may prefer to do so. Although this paper is long we think it is very important to present a single treatment that generates solutions of the CMSSM consistent with all theoretical and experimental constraints, and examines their consequences and predictions.

## II. FORMALISM

### A. Basic assumptions

Several features make the minimal supersymmetric standard model (MSSM) a particularly interesting extension of the standard model. The model is based on the same gauge group as the SM, and its particle content is the minimal one required to implement supersymmetry in a consistent way. It is described by the $R$-parity conserving superpotential

$$W = h^U_{ij}\hat{Q}_i\hat{H}_u\hat{u}^c_j + h^D_{ij}\hat{Q}_i\hat{H}_d\hat{d}^c_j + h^E_{ij}\hat{L}_i\hat{H}_d\hat{e}^c_j + \mu\hat{H}_d\hat{H}_u. \tag{1}$$

Here $\hat{Q}$, $\hat{L}$ represent the quark and lepton SU(2) doublet superfields, $\hat{u}^c$, $\hat{d}^c$, $\hat{e}^c$ the corresponding SU(2) singlets, and $\hat{H}_u$, $\hat{H}_d$ the Higgs superfields whose scalar components give mass to up- and down-type quarks and/or leptons, respectively. Generational indices have been shown explicitly, but group indices have been dropped. In addition, one introduces all the allowed soft supersymmetry-breaking terms. These are given by

$$\begin{aligned}-\mathcal{L}_{\mathrm{soft}} = {} & \left(A^U_{(ij)}h^U_{ij}\widetilde{Q}_iH_u\widetilde{u}^c_j + A^D_{(ij)}h^D_{ij}\widetilde{Q}_iH_d\widetilde{d}^c_j + A^E_{(ij)}h^E_{ij}\widetilde{L}_iH_d\widetilde{e}^c_j + \mathrm{H.c.}\right) + B\mu\,(H_dH_u + \mathrm{H.c.}) \\ & + m^2_{H_d}|H_d|^2 + m^2_{H_u}|H_u|^2 + m^2_{\widetilde{L}}|\widetilde{L}|^2 + m^2_{\widetilde{e}^c}|\widetilde{e}^c|^2 + m^2_{\widetilde{Q}}|\widetilde{Q}|^2 + m^2_{\widetilde{u}^c}|\widetilde{u}^c|^2 + m^2_{\widetilde{d}^c}|\widetilde{d}^c|^2 \\ & + \tfrac{1}{2}\left(M_1\bar{\psi}_B\psi_B + M_2\bar{\psi}^a_W\psi^a_W + m_{\tilde{g}}\bar{\psi}^a_g\psi^a_g + \mathrm{H.c.}\right).\end{aligned} \tag{2}$$

Here the tilded fields are the scalar partners of the quark and lepton fields, while the $\psi_i$ are the spin-$\frac{1}{2}$ partners of the $i$ =U(1)$_Y$,SU(2)$_L$,SU(3)$_c$ gauge bosons. The $A_{(ij)}$, $B$, and all other new parameters in $\mathcal{L}_{\mathrm{soft}}$ are *a priori* unknown mass parameters.

The full Lagrangian consists of the kinetic and gauge terms (which are assumed to be minimal), the terms derived from the superpotential (the $F$ terms), and $\mathcal{L}_{\mathrm{soft}}$. It is important to understand that the Lagrangian we study has the most general set of $R$-parity conserving soft-breaking terms, that is, terms that do not induce quadratic divergences and thereby preserve the existence of two disparate mass scales. We require $R$-parity conservation motivated not only by the lack of fast proton decay in nature, but also by the natural success of the theory in predicting the existence of dark matter. In Section V we will add some other assumptions that relate various soft-breaking terms; these assumptions are somewhat motivated and can easily be removed for further study if theoretical or phenomenological opportunities exist.

The model as defined by Eqs. (1) and (2) is the simplest phenomenologically viable supersymmetric extension of the SM. It is also general in the sense of allowing the most general form [34] of soft terms in Eq. (2). On the other hand, because of the large number of new unknown parameters the model is not very predictive. A natural way of relating them is to think of the MSSM as coming out of some underlying GUT (or string) model.

One possible approach is to select at the start a specific GUT which at low energy would take the form of the MSSM (plus possibly a modified neutrino sector which

we neglect here). This can be done with any GUT which can break into the SM gauge group, the minimal SU(5) being the simplest and most often studied choice. In this approach, however, one must also consider the whole GUT-scale structure with a more complicated Higgs sector. Guided by minimality, one often focuses on the simplest Higgs sector of SU(5). But that model cannot be regarded as realistic or particularly attractive due to the well-known problem of doublet-triplet splitting. Fixing this new "fine-tuning" problem at the GUT scale requires significant modifications of the model. In other words, at present we believe there is no commonly accepted "standard" GUT model.

Another approach is to treat the MSSM as an effective model that could arise from a large class of GUT models while not making any specific choice. Instead, one can make various reasonable assumptions at the GUT scale consistent with general properties of that class of GUT models and next study "corrections" due to a specific GUT. In this approach one therefore initially neglects all possible corrections due to the superheavy states. This is the approach that we will follow here. We will be adopting more and more assumptions at the GUT scale, starting in the next section from just gauge coupling unification and eventually considering the MSSM in the framework of the minimal supergravity model. While we will not choose any specific GUT we will remark below about the importance of some of the possible corrections at the GUT energy scale. We feel it is important to distinguish what we can learn from this approach from the results that would be obtained if we chose a specific unification gauge group.

### B. Light threshold corrections

We first address several issues that can be studied without necessarily introducing further simplifications of the parameter space. We begin by focusing on the running of the gauge couplings alone and in particular on the important role played by the mass thresholds due to the Higgs and supersymmetric particles.

In running the renormalization group equations (RGE's) between the weak and GUT scales the coefficients of the RGE's change at each particle's mass threshold due to the decoupling of states at scales above their masses. Initially, a simplified case was considered [4] where one assumed mass degeneracy for all the sparticles (along with the second Higgs doublet) at some scale usually denoted $M_{\rm SUSY}$. In that case one uses the $\beta$ functions for the gauge couplings of the SM between $Q = m_Z$ and $Q = M_{\rm SUSY}$, and those of the MSSM between $Q = M_{\rm SUSY}$ and $Q = M_X$.

However, the effects of a nondegenerate SUSY spectrum on the gauge coupling $\beta$ functions provide a significant correction to the naive solutions of the RGE's [5,8,40–42]. The assumption that $M_{\rm SUSY}$ could represent some average sparticle mass for highly nondegenerate spectra, such as one gets in superunified models, is in general incorrect and can lead to significant errors on the order of 10% or more in $\alpha_s(m_Z)$, $M_X$, etc. Instead one must take into account the various sparticle thresholds individually, changing the gauge coupling $\beta$-function coefficients for each sparticle as the energy scale crosses its (running) mass, i.e., when it decouples from the RGE's. Accounting for each particle's contribution to the gauge $\beta$-function coefficients, one can write, at one loop [5,8],

$$b_1^{\rm MSSM} = \frac{4}{3}N_g + \frac{1}{10}N_H^{\rm SM} + \frac{2}{5}\theta_{\tilde H} + \frac{1}{10}\theta_{H_2} + \frac{1}{5}\sum_i \left\{ \frac{1}{12}\left(\theta_{\tilde u_{L_i}} + \theta_{\tilde d_{L_i}}\right) + \frac{4}{3}\theta_{\tilde u_{R_i}} + \frac{1}{3}\theta_{\tilde d_{R_i}} + \frac{1}{4}\left(\theta_{\tilde e_{L_i}} + \theta_{\tilde\nu_{L_i}}\right) + \theta_{\tilde e_{R_i}} \right\}, \tag{3}$$

$$b_2^{\rm MSSM} = -\frac{22}{3} + \frac{4}{3}N_g + \frac{1}{6}N_H^{\rm SM} + \frac{4}{3}\theta_{\widetilde W} + \frac{2}{3}\theta_{\tilde H} + \frac{1}{6}\theta_{H_2} + \frac{1}{2}\sum_i \left\{ \theta_{\tilde u_{L_i}}\theta_{\tilde d_{L_i}} + \frac{1}{3}\theta_{\tilde e_{L_i}}\theta_{\tilde\nu_{L_i}} \right\}, \tag{4}$$

$$b_3^{\rm MSSM} = -11 + \frac{4}{3}N_g + 2\,\theta_{\tilde g} + \frac{1}{6}\sum_i \left\{ \theta_{\tilde u_{L_i}} + \theta_{\tilde d_{L_i}} + \theta_{\tilde u_{R_i}} + \theta_{\tilde d_{R_i}} \right\}, \tag{5}$$

where

$$\frac{d\alpha_i}{dt} \equiv \frac{b_i}{2\pi}\alpha_i^2 + \text{two loops}, \qquad t \equiv \ln(Q/m_Z), \qquad \alpha_1 \equiv \frac{5}{3}\alpha_Y, \qquad \theta_x \equiv \theta(Q^2 - m_x^2). \tag{6}$$

In the summations, $i = 1, \ldots, N_g$ where $N_g = 3$ is the number of fermion generations, and $N_H^{\rm SM} = 1$ is the number of SM Higgs doublets. Here also $\tilde H$ represents the (mass degenerate) Higgsino fields, $\widetilde W$ the partners of the $W$ bosons ($m_{\widetilde W} \equiv M_2$), and $\tilde g$ the partner of the gluon, all taken to be mass eigenstates in this approximation. $H_2$ is to be understood as the second Higgs doublet in the approximation where $H_1$ is the SM Higgs doublet containing the neutral $CP$-even Higgs boson with mass $\sim m_Z$. $H_2$ is heavy with each component's mass equal to that of the Higgs pseudoscalar. In this approximation the mixing of the two Higgs doublets is suppressed by inverse powers of the heavy Higgs bosons' masses and are therefore ignored as being of higher order and numerically negligible [42]. (The full two-loop gauge coupling $\beta$ functions for the SM and MSSM which we use in actual calculations can be found in Refs. [43 and 44], respectively. A discussion of two-loop thresholds can be found in Sec. VI B.)

The effect of multiple mass threshold effects on the running of the gauge couplings has been extensively studied recently. Notably, in a semianalytic approach developed by Langacker and Polonsky [10] the effects of the thresholds on the one-loop gauge $\beta$ functions were studied. They showed that in the one-loop calculation of $\alpha_s(m_Z)$ from $\sin^2\theta_W$, $\alpha$, and the GUT-unification condition, the net effect of all low-energy thresholds could be expressed in terms of a single scale $M_{\rm SUSY}^{\rm eff}$ (called $A_{\rm SUSY}$ in Ref. [10]). One can express this scale in terms of all the supersymmetric masses:

$$M_{\rm SUSY}^{\rm eff} = m_{\widetilde{H}} \left(\frac{m_{H_2}}{m_{\widetilde{H}}}\right)^{\frac{3}{19}} \left(\frac{M_2}{m_{\widetilde{H}}}\right)^{\frac{4}{19}} \left(\frac{M_2}{m_{\widetilde{g}}}\right)^{\frac{28}{19}} \left(m_{\tilde{u}_L} m_{\tilde{c}_L} m_{\tilde{t}_L}\right)^{-\frac{15}{114}} \left(m_{\tilde{d}_L} m_{\tilde{s}_L} m_{\tilde{b}_L}\right)^{\frac{1}{2}} \left(m_{\tilde{u}_R} m_{\tilde{c}_R} m_{\tilde{t}_R}\right)^{-\frac{15}{57}}$$
$$\times \left(m_{\tilde{d}_R} m_{\tilde{s}_R} m_{\tilde{b}_R}\right)^{-\frac{9}{57}} \left(m_{\tilde{e}_L} m_{\tilde{\mu}_L} m_{\tilde{\tau}_L}\right)^{\frac{7}{38}} \left(m_{\tilde{e}_R} m_{\tilde{\mu}_R} m_{\tilde{\tau}_R}\right)^{-\frac{2}{19}} \left(m_{\tilde{\nu}_{eL}} m_{\tilde{\nu}_{\mu L}} m_{\tilde{\nu}_{\tau L}}\right)^{-\frac{1}{38}} . \quad (7)$$

In the simplified case in which the spectra of squarks and sleptons are each assumed mass degenerate, and taking only the contributions with leading exponents, Eq. (7) reduces to a similar formula given in Ref. [17]. By using a very crude parametrization in which $m_{\tilde{H}} \simeq |\mu|$, one finds that

$$M_{\rm SUSY}^{\rm eff} \simeq |\mu| \left(\frac{\alpha_2(M_2)}{\alpha_s(m_{\tilde{g}})}\right)^{\frac{28}{19}} \simeq |\mu|/5. \quad (8)$$

This strong dependence on $\mu$ is somewhat unexpected considering that $\mu$ does not break supersymmetry.

The $M_{\rm SUSY}^{\rm eff}$ formalism is useful in providing estimates of the size of the various possible corrections to the running of the gauge couplings. However, it is neither accurate nor practical in the more comprehensive approach that we will adopt below in which the running of gauge couplings is simultaneously considered with the running of Yukawa couplings and mass parameters. Using the SM RGE's between $Q = m_Z$ and $Q = M_{\rm SUSY}^{\rm eff}$ and the SUSY RGE's for $Q > M_{\rm SUSY}^{\rm eff}$ may accurately reproduce $\alpha_s(m_Z)$, but it will not provide the correct value of $\alpha_X$ or $M_X$ (up to 50% errors for the latter), nor will it allow one to calculate correctly the ratio $m_b/m_\tau(M_X)$. Furthermore, in this scheme two-loop corrections to the one-loop value of $\alpha_s(m_Z)$ derived in this method can be added only in an approximate fashion. These two-loop corrections are of the same order as the one-loop threshold corrections, and in fact increase $\alpha_s(m_Z)$ by ~10% when included (see Table III in Sec. VI B). Thus we will not use the technique of an effective SUSY scale except for purposes of comparison in Sec. III.

In the numerical analysis that we will present later, the effect of the threshold corrections is automatically included separately for each contributing particle, not with a single SUSY threshold. We will discuss this, along with some other subtleties involved, in Sec. VI B.

Finally, several authors have emphasized the importance of thresholds at the GUT scale [9–11,13,18,19,36]. In many models, such as minimal SU(5), these corrections can be sizable. In fact, they can be comparable to the corrections coming from the nondegeneracy of the SUSY spectrum at the low scale (see, e.g., Ref. [10]). Consideration of such corrections can even be used to achieve gauge coupling unification in models where none seemed otherwise possible, such as nonsupersymmetric SO(10) [1,7]. Models with nonminimal GUT sectors often give rise to sizable corrections that can alter low-energy predictions [1,45]. However, consideration of these corrections can only be made after (i) a GUT gauge group has been chosen and (ii) the GUT Higgs sector and mass spectrum has been decided upon. Because we wish to study the superunified MSSM in general, without reference to a particular choice of GUT gauge group or spectrum, we ignore all such corrections and leave them for future studies of various proposed unification schemes.

## III. BOTTOM-$\tau$ YUKAWA UNIFICATION

There has been much interest recently in the issue of Yukawa coupling unification within the framework of SUSY. In many GUT models, including minimal SUSY–SU(5), the down-type components of the lepton and quark doublets reside in the same GUT multiplets and, assuming a particularly simple Higgs sector, their Yukawa couplings are often equal at the GUT scale. The experimentally determined ratio $m_b/m_\tau \simeq 3$, which decreases roughly to one at the GUT scale, was considered one of the early successes for GUT's. More recently however after the precise LEP data on gauge couplings became available, it was shown that the bottom-$\tau$ mass unification, while consistent with SUSY–SU(5), was inconsistent with the non-SUSY case [15].

Several groups [16–18] have examined $b-\tau$ mass unification more precisely in minimal SUSY under the assumption of gauge coupling unification. These studies have claimed that in order to achieve $b-\tau$ mass unification one must have a top quark with mass very near to its IR pseudofixed point. That is, to a good approximation $b-\tau$ mass unification implies [16]

$$m_t^{\rm pole} \simeq (200\,{\rm GeV}) \sin\beta. \quad (9)$$

For the range of top quark masses favored by LEP ($130\,{\rm GeV} \lesssim m_t^{\rm pole} \lesssim 170\,{\rm GeV}$) [46] under the assumption of a light Higgs boson, they find that only the small regions $1 \lesssim \tan\beta \lesssim 2$ or $\tan\beta \simeq 60$ are consistent with $b$-$\tau$ mass unification. [Here $m_t^{\rm pole}$ refers to the so-called pole mass of the top quark as opposed to the running or modified minimal subtraction scheme ($\overline{\rm MS}$) mass [47]. For a clear discussion of this point see Ref. [14]. We will usually speak of running masses except where we specify otherwise.]

One is led to ask the following: if the top quark is found to have a mass somewhere in the LEP-favored region, are we absolutely forced to either very small or very large values for $\tan\beta$? In order to answer this question one must consider how stable the stated claim is to perturbations in the inputs of the analysis. Such questions have been briefly considered in Refs. [16–18,48]. We find that the effects of such perturbations are often understated.

In considering how to make the MSSM consistent with a "light" top quark [i.e., one with mass well below that required by Eq. (9)], we find that there are several options for eluding the heavy top or the extreme values of $\tan\beta$ without having to give up on $b$-$\tau$ mass unification completely. First and foremost, it must be remembered that previous attempts to address this issue have suffered from a common problem: they have attempted to study

$b$-$\tau$ mass unification while using only a single threshold approximation for the SUSY mass spectrum. That is, these analyses have claimed that a nondegenerate spectrum of sparticles can be approximated by a single effective scale. Although this is indeed possible for a study of $\alpha_s(m_Z)$ consistent with gauge coupling unification (see discussion in Sec. II B), no single threshold approximation can possibly perform the same task for $b$-$\tau$ mass unification, given the dependence of the Yukawa RGE's on the gauge couplings, the presence of Yukawa couplings in the two-loop RGE's, and the necessary lack of knowledge about the scale of unification in such an approximation.

With this caveat in mind we now begin to explore the stability of Eq. (9) to perturbations in the inputs to the analysis. In this section alone we shall use the very same single threshold approximation about which we have just warned the reader. We do so because we are only interested in general numerical studies that point to possible approaches to this question, and because we have a consistent approach in the following sections whose results do not depend on the single threshold approximation for the gauge couplings.

The one scale that we use here should not be confused with the $M_{\rm SUSY}^{\rm eff}$ introduced earlier, for we will choose $\alpha_s(m_Z)$ in this case without regard to the condition of gauge coupling unification. This new effective scale is in fact nothing more than the naive SUSY scale used in the studies of Ref. [16] and in many early SUSY studies. In displaying our results, we will choose this effective SUSY scale to be equal to $m_Z$; once again the exact value is unimportant for our general conclusions. We also have to choose a value for the $b$-quark pole mass. In this section, we will take the range $4.7 \leq m_b^{\rm pole} \leq 5.1\,{\rm GeV}$, which is the $3\sigma$ bound from the recent analysis of Ref. [49].

In addition to the innate error resulting from a single threshold approximation, there remain other simple routes by which Eq. (9) can be modified. We find that by (i) allowing corrections to the Yukawa unification or (ii) allowing the strong coupling constant to take on values near the lower end of its experimental range, one can avoid the requirement of a heavy top.

The first of these routes requires one to consider corrections to the requirement that $m_b/m_\tau = 1$ at $M_X$. This is because in the interesting regions of the $m_t^{\rm pole} - \tan\beta$ plane, one finds that in general $m_b/m_\tau < 1$ at $M_X$. Corrections could be induced through radiative corrections, through effects from heavy state decoupling, through nonrenormalizable operators, or simply by the scale of $b$-$\tau$ mass unification becoming displaced from the scale of gauge coupling unification. Without choosing any particular source, such corrections have been considered [16,18,48]. But how large must these corrections become in order to significantly alter the central claim of Eq. (9)? In Fig. 1 we have shown the regions consistent with $m_b/m_\tau = 1$ for bottom quark masses in the range $4.7 \leq m_b^{\rm pole} \leq 5.1\,{\rm GeV}$ and $\alpha_s(m_Z) = 0.120$ (within the solid lines). We have also shown the region for the same range of bottom masses, but now with corrections to Yukawa unification of 10% (dashed lines). This or similar plots are most often shown in the literature as evidence for the stability of Eq. (9).

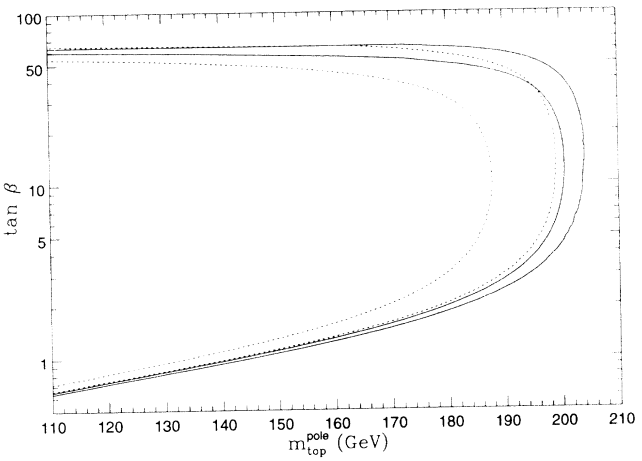


FIG. 1. Regions in the $m_t^{\rm pole} - \tan\beta$ plane consistent with bottom-$\tau$ Yukawa unification. The region bounded by the solid lines represents the region of parameter space consistent with $m_b/m_\tau = 1$ at $M_X$ for $4.7 \leq m_b^{\rm pole} \leq 5.1\,{\rm GeV}$. The region between the dashed lines is consistent with $m_b/m_\tau = 0.9$ at $M_X$. Here we have taken the effective scale of SUSY to be 90 GeV and $\alpha_s(m_Z) = 0.120$.

Although Fig. 1 suggests that Eq. (9) is stable to a 10% correction one might also wish to explore the effect of varying the strong coupling constant on the Yukawa unification. Current measurements of $\alpha_s(m_Z)$ from a variety of sources indicates that $0.110 \lesssim \alpha_s(m_Z) \lesssim 0.130$. Values of $\alpha_s(m_Z)$ in the lower half of this range in combination with a 10% uncertainty in the GUT relation $m_b/m_\tau = 1$ significantly widen the available parameter space in the $m_t^{\rm pole} - \tan\beta$ plane. (Given the analyses of Ref. [50], perhaps such low values for $\alpha_s(m_Z)$ should be included in a careful consideration of these questions.) Such an effect is shown in Fig. 2 where we have taken $\alpha_s(m_Z) = 0.112$. It must be emphasized that such a small value for $\alpha_s(m_Z)$ is inconsistent with the simplest SUSY-GUT unification unless we require the scale of SUSY masses to be $\sim$ 10 TeV. In particular, we would need a very heavy Higgsino. Nonetheless, such

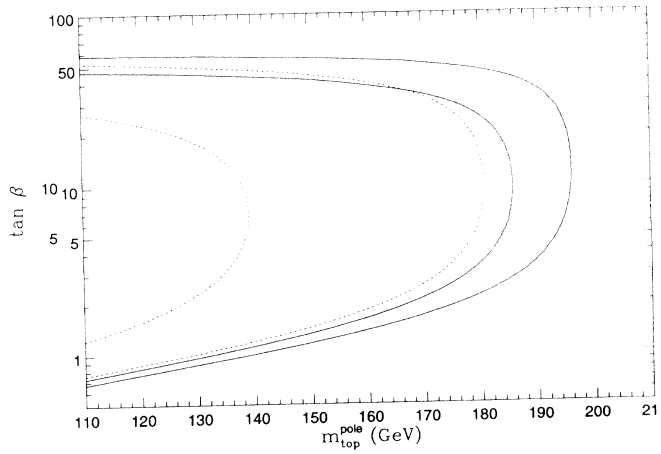


FIG. 2. Same as Fig. 1 but now with $\alpha_s(m_Z) = 0.112$. Notice that the available parameter space has increased markedly.

a small $\alpha_s(m_Z)$ could come from other sources, such as heavy threshold effects or nonrenormalizable operators. Fig. 2 clearly shows that for $m_t^{\rm pole} \gtrsim 140\,{\rm GeV}$, all values of $\tan\beta$ consistent with perturbative unification become allowed. Essentially, combining two 10% effects has eliminated the constraint among $m_b$, $m_t$, and $\tan\beta$.

As we have tried to emphasize, the conclusions drawn by demanding strict $b-\tau$ mass unification can be quite strong, yet fairly small effects due to unknowns in the analysis can change the results considerably. Therefore we take the following approach in the remainder of this paper. We will always take the $\tau$ mass as given very precisely by experiment and use it to determine $m_\tau(M_X)$. Although the experimental uncertainty to the central value of 4.9 GeV is larger, we will do the same for the bottom quark mass. We will not demand exact $b$-$\tau$ mass unification. Because we make no specific choice of GUT group or spectrum in this paper, we have no mechanism otherwise for escaping the constraints imposed by $b$-$\tau$ mass unification. Yet we also understand that corrections that will come from any eventual choice of GUT can, as we demonstrated above, allow a larger region of parameter space to become available. When we do require exact $b$-$\tau$ mass unification in our full analysis we find agreement with Eq. (9). Further, even when we do not require unification, all solutions generated still preserve unification to about 20%.

Because we wish this analysis to be general and to provide insights over the entire range of perturbatively allowed values of $\tan\beta$ in particular, we must do without precise $b$-$\tau$ mass unification. At the same time we still include everything that would otherwise follow from imposing this unification because solutions we find in the regions of parameter space consistent with Eq. (9) do indeed lead to $b$-$\tau$ mass unification. In this sense, our results are more general than the previously cited analyses. We think it is likely that the approximate unification of $m_b$ and $m_\tau$ is telling us important physics, but we think it is perhaps premature to draw conclusions from it.

## IV. ELECTROWEAK GAUGE SYMMETRY BREAKING

One of the most remarkable features of the MSSM is a "built-in" mechanism for dynamical electroweak symmetry breaking (EWSB) [32]. The renormalization group improved supersymmetric Higgs potential naturally breaks $\mathrm{SU(2)\times U(1)_Y} \to \mathrm{U(1)_{em}}$ if the top quark Yukawa coupling is sufficiently large compared to the gauge couplings. As we outline below this will allow us to reduce the number of free parameters in the theory and express some GUT-scale free parameters in terms of more useful low-energy ones.

The tree-level Higgs potential can be derived from the expressions for $W$, Eq. (1), the so-called $D$ terms, and $\mathcal{L}_{\rm soft}$, Eq. (2):

$$V_0 = m_1^2|H_d^0|^2 + m_2^2|H_u^0|^2 + m_3^2(H_d^0 H_u^0 + \text{H.c.}) + \frac{g_1^2+g_2^2}{8}(|H_d^0|^2 - |H_u^0|^2)^2, \quad (10)$$

where $m_{1,2}^2 \equiv m_{H_{d,u}}^2 + \mu^2, m_3^2 \equiv B\mu$, and the phases of the fields are chosen such that $m_3^2 < 0$.

Using the RGE's, one may define the renormalization group improved tree-level Higgs potential $V_0(Q)$ at any scale $Q$. $V_0(Q)$ is understood to be the tree-level $V_0$ where the fields and coefficients have attained a scale dependence through their one- or two-loop RGE's. However, as was emphasized in Ref. [51], in general $V_0(Q)$ can depend strongly on the energy scale at which it is evaluated. In other words, minimizing $V_0(Q)$ at, say, $Q = m_Z$ and again at some slightly larger $Q$ may lead to very different values of $v_d$, $v_u$, and therefore $\tan\beta \equiv v_u/v_d$. This behavior is due to large radiative corrections coming particularly from mass splitting in the $t$-$\tilde{t}$ system. If one knew the scale $Q = O(m_Z)$ at which these corrections were small, one could safely minimize $V_0(Q)$ there. However, this scale in unknown *a priori*. A much more satisfactory solution is achieved by minimizing the full one-loop Higgs effective potential. The full Higgs potential can be written as

$$V_{\rm Higgs}(Q) = V_0(Q) + \Delta V(Q), \quad (11)$$

where (see, e.g., Ref. [52])

$$\Delta V(Q) = \frac{1}{64\pi^2} S\mathrm{Tr}\, M^4 \left(\log\frac{M^2}{Q^2} - \frac{3}{2}\right) \quad (12)$$

is the one-loop contribution to $V_{\rm Higgs}$ and $S\mathrm{Tr}\, f(M^2) \equiv \sum_j (-1)^{2j}(2j+1)\mathrm{Tr}\, f(M^2)$ where $M$ and $j$ are the (field-dependent) mass and the spin of a given state, and the sum is over all states in the Lagrangian.

Electroweak symmetry breaking can occur if the following two conditions are met: (i) $V_{\rm Higgs}$ is bounded from below (i.e., $m_1^2 + m_2^2 \geq 2|m_3^2|$) and (ii) the minimum of $V_{\rm Higgs}$ occurs at nonzero field configurations (i.e., $m_1^2 m_2^2 \leq m_3^4$). It was realized early that, given a "large" top quark mass, EWSB could be achieved radiatively [32]. That is, despite taking $m_{H_d}^2, m_{H_u}^2, \mu^2 > 0$ at $M_X$, requirement (ii) above can still be satisfied. For a "large" $m_t \gtrsim 80\,{\rm GeV}$, the running of $m_2^2$ is dominated by $h_t$, the top Yukawa. As the scale $Q$ decreases from the GUT scale, $m_2^2$ is driven negative while $m_1^2$ and $\mu^2$ remain positive.

Minimization of $V_{\rm Higgs}$ leads to the system of equations

$$\frac{\partial V_{\rm Higgs}}{\partial v_d^2} = m_1^2 + m_3^2\tan\beta + \frac{1}{2}m_Z^2\cos 2\beta + \Sigma_1 = 0, \quad (13)$$

$$\frac{\partial V_{\rm Higgs}}{\partial v_u^2} = m_2^2 + m_3^2\cot\beta - \frac{1}{2}m_Z^2\cos 2\beta + \Sigma_2 = 0, \quad (14)$$

where $\Sigma_{1,2} \equiv \partial\Delta V/\partial v_{d,u}^2$ and all terms are implicitly $Q$ dependent.

Solving Eqs. (13) and (14) one finds

$$\sin 2\beta(Q) = \frac{-2m_3^2(Q)}{\mu_1^2(Q) + \mu_2^2(Q)} \quad (15)$$

and

$$\frac{1}{2}m_Z^2(Q) = \frac{\mu_1^2(Q) - \mu_2^2(Q)\tan^2\beta(Q)}{\tan^2\beta(Q) - 1}. \quad (16)$$

We have introduced two parameters:

$$\mu_{1,2}^2(Q) \equiv m_{1,2}^2(Q) + \Sigma_{1,2}(Q) = m_{H_{d,u}}^2(Q) + \mu^2(Q) + \Sigma_{1,2}(Q). \quad (17)$$

Examining Eqs. (13)–(16) we find that, in fact, EWSB can occur for any value of $m_t$ so long as $m_t > m_b$. In the limit $m_t$ approaches $m_b$ (ignoring for now the contributions beyond the tree level), $\mu_2^2$ approaches $\mu_1^2$ from below, but is not driven negative as in the large $m_t$ limit. Equation (16) can now only be satisfied as $\tan\beta$ approaches 1 from above. One concludes therefore that radiative EWSB can occur for any $m_t > m_b$, though small $m_t$ ($\lesssim m_W$) would have required $\tan\beta \simeq 1$. From a rough search of the parameter space we find that although the condition $m_t \gtrsim m_W$ is always sufficient for EWSB (assuming appropriate values for the other parameters), it is also *necessary* in order to obtain values of $\tan\beta \gtrsim 2$.

It would be simplest if we could always minimize $V_{\rm Higgs}(Q)$ at $Q = m_Z$ because we know from experiment the value for $m_Z(m_Z)$ in Eq. (16) above. In minimizing $V_0(Q)$, this would be dangerous. But $V_{\rm Higgs}(Q)$, unlike $V_0(Q)$, is relatively stable with respect to $Q$, so that we can choose $Q = m_Z$ with confidence.

The complete forms of $\Sigma_1$ and $\Sigma_2$ are included in Ref. [53]. It has been emphasized [53,54] that the use of only the leading $t$-$\tilde{t}$ contributions to $\Delta V$ can be misleading due to potentially large cancellations that can occur with other terms that are not included. Throughout our analysis, all contributions to the complete one-loop effective potential have been included. Because use of the full potential requires knowledge of the complete SUSY spectrum, the iterative procedure that will be outlined in Sec. VI is ideally suited for considering this issue.

## V. SUPERGRAVITY-BASED CONSTRAINTS

While the phenomenology of the MSSM is sometimes studied without referring to its GUT-scale origin we want to consider in this study a highly constrained SUSY scenario with as many well-motivated assumptions as possible. This will of course enhance predictability for the ranges of parameters where SUSY may be realized. (Later we can examine what modifications result from relaxing assumptions.)

As we mentioned in Sec. II A, a natural and often considered approach is to couple the MSSM to minimal $N = 1$ supergravity from which the following set of assumptions emerges.

(1) *Common gaugino mass* $m_{1/2}$. The soft SUSY-breaking gaugino mass terms are equal to $m_{1/2}$ at $M_X$:

$$M_1(M_X) = M_2(M_X) = m_{\tilde{g}}(M_X) \equiv m_{1/2}. \quad (18)$$

(2) *Common scalar mass* $m_0$. The soft SUSY-breaking scalar mass terms contributing to the squark, slepton, and Higgs boson masses are equal to $m_0$ at $M_X$:

$$m_{\tilde{Q}}^2(M_X) = m_{\tilde{u}^c}^2(M_X) = \cdots = m_{H_d}^2(M_X) = m_{H_u}^2(M_X) \equiv m_0^2. \quad (19)$$

(3) *Common trilinear scalar coupling* $A_0$. The soft trilinear SUSY-breaking terms are all equal to $A_0$ at $M_X$,

$$A_t(M_X) = A_b(M_X) = A_\tau(M_X) = \cdots \equiv A_0. \quad (20)$$

Through the RGE's of the MSSM, assumption (18) is often expressed

$$M_1 = \tfrac{5}{3}\tan^2\theta_W M_2 \simeq 0.5 M_2, \quad (21)$$

$$M_2 = \frac{\alpha_2}{\alpha_s} m_{\tilde{g}} \simeq 0.3 m_{\tilde{g}}, \quad (22)$$

with $M_1$, $M_2$, and $m_{\tilde{g}}$ evaluated at the electroweak scale. One also derives $m_{1/2} \simeq 1.2 M_2 \simeq 0.36 m_{\tilde{g}}$.

Assumptions (18) and (19), in conjunction with SUSY and the gauge structure, lead to the following expressions for the masses of the sfermions (except for the third generation sfermions) at the electroweak scale (see, e.g., Ref. [55]):

$$m_{\tilde{f}_{L,R}}^2 = m_f^2 + m_0^2 + b_{\tilde{f}_{L,R}} m_{1/2}^2 \pm m_Z^2 \cos 2\beta\,[T_3^{f_{L,R}} - Q_{f_{L,R}}\sin^2\theta_W], \quad (23)$$

where $\tilde{f}_{L,R}$ is the left (right) sfermion corresponding to an ordinary left (right) fermion, $T_3^{f_{L,R}}$ and $Q_{f_{L,R}}$ are the third component of the weak isospin and the electric charge of the corresponding fermion $f$, and the coefficients $b$ can be expressed as functions of the gauge couplings at $m_Z$ and are $b \simeq 6$ for squarks, $\simeq 0.5$ for left sleptons, and $\simeq 0.15$ for right sleptons (see, e.g., Ref. [56]). Their exact values vary somewhat with different input parameters.

While the assumptions (18), (19), and (20) derive from theoretical speculations at the GUT scale, we want to stress that some motivation for assuming at least the common scalar mass is provided by experiment. The near mass degeneracy in the $K^0$-$\bar{K}^0$ system implies a near mass degeneracy between $\tilde{s}_L$ and $\tilde{d}_L$ [57]. Similarly, slepton masses have to be strongly degenerate from stringent bounds on $\mu \to e\gamma$ [57]. It is thus sensible to generalize this property to all the mass terms, especially since there exists a well-motivated theoretical framework providing it. Alternative approaches exist [35,58], though we do not consider them in this study. We note that for almost all topics and applications only $A_t$ among the trilinear soft terms plays a role, so in practice we did not have to impose the condition (20). The assumptions (18), (19) will be easily tested with any superpartner data.

Many past analyses have also relied on the further assumption that $B_0 = A_0 - m_0$ [$B_0 = B(M_X)$, etc.], which follows from a restricted class of supergravity (SUGRA) models. As has been shown in Ref. [59], even if this relation is present at the tree level in the full theory, it can be altered dramatically as heavy states are decoupled at $M_X$. We do not impose this constraint anywhere in the analysis.

## VI. PROCEDURE

### A. Choice of independent parameters

After making the (SUGRA-inspired) reduction of the parameter space outlined above, we are left with six "fundamental" input parameters at the GUT scale: $m_0$, $m_{1/2}$, $A_0$, $B_0$, $\mu_0$, and $h_{t0}$. (In addition, we include all effects due to $h_b$ and $h_\tau$ in the analysis.) However, not all of the parameters remain independent when we impose radiative EWSB. Equation (16) allows us to eliminate $\mu^2(m_Z)$ as a free parameter in favor of $m_Z^2$, though the sign of $\mu$ is still free. Similarly, we can eliminate $B(m_Z)$ in favor of $\tan\beta(m_Z)$ via Eq. (15). Finally, given $\tan\beta$ and the RGE's we can replace $h_{t0}$ by $m_t^{\rm pole}$. Table I summarizes our choices.

This "mixed" set of input parameters, $m_0$, $m_{1/2}$, $A_0$, $\mu_0$, $\tan\beta$, and $m_t^{\rm pole}$, has been commonly used in the literature because of its technical convenience. This convenience becomes apparent upon inspection of the system of RGE's, in which $\mu$ and $B$ do not affect the running of any of the other parameters in the low-energy effective Lagrangian. Their values at the weak scale may be calculated from Eqs. (15) and (16), and run back up to $M_X$ in order to determine $\mu_0$ and $B_0$. The sign of $\mu$ is scale independent. Note that when we consider $\tan\beta$ in this analysis, we will always assume $\tan\beta(Q) = \tan\beta(m_Z)$ for all $Q = O(m_Z)$; this is well motivated by the very slow running of $\tan\beta$ and the small range of scales over which we consider the phenomenology of the MSSM, and so introduces only negligible errors.

There is another reason for the above choice of input parameters. In some schemes it is possible to determine $m_t$ as an output. We feel, however, that $m_t$ should be an input into any routine. Current LEP data put strong constraints on $m_t$, and direct discovery of the top quark at the Fermilab Tevatron may be forthcoming. Thus $m_t$ will soon serve as a relatively well-known input parameter. Therefore, analyses that give $m_t$ as an output will not be efficient in exploring the parameter space consistent with a known $m_t$.

There is however a certain technical difficulty associated with using the "mixed" parametrization. Some input parameters, such as the Yukawa couplings of the third generation, the gauge couplings, and $\tan\beta$, are known or chosen at the $Z$ scale. But others such as $m_0$, $m_{1/2}$, and $A_0$ are chosen at the GUT scale. Furthermore, the two scales are mixed in the sense that we must calculate the values of $M_X$ and $\alpha_X$ through the running of the low-energy values of the gauge couplings. This running is in turn dependent on the low-energy mass spectrum of the SUSY particles, which depends most heavily on the values of $m_0$ and $m_{1/2}$ at the GUT scale. Therefore we employ an iterative numerical procedure that converges on a consistent solution given all the input parameters. We discuss it below.

### B. Running the RGE's

We begin our numerical procedure at the electroweak scale, which we take to be $m_Z$. This is an obvious choice since many experimental quantities are now available at that scale.

At $Q = m_Z$ we take as input the well-measured values of the $Z$ mass [46],

$$m_Z = 91.187 \pm 0.007\,\text{GeV}, \tag{24}$$

the electromagnetic coupling constant

$$\alpha(m_Z) = \frac{1}{127.9 \pm 0.1}, \tag{25}$$

and the weak mixing angle $\sin^2\theta_W(m_Z)$, in the $\overline{\rm MS}$ scheme. [The $\overline{\rm MS}$ value of $\sin^2\theta_W$ at the $Z$ pole is defined so that $\sin^2\theta_W\cos^2\theta_W \equiv (\pi\alpha/\sqrt{2}G_F)/m_Z^2(1-\Delta\hat{r})$, where the radiative correction function $\Delta\hat{r}$ depends on both $m_t$ and $m_h$.] The current world average for the weak mixing angle is $\sin^2\theta_W = 0.2324 \pm 0.0008 \pm 0.0003$ [10], where the first error is due to uncertainty in the value of $m_t$ and the second error is dominated by the Higgs boson mass uncertainty. Because we take $m_t$ as a known input parameter in this analysis, the uncertainty due to top quark mass is replaced by a functional dependence of $\sin^2\theta_W$ on $m_t^{\rm pole}$ [10]:

$$\sin^2\theta_W = 0.2324 - 1.03\times10^{-7}\left[(m_t^{\rm pole})^2 - (138\,\text{GeV})^2\right] \pm 0.0003. \tag{26}$$

One can see the dependence of the gauge couplings on this parametrization in Table II, where we have shown the values of $\alpha_s(m_Z)$, $\alpha_X$, and $M_X$ for several values of

TABLE I. Summary of input to and outputs from our analysis. Note that the choice between $m_b$ and $\frac{m_b}{m_\tau}|_{M_X}$ depends on whether we are testing the assumption of GUT-scale Yukawa unification as in Sec. III or requiring physically realistic bottom quark masses as in this section and those that follow.

| | |
|---|---|
| Inputs: | $m_0$, $m_{1/2}$, $A_0$, $\text{sgn}\,\mu_0$, $m_t^{\rm pole}$, $\tan\beta$<br>$\alpha(m_Z)$, $\sin^2\theta_W(m_Z)$, $m_\tau$, ($m_b$ or $\frac{m_b}{m_\tau}|_{M_X}$) |
| Outputs: | $B_0$, $\lvert\mu_0\rvert$, $\alpha_s(m_Z)$, ($\frac{m_b}{m_\tau}|_{M_X}$ or $m_b$)<br>$M_1$, $M_2$, masses and mixing angles of gluinos, neutralinos, charginos, squarks, sleptons, and Higgs bosons; $\Omega_\chi h_0^2$, BR($b\to s\gamma$), etc. |

TABLE II. Typical effect of dependence of $\sin^2\theta_W$ on $m_t$ for $m_t^{\rm pole} = 120$, 145, 170 GeV on $\alpha_s(m_Z)$, $\alpha_X$, and $M_X$. For this table we have chosen $m_0 = m_{1/2} = 200$ GeV, $\tan\beta = 5$, $A_0 = 0$, and $\mu > 0$.

| | $m_t^{\rm pole}$(GeV) | | |
|---|---|---|---|
| | 120 | 145 | 170 |
| $\sin^2\theta_W$ | 0.2329 | 0.2322 | 0.2314 |
| $\alpha_s(m_Z)$ | 0.126 | 0.127 | 0.129 |
| $\alpha_X$ | 0.0414 | 0.0413 | 0.0414 |
| $M_X/10^{16}$ GeV | 1.76 | 1.94 | 2.26 |

$m_t^{\rm pole}$, using Eq. (26), for a set of sample input parameters. It is also interesting to note that this dependence of $\sin^2\theta_W$ on the top quark mass leads to a strong dependence of $\alpha_s(m_Z)$ on the top mass as well. For constant $\sin^2\theta_W$, larger values of the top quark mass tend to decrease the value of $\alpha_s(m_Z)$ by about 3% over the allowed range of $m_t$. However, because of the strong dependence of $\sin^2\theta_W$ on $m_t$, the value of $\alpha_s(m_Z)$ actually increases by about 3% over the same range.

In addition to the values of the gauge couplings at $Q = m_Z$, one also needs the Yukawa couplings of the third generation of quarks and leptons at $m_Z$. The mass of the $\tau$ is now very precisely known, $m_\tau = 1776.9 \pm 0.5\,\text{MeV}$ [60]. The mass of the $b$ quark, however, has a larger uncertainty. Following the analyses of Refs. [14,49] we take the central value of $m_b^{\rm pole}(m_b^{\rm pole})$ to be 4.9 GeV. In order to determine $h_b$ and $h_\tau$ at $Q = m_Z$ we run the gauge couplings $\alpha$ and $\alpha_s$ from their experimental values at $Q = m_Z$ down to the $b$- and $\tau$-mass scales using three-loop QCD and two-loop QED RGE's [61]. At the mass thresholds we translate [47] the experimentally measured pole masses to the $\overline{\rm MS}$ scheme and run these masses back up to the $Z$ scale. Similarly we arrive at $h_t(m_Z)$ by running gauge couplings up to the top quark mass threshold and then running $h_t$ back down to $m_Z$.

Now we return to a careful treatment of the threshold corrections in the running of the gauge couplings already mentioned in Sec. II B. In the present analysis all thresholds are handled as an intrinsic part of the numerical routines. Because we determine the (running) mass of each sparticle at the scale $Q = m_i(Q)$ anyway, we can simultaneously change the gauge coupling $\beta$-function coefficients to reflect the coupling or decoupling of this particular state. We have already argued in Sec. II B that the RGE's must be run at two-loops with correct one-loop thresholds, which is what we do. In Table III we demonstrate the importance of both these requirements. Notice in particular that the net effect of the two-loop running is to increase $\alpha_s(m_Z)$ by $\sim 10\%$. Also notice that had we considered proton decay in this analysis, we would have found that the proton lifetime coming from dimension-6 operators increases when using two-loop running instead of one-loop by a factor of $\sim 5$ since $M_X$ has increased by $\sim 50\%$ and the lifetime scales as $M_X^4$.

When running the gauge coupling RGE's we follow the decoupling prescription outlined in Eqs. (3)–(5). However, there are some minor simplifications and ambiguities to consider [40]. First, we decouple all Higgsinos at the common scale $Q = \mu(Q)$, $b$-inos at $Q = M_1(Q)$, $W$-inos at $Q = M_2(Q)$, and the second Higgs doublet at $Q = m_A(Q)$. For the top quark one could either choose to decouple it at its mass threshold, or simply at $m_Z$; numerically either procedure is essentially equivalent. One other ambiguity in the one-loop RGE's arises for weak isodoublets decoupling from $\beta_2$. Here, because they will always appear in $T_3 = \pm\frac{1}{2}$ pairs in the loops, we only couple the doublet when the scale is larger than the heavier member of the doublet. This can be seen in Eq. (4). At two loops many such ambiguities arise; however, the effects of individual thresholds in the two-loop RGE's are of higher order and can be safely ignored. Therefore we have changed the two-loop coefficients with a single threshold at $Q = m_{1/2}$ above which we use MSSM two-loop coefficients and below which we use those of a two-Higgs doublet SM. We have checked that dramatically varying the scale $Q$ at which the two-loop coefficients are changed from their SM values to the SUSY ones causes typically an $\sim 2\%$ variation in $\alpha_s(m_Z)$ [$\Delta\alpha_s(m_Z) \lesssim 0.002$]. Thus, we feel that our approximation is justified.

It is important to reiterate that we only decouple states in the running of the gauge couplings. This decoupling is necessary in order to determine realistic values for $\alpha_s(m_Z)$. However, were one to decouple states, say, from the soft mass RGE's, then one would need to reconsider the effective Lagrangian and matching conditions at scales below each threshold, where this Lagrangian, its couplings, and their RGE's would no longer be supersymmetric. By minimizing the one-loop effective potential with all states included down to $Q = m_Z$, we effectively include the contributions from their decoupling. Therefore, in all RGE's other than those of the gauge couplings, we have left all states coupled down to $Q = m_Z$ where we minimize the full one-loop effective potential.

Once the boundary conditions at the GUT scale have been set we run the RGE's of the system in order to determine the value of a parameter at any scale $Q$ below $M_X$. The RGE's for minimal SUSY have appeared in numerous places in the literature, including Refs. [43,62]; we follow essentially the conventions of Ref. [62]. Although various authors have offered semianalytic, approximate solutions to the full set of RGE's under various simplifying assumptions, a full analysis of the parameter space requires that the RGE's be solved numerically, given the level of accuracy that we are maintaining.

TABLE III. Typical effect of dependence of $\alpha_s(m_Z)$, $\alpha_X$, and $M_X$ on one-loop running, two-loop running, and two-loop running with the "effective scale" of Eq. (7) for two spectra of SUSY particles. For case 1 we take $m_0 = m_{1/2} = 100\,\text{GeV}$, $\tan\beta = 5$, $m_t^{\rm pole} = 145\,\text{GeV}$, $A_0 = 0$, and $\mu > 0$. Case 2 is the same as case 1 except $m_0 = m_{1/2} = 1\,\text{TeV}$. For the two cases, $M_{\rm SUSY}^{\rm eff} = 13,177\,\text{GeV}$, respectively. Recall that $M_{\rm SUSY}^{\rm eff}$ is defined to reproduce the one-loop value for $\alpha_s(m_Z)$. We calculate the values of $\alpha_X$ and $M_X$ for $M_{\rm SUSY}^{\rm eff}$ as in Ref. [17].

| | Example 1 | | | Example 2 | | |
|---|---|---|---|---|---|---|
| | One loop | Two loop | $M_{\rm SUSY}^{\rm eff}$ | One loop | Two loop | $M_{\rm SUSY}^{\rm eff}$ |
| $\alpha_s(m_Z)$ | 0.117 | 0.129 | 0.117 + 2 loops | 0.111 | 0.121 | 0.111 + 2 loops |
| $\alpha_X$ | 0.0404 | 0.0422 | 0.0456 | 0.0380 | 0.0394 | 0.0417 |
| $M_X/10^{16}\,\text{GeV}$ | 1.50 | 2.37 | 4.30 | 0.79 | 1.18 | 1.81 |

The procedure that we adopt essentially consists of repeatedly running the RGE's between $Q = m_Z$ and $Q = M_X$ until a self-consistent solution has been isolated.

In the first iteration for any given set of input parameters, an approximate SUSY spectrum is generated. The six RGE's of the gauge and Yukawa couplings, are simultaneously run up first to the GUT scale using the method of Runge-Kutta. We run the gauge couplings above the $Z$ scale in the SUSY-consistent dimensional reduction ($\overline{\text{DR}}$) scheme as opposed to the $\overline{\text{MS}}$ scheme which we used below the $Z$ scale, and so we impose the matching condition for the two schemes at $Q = m_Z$ [40]. (The net effect of the scheme change is less than 1% however [10,40].) Running up, we define $M_X$ as that point at which $\alpha_1(M_X) = \alpha_2(M_X) \equiv \alpha_X$. We then set $\alpha_s(M_X) = \alpha_X$. All scalar masses are set equal to $m_0$, all gaugino masses to $m_{1/2}$, and all $A$ parameters to $A_0$.

The RGE's for all the 26 running parameters (the gauge and Yukawa couplings, the $\mu$-parameter, and the soft mass terms) are run back from $Q = M_X$ down to $Q = m_Z$. For the gauge couplings, two-loop RGE's with one-loop thresholds are used throughout, while two-loop RGE's without thresholds are used for the Yukawa couplings. Only the one-loop RGE's are used for the SUSY soft mass parameters. Along the way we decouple any particle $i$ in the spectrum from the gauge coupling RGE's at the scale $Q = m_i(Q)$. As described earlier, thresholds in the one-loop gauge coupling RGE's are used to account for the effects of the decoupling of the various sparticles at masses greater than $m_Z$. At $Q = m_Z$ a value for $\alpha_s(m_Z)$ is found consistent with unification assumptions, and the full one-loop effective scalar potential is minimized in order to determine the values of $\mu^2(m_Z)$ and $B(m_Z)$ that produce proper EWSB. On the next iteration when the entire set of parameters is again run up from $Q = m_Z$ to a newly determined $M_X$, the parameters $\mu$ and $B$ will also run, providing their corresponding values at the GUT scale.

This entire procedure is repeated several times, terminating only after changes in the solutions to the RGE's are small compared to the values themselves or to the experimental errors, whichever are relevant. Each iteration provides a more precise spectrum of sparticles, which in turn provides more precise running of the gauge and Yukawa couplings. We find that the whole procedure is extremely stable, usually converging to a solution in just a few iterations.

In Fig. 3 we give an example of the running of various sparticle masses from the GUT scale down to the electroweak scale. Notice that the mass of the Higgs boson that couples to the top quark is driven imaginary (i.e., its mass squared is driven negative) at scales $\sim 1$ TeV, signaling the onset of EWSB. This is shown in the plot as the mass itself going "negative" for convenience of presentation.

When the program has isolated a solution we have as our output all sparticle masses and mixings valid to one loop, Higgs boson masses which include all third generation contributions to the one-loop radiative corrections [63], $\alpha_s(m_Z)$, $\alpha_X$, and $M_X$ valid to two-loops, and the GUT-scale parameters $B_0$ and $\mu_0$.

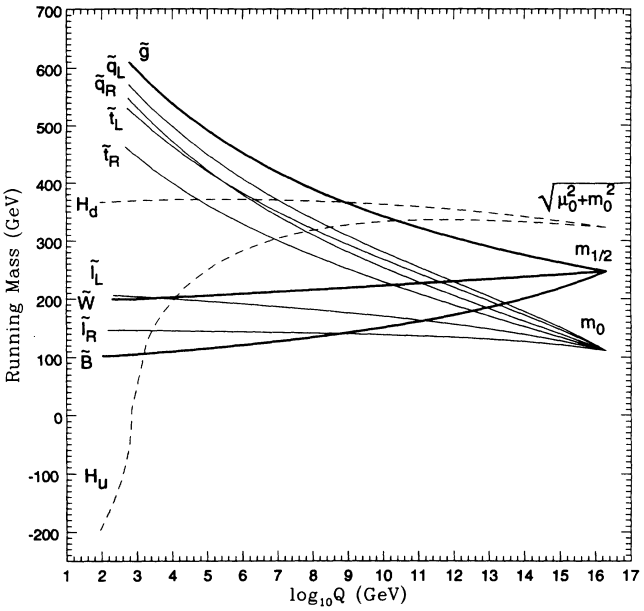


FIG. 3. The running of the sparticle masses from the GUT scale to the electroweak scale, for a sample set of input parameters (see "Solution 3" in Table VIII later in this paper). The bold lines are the three soft gaugino masses $m_{\tilde{g}}$, $M_2$ (labeled $\widetilde{W}$), and $M_1$ (labeled $\widetilde{B}$). The light solid lines are the squark ($\tilde{q}_L$, $\tilde{q}_R$, $\tilde{t}_L$, $\tilde{t}_R$) and slepton ($\tilde{l}_L$, $\tilde{l}_R$) soft masses, where we ignore $D$-term contributions and the mixing of the stops for this figure. Finally, the dashed lines represent the soft Higgs boson masses, $m_1$ and $m_2$ [see Eq. (10)], labeled by $H_d$ and $H_u$. The onset of EWSB is signaled by $m_2^2$ going negative, which is shown on the plot as $m_2$ going negative for convenience.

## VII. CONSTRAINTS

In applying the numerical procedure described in the previous section we have required the gauge coupling to unify, and from the input values of $\alpha$, Eq. (25), and $\sin^2\theta_W$, Eq. (26), obtained a range of $\alpha_s(m_Z)$ as a function of independent parameters. We have also demanded proper EWSB yielding the experimentally measured value of $m_Z$. We have parametrized the many mass parameters of the MSSM in the usual way, assuming common gaugino and scalar masses and the $A$ parameters, Eqs. (18), (19), and (20), as implied by minimal SUGRA. Before we present our results in the next section, we now list and briefly elaborate on several other constraints that we will impose on the output of our numerical analysis. As we explained in Sec. III we do not impose the condition $m_b = m_\tau$ at the GUT scale because the resulting bottom quark mass is likely to be very sensitive to the threshold corrections at $M_X$, which we cannot include without selecting a specific GUT model. Without such corrections we obtain the values of $m_b^{\text{pole}}$ about 20% above the current experimental range, except for very large $m_t$.

### A. Limits from experimental searches

LEP experiments have placed lower limits on the chargino mass of about 47 GeV, and on the charged slep-

ton, sneutrino, and squark masses of about 43 GeV [64]. The lightest top squark mass bound is dependent on the left-right top squark mixing, which can reduce its coupling to the $Z$ boson. DELPHI [65] has excluded $m_{\tilde{t}_1}$ below about 45 GeV, except for a rather tiny range of the mixing angle which allows $m_{\tilde{t}_1} > 37\,\mathrm{GeV}$.

Placing an experimental lower limit on the masses of the Higgs bosons is in principle more complicated since either $h$ or $A$, or both, can be light, and because of potentially sizable radiative corrections to their masses due to the heavy top quark. Assuming reasonable ranges of value for $m_t$, $m_{\tilde{t}}$, and $\tan\beta > 1$ the bounds $m_h > 44\,\mathrm{GeV}$ and $m_A > 21\,\mathrm{GeV}$ have been derived by ALEPH [64]. Other LEP experiments obtained similar limits. However, once we impose the unification and EWSB conditions, we find that $h$ couplings are very SM-like [$\sin^2(\beta-\alpha) \approx 1$] so that in practice the LEP limit of about 62 GeV [66] for the SM Higgs boson applies to $h$ as well. For related reasons, $A$ is always heavier than $m_Z$ for us, so that the LEP limits on $A$ place no serious bound.

Lower mass bounds on the squarks and gluino have been reported at 126 GeV and 141 GeV [67], respectively, assuming no cascade decays. By including cascade decays one can reduce those bounds by some 20 GeV or more [68]. The squark masses could become even as light as allowed by LEP if $m_{\tilde{g}}$ becomes large. All squark and gluino bounds are very model dependent.

LEP experiments alone cannot place a lower bound on the mass of the lightest neutralino because its coupling to the $Z$ can be strongly suppressed and it is not directly detectable. It is only by combining LEP direct chargino and neutralino searches with indirect ($Z$ line shape) searches and with the lower bound on $m_{\tilde{g}}$ from the Tevatron [via Eq. (22)] that a bound $m_\chi \gtrsim 18\,\mathrm{GeV}$ [69] can be derived for any $\tan\beta > 1$.

### B. $b \to s\gamma$

Recently, CLEO has reported an upper bound on $B(b \to s\gamma) < 5.4 \times 10^{-4}$ [70]. A central value ($3.5 \times 10^{-4}$) and a lower limit ($1.5 \times 10^{-4}$) is obtained from the detection of $B \to K^*\gamma$ [70] and assuming that the ratio of $B(B \to K^*\gamma)$ to $B(b \to s\gamma)$ is 15% [71]. In addition to the SM contribution, SUSY allows for one-loop diagrams with the exchange of the charged Higgs boson and the charginos and neutralinos [72–76]. We calculate $B(b \to s\gamma)$ with the formulas of Ref. [73]. These use QCD corrections that are less accurate than has been done for the SM case recently [77]. We are in the process of combining our results with those of Ref. [77] to obtain improved QCD corrected CMSSM predictions.

In Sec. VIII we will apply the *upper* bound $B(b \to s\gamma) < 5.4 \times 10^{-4}$. In Sec. IX D we will present the *predictions* of CMSSM for $B(b \to s\gamma)$ and show that the range favored by CMSSM naturally falls into the range resulting from the CLEO analysis. We will also show that the claims [74] of a stringent bound on the charged Higgs boson mass are too strong in the CMSSM.

### C. Color and charge breaking

In the MSSM the Higgs potential automatically conserves color and charge but the same is not necessarily true with the full scalar potential. If one wishes to determine the form of the global minima, one must numerically search for all local minima of the full scalar potential, including the charged and colored states, and determine the broken symmetries associated with each. This is outside the realm of the study we are reporting on here and so we only demand that the (mass)$^2$ of any charged or colored mass eigenstate remains positive. In fact, this will be an important constraint in some regions of the parameter space (especially for large $A_0$) where the lighter top squark (mass)$^2$ can become negative due to a large $\tilde{t}_L$-$\tilde{t}_R$ mass splitting.

It is sometimes stated in the literature that a necessary condition for avoiding color breaking [78] is to demand that $|A_0|/m_0 < 3$. However, as pointed out by Ref. [79], this condition is really neither sufficient nor necessary. Therefore, we consider values for $|A_0|/m_0$ slightly larger than three. Knowing that minimization of the full scalar potential may lead to color- or charge-breaking minima for such large ratios, the constraints coming from our analysis can only be strengthened by a full treatment of this color and/or charge breaking.

Nonetheless, as will be discussed in the next section, $m^2_{\tilde{t}_1}$ never goes negative for smaller values of $A_0$ ($|A_0|/m_0 \lesssim 1$) simply because the $\tilde{t}_L - \tilde{t}_R$ mass splitting is dominated by $A_0$.

### D. Lightest neutralino as the LSP and dark matter candidate

In the absence of $R$-parity breaking the LSP remains absolutely stable. Depending on its nature it may have to face potentially tight cosmological constraints which we will discuss below. It will also have important experimental consequences for possible SUSY signatures. In the MSSM, any of the superpartners could in principle be the LSP because their masses are virtually unrelated. In the CMSSM the picture is very different: the masses of the superpartners are highly correlated. These relations are determined by the assumptions of Eqs. (18)–(20) and lead to a hierarchy among the sparticle masses. As a result there are very few possible candidates for the LSP. Typically it is the lightest of the four neutralinos that comes out to be the LSP, and it has been usually favored in most phenomenological and cosmological studies. However, for some combinations of parameters some other sparticle, such as the top squark, the stau, or the sneutrino can be the LSP. Each of the resulting types of the LSP must meet cosmological constraints.

As we have already discussed in Sec. VII C, due to a large mass splitting in the $\tilde{t}_L - \tilde{t}_R$ sector, the lighter top squark mass eigenstate ($\tilde{t}_1$) may in certain cases become very light. In fact, one may even encounter $m^2_{\tilde{t}_1} < 0$. On the other hand, the lighter stau sometimes becomes the LSP. As concerns the sneutrino, after we apply experi-

mental limits and reject unphysical cases, we never find it to be the LSP.

#### 1. Neutral LSP

It would be difficult to imagine that an electrically charged or colored massive stable particle, such as the stau or the top squark, could exist in any meaningful amount in the Universe [80,81]. If it did, it would interact with photons and become detectable. It would also interact with ordinary matter and dissipate its energy thus falling toward the cores of galaxies. It would form stable isotopes of chemical elements. For these and other reasons, only electrically neutral and colorless particles are believed to be able to exist in the Universe in the form of dark matter [80,81]. We will therefore reject those regions of the parameter space where either the top squark or stau are the LSP. In the rest of the study we will only deal with the neutralino as the LSP.

#### 2. Neutralino relic abundance

Any stable (or metastable) species predicted by theory would contribute to the total mass energy of the Universe. A relic abundance is usually expressed as the ratio of the particle's relic density to the critical density $\rho_{\rm crit} \equiv 3H_0^2/8\pi G = 1.9 \times 10^{-29}(h_0^2)g/{\rm cm}^3$,

$$\Omega_\chi \equiv \frac{\rho_\chi}{\rho_{\rm crit}}, \tag{27}$$

where $\rho_{\rm crit}$ corresponds to the flat Universe and $h_0$ is the present value of the Hubble parameter $H_0$ in units 100 km/s Mpc ($h_0 = \frac{H_0}{100\ {\rm km/s\,Mpc}}$). Current estimates only require $0.4 \lesssim h_0 \lesssim 1$ [80].

A supersymmetric LSP, being stable, cannot decay on its own but can pair annihilate into ordinary matter. Its relic abundance $\Omega_\chi h_0^2$ is inversely proportional to the LSP annihilation cross section and thus depends on the masses and couplings of the final and exchanged particles. In calculating the neutralino relic abundance we include *all* the relevant LSP pair annihilation channels into ordinary matter that are kinematically allowed. Lighter $\chi$'s annihilate only (except for rare radiative processes) into pairs of ordinary fermions via the exchange of the $Z$ and the Higgs bosons, and the respective sfermions (We do not include final-state gluons since the relevant cross section has been shown to be relatively insignificant in calculating the relic abundance in the early Universe [82].) As $m_\chi$ grows new final states open up: pairs of Higgs bosons, gauge and Higgs bosons, $ZZ$ and $WW$, and $t\bar{t}$, all of which we include in our analysis. The actual procedure of calculating the relic abundance is quite involved and has been adequately described elsewhere (see, e.g., Refs. [80,83,84]). We use the technique developed in Ref. [83] which allows for a reliable (except near poles and thresholds) computation of the thermally averaged annihilation cross section in the nonrelativistic limit and integration of the Boltzmann equation. This technique is applicable to calculating the relic abundance in most of the parameter space.

As was first pointed out in Ref. [85], and rediscovered and elaborated by Griest and Seckel [86], special care must be applied to calculating the relic abundance near the poles of exchanged particles and when new mass thresholds become kinematically accessible. In particular, proper treatment of narrow poles has been provided in Refs. [23,28,87] and it was shown that standard techniques may lead to errors reaching even 2 or 3 orders of magnitude in the vicinity of a pole. This is especially true for the lightest Higgs boson because the width of $h$ is extremely narrow, and also near the $Z$-boson pole where the effective coupling is somewhat stronger. We find that the regions of the parameter space where our (standard) calculation fails are relatively small albeit non-negligible. In presenting our results in the next section we will therefore point out those regions where the presented results for the neutralino relic abundance are not trustworthy. It has been argued in Refs. [23,28] that the regions where the $h$ and $Z$ poles dominate are favored by current limits on the proton decay in the SUSY SU(5) model. Since we do not select SU(5) as a GUT symmetry, nor view it as particularly attractive, at this point we choose not to pay special attention to calculating the relic abundance near the poles. We will comment on these effects in discussing results.

#### 3. Age of the Universe

In the standard cosmological model the age of the Universe depends on the total relic abundance $\Omega_{\rm tot}$. Conversely, estimates of the Universe's age place a constraint on $\Omega_\chi < \Omega_{\rm tot}$. A conservative assumption that the Universe is at least 10 billion years old (and $h_0 > 0.4$) leads to [80]

$$\Omega_\chi h_0^2 \lesssim 1. \tag{28}$$

If the age of the Universe is at least 15 billion years, as many currently believe, then the bound (28) becomes much stronger: $\Omega_\chi h_0^2 \lesssim 0.25$ [80]. This is because an older Universe corresponds to a smaller expansion rate $h_0$. No stable particle can contribute to $\Omega_{\rm tot}$ more than is allowed by at least the bound (28) without distorting the Universe's evolution. This constraint is independent of the nature (or even existence) of dark matter (DM) in the Universe. The bound of Eq. (28) must be satisfied for any choice of free parameters and, as we will see in the next section, it provides a very strong constraint on the parameter space.

#### 4. Dark matter

The visible matter in the Universe accounts for about 1% of the critical density. There is at present abundant evidence for the existence of significant amounts of dark matter in galactic halos ($\Omega \sim 0.1$) and in clusters of galaxies ($\Omega \gtrsim 0.2$) [80]. Big bang nucleosynthesis (BBN) constrains the allowed range of baryonic matter in the

Universe to the range $0.02 < \Omega_B < 0.11$ [88] (and more recently $\Omega_B \approx 0.05$; see the second paper of Ref. [88]). The value $\Omega_{\rm tot} = 1$ is strongly preferred by theory since it is predicted by the models of cosmic inflation and is the only stable value for Friedmann-Robertson-Walker models. Values of $\Omega_{\rm tot}$ larger than those "directly" observed are also strongly supported by most models of large structure formation. This, along with estimates given above, implies that (i) most baryonic matter in the Universe is invisible to us and (ii) already in halos of galaxies one might need a substantial amount of nonbaryonic DM. If $\Omega_{\rm tot} = 1$ then most (about 95%) of the matter in the Universe is nonbaryonic and dark. Current estimates of $h_0$ give, for $\Omega_{\rm tot} = 1$, $0.5 \lesssim h_0 \lesssim 0.7$ (the upper bound coming from assuming the age of the Universe above 10 billion years), in which case one expects $0.25 \lesssim \Omega_{\rm tot} h_0^2 \lesssim 0.5$. While it is not unlikely that the galactic halos consist to a large degree of various extended Massive Compact Halo Objects[1] (MACHO's) (such as Jupiter's, brown dwarfs, etc.), it would be very hard to believe that such objects could fill out the whole Universe without condensing into galaxies. This, along with the bound on baryonic matter provided by BBN has led to a widely accepted hypothesis that the bulk of DM in the Universe consists of some kind of weakly interacting massive particles (WIMP's). The relic abundance of the lightest neutralino $\chi$ (most naturally of $b$-ino-type [91]) often comes out to be in the desired range thus making it one of the best candidates for DM [92]. Being nonrelativistic, it falls into the category of cold DM (CDM) which has been favored by models of large structure formation, in contrast with hot DM (HDM), such as light neutrinos. In a purely CDM scenario one assumes that the LSP dominates the mass of the Universe, leading roughly to

$$0.25 \lesssim \Omega_\chi h_0^2 \lesssim 0.5 \quad \text{(CDM)}. \tag{29}$$

Motivated by the theoretical expectation that SUSY GUT theories will also have massive neutrinos, and phenomenologically by the result that [in the aftermath of the Cosmic Background Explorer (COBE)] a mixed CDM+HDM picture (MDM) seems to fit the astrophysical data better [93] than the pure CDM model, we also consider a smaller value of $\Omega_\chi$. In the mixed scenario one assumes about 30% of HDM (such as light neutrinos with $m_\nu \simeq 6\,\text{eV}$) and about 65% of CDM ($b$-ino-like neutralino), with baryons contributing the remaining 5%. In this case the favored range for $\Omega_\chi h_0^2$ is approximately given by

$$0.16 \lesssim \Omega_\chi h_0^2 \lesssim 0.33 \qquad \text{(MDM)}. \tag{30}$$

[1]Recently, a few candidate events for MACHO's with mass $\sim 0.1 M_\odot$ have been reported by microlensing experiments [89] thus implying that some sort of small stars comprise a significant component of the halo of our Galaxy. We note that, with the present efficiency, this discovery does not, and will not for the next several years, be able to eliminate other kinds of candidates for the dark matter [90].

[Strictly speaking, in the MSSM the neutrinos are massless and as such could not constitute interesting HDM. But it is straightforward to extend the model to include right-handed neutrinos (and their sneutrino partners) and give them mass terms. We do not expect this extension to sizably modify the running of all the other parameters of the MSSM. It is with this implicit assumption that we will apply the range given by (30) in analyzing the resulting implications for SUSY searches.]

Both scenarios assume a significant amount of LSP DM. The sneutrino, an early candidate [94] for DM, is now strongly disfavored. After the LEP experiments have placed a limit on its mass $m_{\tilde\nu} > 43\,\text{GeV}$, its relic abundance can now only be negligibly small ($\Omega_{\tilde\nu} \sim 10^{-3}$). We thus find it remarkable that we never find the sneutrino to be the LSP. Had it been the LSP instead of the neutralino in most of the parameter space then the CMSSM would not have provided a viable candidate for the DM problem.

## VIII. RESULTS

We now proceed to discuss the numerical results obtained by using the procedure for generating low-energy output described in Sec. VI. We will first analyze the impact of several experimental, theoretical, and cosmological constraints on the parameter space. Next, we will focus on the region of the model's parameter space consistent with all the adopted constraints and discuss the resulting consequences for the value of $\alpha_s(m_Z)$, the mass spectra of the Higgs boson and supersymmetric particles, and other predictions.

### A. Effect of constraints

We have generated a large set of solutions for a broad range of input parameters. We explore wide ranges of both $m_{1/2}$ and $m_0$, each between 50 GeV and approximately 3 TeV in 22 logarithmic steps, for discrete values of $m_t^{\rm pole} = 120, 145, 170\,\text{GeV}$, $\tan\beta = 1.1$, 1.5, 3, 5, 10, 15, 20, 30, 40, 50, and $A_0/m_0$ between $-3.5$ and 3.5 in increments of 0.5. We also consider both signs of $\mu_0$.

The choice of a logarithmic scale for $m_{1/2}$ and $m_0$ is technically motivated. We are interested most particularly in lower values of the soft masses where the fine-tuning reintroduced by SUSY breaking is smallest and where we can expect currently planned facilities to best probe the parameter space. Likewise, the difference between $\tan\beta = 1.5$ and $\tan\beta = 3$ is more significant than that between $\tan\beta = 40$ and $\tan\beta = 50$. Lastly, the scaling of $A_0$ with $m_0$ is motivated by SUGRA, with bounds motivated by the fear of color-breaking global minima for large $A_0$.

Mass scales above 1 TeV may seem unnatural but we also wish to explore the asymptotic behavior of our results. For the top mass, the three representative values, $m_t^{\rm pole} = 120$, 145, 170 GeV, help us sample the whole region of top mass preferred by the analysis of the LEP data. We pay particular attention to the middle value,

$m_t^{\rm pole} = 145\,{\rm GeV}$, as being favored by LEP (when one includes a light Higgs boson as required by SUSY) and perhaps by the cross section for candidates from the Tevatron. For $\tan\beta$ we sample a spectrum of values over the entire region consistent with the Yukawa couplings of the third generation remaining perturbative all the way up to the scale of unification. Values of $\tan\beta \lesssim 1.1$ become difficult to study due to a dangerous cancellation in Eq. (16) and because we are close to the perturbative limit of the top Yukawa couplings, values of $\tan\beta \gtrsim 50$ become difficult because the bottom and $\tau$ Yukawa couplings are likewise close to their perturbative limits.

Overall, we explore well over 100 000 combinations, each representing a unique point in the space of $m_t^{\rm pole}$, $\tan\beta$, $m_{1/2}$, $m_0$, $A_0$, and $\mathrm{sgn}\,\mu_0$. We present some representative solutions in Figs. 4–9 in the plane $(m_{1/2}, m_0)$. In this section we focus mostly on the case $m_t^{\rm pole} = 145\,{\rm GeV}$ and several representative choices of $\tan\beta$ and $A_0$. We will also display the dependence on $m_t^{\rm pole}$ below.

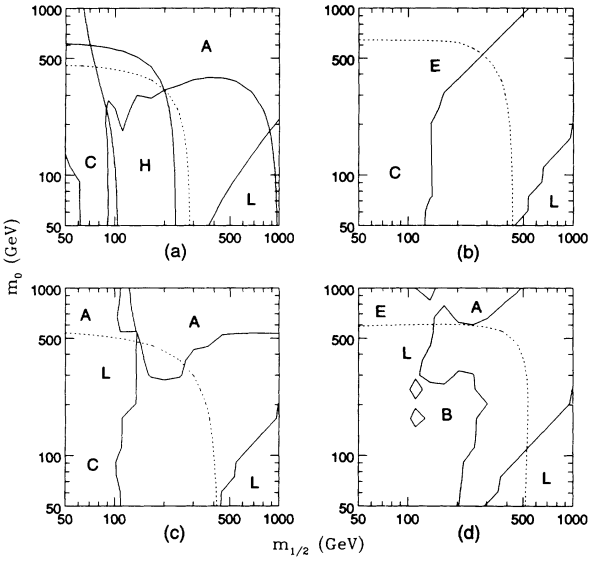


FIG. 4. Plots of the $(m_{1/2}, m_0)$ plane showing regions excluded by lack of EWSB (labeled E), neutralino not being the LSP (L), the age of the Universe less than 10 billion years (A), $m_{\chi_1^\pm} < 47\,{\rm GeV}$ (C), $B(b \to s\gamma) > 5.4 \times 10^{-4}$ (B), and SM-like lightest Higgs boson mass $m_h < 60\,{\rm GeV}$ (H). We take $m_t^{\rm pole} = 145\,{\rm GeV}$, $\mathrm{sgn}\,\mu_0 = -1$, and several representative choices of $\tan\beta$ and $A_0$. In window (a) $\tan\beta = 1.5$, $A_0/m_0 = 0$, in (b) $\tan\beta = 5$, $A_0/m_0 = 0$, in (c) $\tan\beta = 5$, $A_0/m_0 = -2$, and in (d) $\tan\beta = 20$, $A_0/m_0 = 3$. In window (a), the regions excluded by each criterion are identified separately, while for windows (b)–(d) only the total envelope is shown. For each case, the limit imposed by our fine-tuning constraint $f \leq 50$ is shown as a dotted line, disfavoring regions above and to the right of the line. Notice the importance of combining several different criteria in constraining the parameter space. (Only the most limiting constraints are marked.) Note that in window (a) the $(m_{1/2}, m_0)$ allowed region is bounded entirely by the physics constraints, without a fine-tuning constraint, though $m_{1/2}$ extends to larger values than allowed by this constraint (see also Fig. 7).

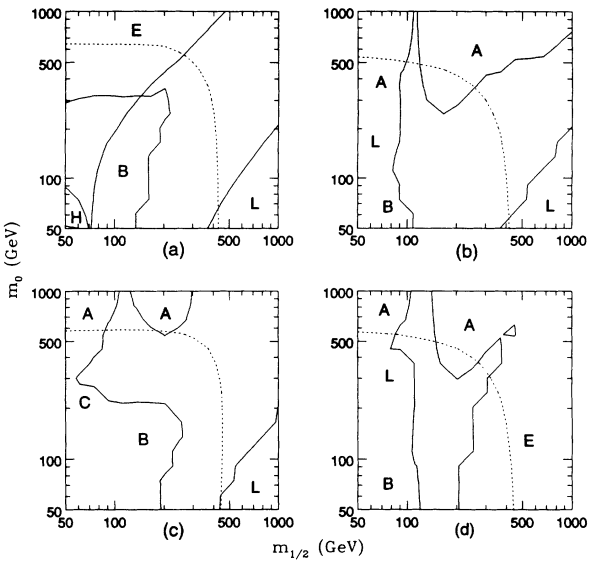


FIG. 5. Same as in Fig. 4 but for $m_t^{\rm pole} = 145\,{\rm GeV}$, $\mathrm{sgn}\,\mu_0 = +1$, and in (a) $\tan\beta = 5$, $A_0/m_0 = 0$, in (b) $\tan\beta = 5$, $A_0/m_0 = -2$, in (c) $\tan\beta = 5$, $A_0/m_0 = 2$, and in (d) $\tan\beta = 10$, $A_0/m_0 = -2$.

### *1. Constraints from experimental searches*

As we can see from Figs. 4–9, at present the regions of the plane $(m_{1/2}, m_0)$ excluded by direct and indirect searches for SUSY at LEP and Fermilab (see Sec. VII A) are limited at best. The strongest direct constraints on $m_{1/2}$ come from $m_{\chi_1^\pm} > 47\,{\rm GeV}$ and/or the Collider Detector at Fermilab (CDF) gluino mass bound. Assuming $m_{\tilde{g}} > 141\,{\rm GeV}$, and neglecting cascade decays, corre-

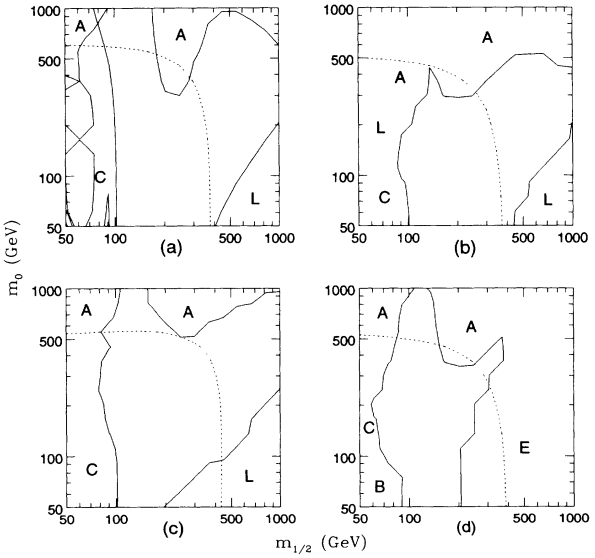


FIG. 6. Same as in Fig. 4 but now with $m_t^{\rm pole} = 170\,{\rm GeV}$, $\mathrm{sgn}\,\mu_0 = -1$ and (a) $\tan\beta = 5$, $A_0/m_0 = 0$, in (b) $\tan\beta = 5$, $A_0/m_0 = -2$, and in (c) $\tan\beta = 20$, $A_0/m_0 = 3$. In (d) we take $\tan\beta = 10$, $A_0/m_0 = -2$, and $\mathrm{sgn}\,\mu_0 = +1$. Generally, for $m_t^{\rm pole} = 170\,{\rm GeV}$ we find both $m_{1/2}$ and $m_0$ bounded from above by physical constraints.

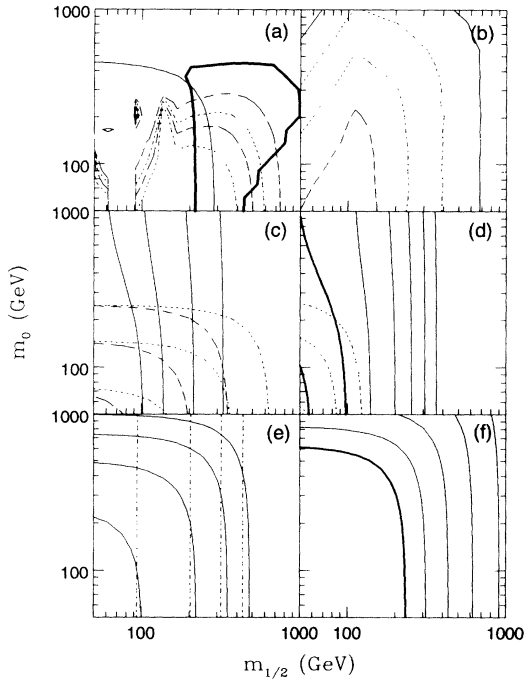


FIG. 7. The $(m_{1/2}, m_0)$ plane displayed for $m_t^{\rm pole}$ =145 GeV, $\tan\beta = 1.5$, $A_0/m_0 = 0$, and $\mathrm{sgn}\,\mu_0 = -1$. We show in window (a) the region allowed by all constraints (dark solid) [compare Fig. 4(a)]. We also mark the bands favored by the CDM (between dashed lines) and MDM scenarios (between dotted lines) and the limit imposed by our fine-tuning constraint $f \leq 50$ (light solid). We also plot in window (b) $\alpha_s(m_Z)$ at 0.120 through 0.132 in steps of 0.002, decreasing for larger $(m_{1/2}, m_0)$ with 0.120 solid, 0.126 dashed and any others dotted; in (c) $m_{\chi_1^\pm}$ (solid), $m_{\tilde{l}_L}$ (dashes), and $m_{\tilde{l}_R}$ (dots) at 45, 80, 150, and 250 GeV. (In the two latter cases only the last three values occur in the graph.) In window (d) we plot $m_\chi$ (solid) at 18 (thick), 45, 75, 100, 125, and 150 GeV. We also display the gaugino purity ($Z_{11}^2 + Z_{12}^2$, dots) of 0.8 and 0.9 increasing to the right. In window (e) we plot $m_{\tilde{g}}$ (dots) and average $m_{\tilde{q}}$ (other than $m_{\tilde{t}}$) (solid) at 250, 500, 750, and 1000 GeV, and in window (f) $m_h$ between 60 and 130 GeV in 5 GeV intervals (60, 120 dark solid, 90 dark dashes, all others light solid). Mass contours in each window increase with increasing $(m_{1/2}, m_0)$.

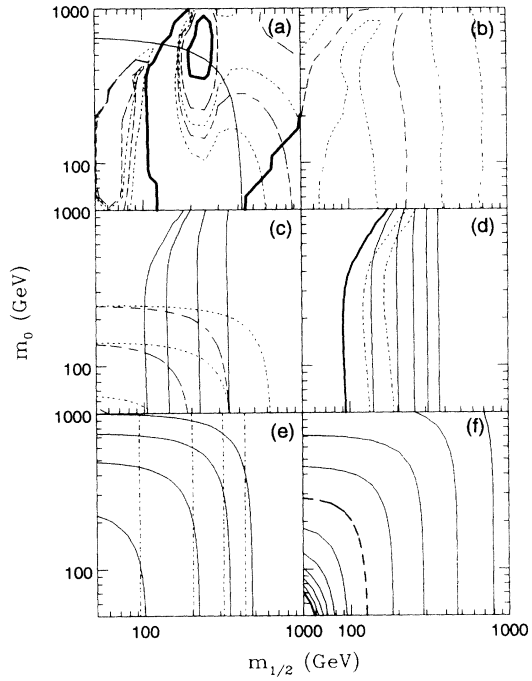


FIG. 8. Same as in Fig. 7 but for $m_t^{\rm pole} = 145$ GeV, $\tan\beta = 5$, $A_0/m_0 = -1$, and $\mathrm{sgn}\,\mu_0 = -1$. Window (a) also demonstrates the importance of including final states other than $f\bar{f}$ (in this case $hh$) in the calculation of $\Omega_\chi h_0^2$ (see Sec. VIII A 7).

sponds roughly to $m_{1/2} \gtrsim 50$ GeV. On the other hand, in general there is no lower bound on $m_0$ except for small $m_{1/2}$ from the experimental lower bounds on the slepton and squark masses. As an example, we present in Fig. 10 the region of the plane $(m_{1/2}, m_0)$ ruled out by the LEP bound $m_{\tilde{\nu}} > 43$ GeV for two extreme values of $\tan\beta$ and by $m_{\tilde{g}} > 141$ GeV. For $m_{1/2} \gg m_0$ the exact value of $m_0$ becomes unimportant, as $m_{1/2}$ will come to dominate the values of all masses and will dictate how EWSB occurs. Although for the major portions of this study we have taken $m_0 \geq 50$ GeV, we have explored the regions of much lower $m_0$ and found nothing to change our conclusions as reported in Secs. VIII and IX.

In addition, we find some regions where the lighter top squark mass becomes smaller than the current ex-

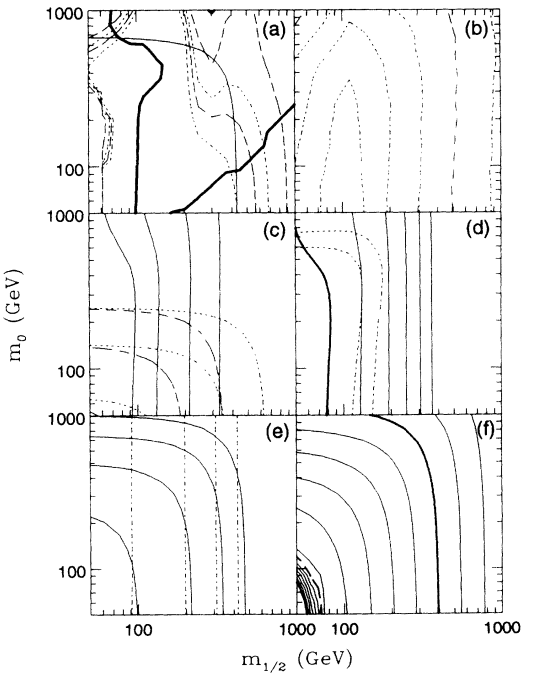


FIG. 9. Same as in Fig. 7 but for $m_t^{\rm pole} = 170$ GeV, $\tan\beta = 20$, $A_0/m_0 = 1$, and $\mathrm{sgn}\,\mu_0 = -1$.

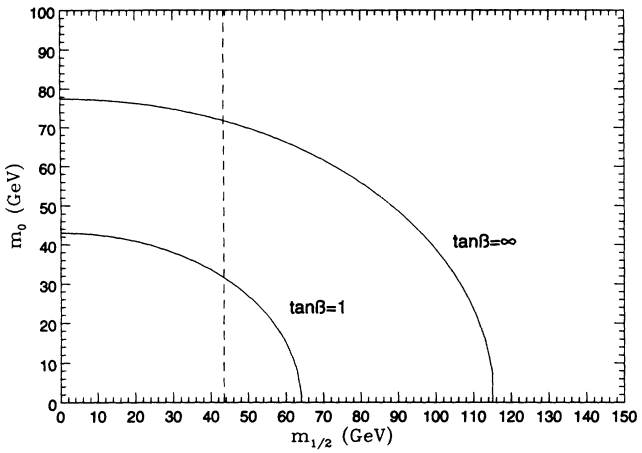


FIG. 10. Region in the $(m_{1/2}, m_0)$ plane ruled out by the LEP bound on the sneutrino mass, $m_{\tilde{\nu}} > 43\,\text{GeV}$, for both small and large $\tan\beta$ and by the CDF bound $m_{\tilde{g}} > 141\,\text{GeV}$ (dashes, cascade decays neglected). The chargino mass bound $m_{\chi_1^\pm} > 47\,\text{GeV}$ often (but not always) leads to additional excluded regions.

perimental bound of about 37 GeV and quickly becomes tachyonic as will be discussed below.

#### 2. Constraints from $b \to s\gamma$

Following Sec. VII B we apply the upper bound $B(b \to s\gamma) < 5.4 \times 10^{-4}$. Interestingly, this bound is often quite important and particularly probes regions of small to moderate $m_{1/2}$ and $m_0$ (Figs. 4–6). As $m_{1/2}$ and $m_0$ grow, $B(\to s\gamma)$ tends to decrease and produce the range of values consistent with CLEO for a wide range of parameters as will be shown in Sec. IX D.

#### 3. Constraints from and on $\alpha_s(m_Z)$

As we can see from Figs. 7–9, the values of $\alpha_s(m_Z)$ resulting from our analysis generally fall into the experimentally allowed range. LEP event shape measurements alone give $\alpha_s(m_Z) = 0.123 \pm 0.006$ [46] while other LEP analyses and low-energy experiments typically yield somewhat lower ranges leading to the world average $\alpha_s(m_Z) = 0.120 \pm 0.006 \pm 0.002$ [46]. (We note, however, that much smaller values of $\alpha_s(m_Z) = 0.107 \pm 0.003$ have been derived in Ref. [50].) We find that $\alpha_s(m_Z)$ generally decreases with growing $m_{1/2}$ and $m_0$, and increases with $m_t$ (see Table II and Sec. VI B). Since small $m_{1/2}$ and $m_0$ are excluded by some experimental constraints (Sec. VIII A 1), we find $\alpha_s(m_Z) \lesssim 0.133$, including the range of very small $m_0$. This is a significant constraint on the entire picture and an important prediction. No interesting upper bound on the plane $(m_{1/2}, m_0)$ can be derived from a lower bound on $\alpha_s(m_Z)$ because $\alpha_s(m_Z)$ decreases very slowly and reaches 0.110 for $m_{1/2}$ and/or $m_0$ in the range of tens of TeV. Keeping SUSY masses below about 1 TeV provides a lower bound $\alpha_s(m_Z) \gtrsim 0.119$, while requiring no fine-tuning ($f \leq 50$, see Sec. VIII A 8) gives $\alpha_s(m_Z) \gtrsim 0.118$. Clearly, as the graphs show, larger values of $\alpha_s(m_Z)$ are favored by low-energy SUSY.

#### 4. Constraints from EWSB

Proper EWSB is not automatic and requiring it places additional strong constraints on the allowed combinations of parameters. As can be seen in Figs. 4–6, this constraint excludes significant regions in the upper left corner ($m_0 \gg m_{1/2}$) of the plane $(m_{1/2}, m_0)$, unless $\tan\beta$ is close to one or $A_0$ is larger and negative. For $\mu_0 > 0$ there are additional regions in the lower right-hand corner ($m_{1/2} \gg m_0$) of the plane $(m_{1/2}, m_0)$ which are also excluded for larger values of $\tan\beta$. This is because the full one-loop effective potential has become unbounded from below in those regions.

#### 5. Constraints from avoiding color breaking

As we said above, sometimes $m_{\tilde{t}_1}^2$ becomes negative. As one can see from the presented figures, this usually happens roughly for $m_0 \gtrsim m_{1/2}$ for rather large values of $|A_0|$ [see symbol "$L$" in these areas in, e.g., Figs. 4(c) and 4(d)]. The regions where $m_{\tilde{t}_1}^2 < 0$ always grow with increasing $\tan\beta$. More specifically, for $\mu_0 < 0$, color breaking occurs when $A_0/m_0 \lesssim -2$ for the whole range of $\tan\beta$, and also to some extent for $A_0/m_0 \gtrsim 3$ and large $\tan\beta$. For the smaller values of $A_0$ $m_{\tilde{t}_1}^2$ is always positive, as expected. For $\mu_0 > 0$ the situation is generally similar for a reversed sign of $A_0$.

#### 6. Constraints from neutralino LSP

As we have argued in Sec. VII D 1, only the lightest neutralino LSP remains a viable candidate for DM. On the other hand, for $m_{1/2} \gg m_0$ we invariably find that the lighter stau is the LSP, and not the neutralino, as one can see in Figs. 4–6. This is expected since the mass of the neutralino $m_\chi$ is given roughly by $m_\chi \simeq M_1 \simeq 0.4 m_{1/2}$. On the other hand, the mass of the lighter stau $\tilde{\tau}_R$ [see Eq. (23)] grows somewhat more slowly with $m_{1/2}$, $m_\chi \sim 0.38 m_{1/2}$. In the region of large $m_{1/2}$ ($\gtrsim 400\,\text{GeV}$) and small $m_0$, $\tilde{\tau}_R$ (and in fact also $\tilde{e}_R$ and $\tilde{\mu}_R$) become lighter than the lightest neutralino. For a fixed $m_{1/2}$, as $m_0$ grows, so does $m_{\tilde{l}_R}$ and $\chi$ becomes the LSP again. Insisting on the neutralino LSP provides a very important constraint on the plane $(m_{1/2}, m_0)$, excluding the region $m_{1/2} \gg m_0$. We note, however, that the regions where $\chi$ is not the LSP correspond to large $m_{\tilde{g}} \gtrsim 1\,\text{TeV}$. Also, we never find the sneutrino to be the LSP: regions of small $m_{1/2}$ where this could take place have been excluded by LEP. We thus find that, in the most interesting region of low-energy SUSY it is the neutralino which is most often the LSP. It is also mostly gaugino-type ($b$-ino-type) – this will be discussed in more detail in Sec. VIII B.

### 7. Constraints from the age of the Universe

For gauginolike $\chi$'s the relic abundance $\Omega_\chi h_0^2$ depends most strongly on the mass of the lightest exchanged sfermion in $\chi\chi \to f\bar{f}$; roughly $\Omega_\chi h_0^2 \propto m_{\tilde{f}}^4/m_\chi^2$ [84]. All sfermion masses grow with increasing $m_0$, and in the case of sleptons much more slowly with $m_{1/2}$, so one expects that the bound $\Omega_\chi h_0^2 \lesssim 1$ which results from requiring that the age of the Universe be at least 10 billion years (see Sec. VII D 3), will be stronger for $m_0$ than for $m_{1/2}$. This is indeed often the case in the remaining regions of the parameter space. The constraint (28) excludes large values of $m_0$ roughly above 1 TeV and often even above a few hundred GeV.

For small $\tan\beta$ ($\tan\beta \approx 1$), the bound (28) is typically much stronger and excludes $m_0 \gtrsim 300\,\text{GeV}$ and $m_{1/2} \gtrsim 1\,\text{TeV}$. As $\tan\beta$ grows slightly to at least moderate values (2 and above), the bound becomes less constraining primarily for $A_0$ around zero or positive allowing for somewhat larger values of $m_0$ and also opening the region $m_0 \sim m_{1/2}$ above 1 TeV. This is because the $s$-channel $Z$ exchange in the process $\chi\chi \to f\bar{f}$ and the $\chi$ pair annihilation into pairs of of light Higgs bosons $h$ become unsuppressed and can reduce the LSP relic abundance. The $Z$-pole effect is clearly visible in the region $m_0 \gg m_{1/2} \simeq 120\,\text{GeV}$ [see, e.g., Figs. 4(a), 4(d), or 5(c)]. But it is also in the region near this pole (and likewise near the $h$ pole) that the exact calculation of the relic abundance becomes difficult. We have highlighted these regions in Fig. 11.

The process $\chi\chi \to hh$ is rarely dominant but it can reduce the relic abundance considerably, especially in the most interesting region of $m_{1/2}$ and $m_0$ in the range of a few hundred GeV for larger values of $\tan\beta$. This is clearly visible in Fig. 8 (see also Fig. 15) where the region to the right of an "island" of $\Omega_\chi h_0^2 > 1$ (large $m_0$ and $m_{1/2} \sim 270\,\text{GeV}$) is again allowed because the final-state $hh$ becomes kinematically allowed. This effect is not present for small $\tan\beta \approx 1$ (compare Fig. 7) because the coupling $h\chi\chi$ vanishes there.

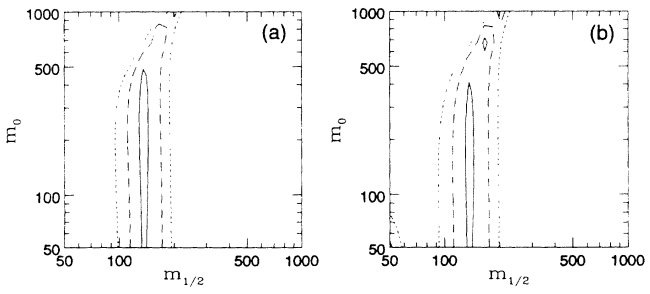


FIG. 11. For the case presented in Fig. 8 ($m_t^{\text{pole}} = 145\,\text{GeV}$, $\tan\beta = 5$, $A_0/m_0 = -1$, and $\text{sgn}\,\mu_0 = -1$) we delineate the regions close to the $Z$ [window (a)] and $h$ [window (b)] poles in the process $\chi\chi \to \bar{f}f$ where our calculation of $\Omega_\chi h_0^2$ cannot be trusted. (The effect of other poles is much less significant.) In window (a) $|m_\chi - m_Z/2| = 25$ (dots), 15 (dashes), and 5 GeV (solid). For $|m_\chi - m_Z/2| \gtrsim 15\,\text{GeV}$ our calculation of $\Omega_\chi h_0^2$ is sufficiently reliable. In window (b) the same for the light Higgs boson $h$.

Overall, the bound $\Omega_\chi h_0^2 \lesssim 1$ typically provides a very stringent constraint on the regions of the parameter space not already excluded by other criteria. It excludes $m_0$ roughly above 1 TeV, except for large $m_{1/2}$ where some SUSY sparticle masses (e.g., $m_{\tilde{g}}$) become very much larger than 1 TeV and are therefore disfavored by the fine-tuning criterion.

### 8. Constraints from requiring no fine-tuning

Finally, it is clear that if SUSY is to replace the SM as an effective theory at the electroweak scale, its mass parameters should not be much larger than $m_Z$. Stated differently, since the combination of $m_1^2$ and $m_2^2$ in Eq. (16) has to give $m_Z^2$, one would have to tune those parameters to a high precision, unless they were broadly within a 1 TeV mass range [95]. This fine-tuning in the potential minimization is a remnant of the fine-tuning exhibited by the full theory. In the full theory, one would parametrize fine-tuning most naturally by $f \equiv \Lambda_{\text{SUSY}}^2/m_Z^2$. Instead, because radiative EWSB connects the SUSY scale to the electroweak scale, we choose to parametrize it by

$$f \equiv |m_1^2|/m_Z^2 \tag{31}$$

which is particularly stable in terms of the running of the RGE's and the minimization of the one-loop effective Higgs potential. (At the tree-level our definition is similar but not identical to the definition of Ross and Roberts [8].) The concept of fine-tuning is somewhat subjective and various authors have used different definitions and criteria.

Figure 12 shows the typical scaling of the fine-tuning

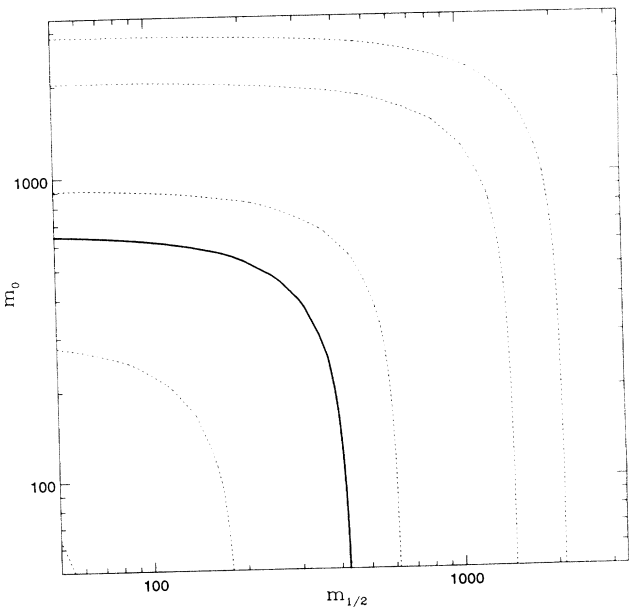


FIG. 12. Scaling behavior of the fine-tuning constant with the SUSY scale. The solid line represents a fine-tuning of 50 which typically corresponds to $m_{\tilde{q}}, m_{\tilde{g}} \lesssim 1\,\text{TeV}$. The other lines are (left to right) for 1, 10, 100, 500, and 1000. Here we have taken $m_t^{\text{pole}} = 145\,\text{GeV}$, $\tan\beta = 5$, $A_0/m_0 = -1$, and $\mu < 0$.

constant with the scale of SUSY for a sample choice of input parameters. In order to exclude regions where large fine-tuning must be invoked, we will later place an upper bound of $f \leq 50$. As we can see from Fig. 13, this criterion typically selects the heaviest sparticle masses below roughly 1 TeV. It is worth stressing however that, for large $\tan\beta$, both $m_{\tilde{g}}$ and $m_{\tilde{q}}$ can be significantly larger without any excessive fine-tuning. Thus simple cuts $m_{\tilde{g}}, m_{\tilde{q}} < 1\,\text{TeV}$ often made in the literature [19,21,22] may in general be too strong.

One might hope that physics constraints would eliminate the need for adding a separate fine-tuning constraint. That indeed is the case for large ranges of parameters, which is very encouraging. For example, for large $m_t^{\text{pole}} = 170\,\text{GeV}$ we find that the constraint $\Omega_\chi h_0^2 < 1$ cannot be satisfied if $m_0$ or $m_{1/2}$ are larger than several hundred GeV. This is also true for smaller $m_t^{\text{pole}}$ if $\tan\beta$ is close to one. In general much larger $m_0$ and $m_{1/2}$ become allowed as $\tan\beta$ grows, but this does demonstrate the kind of argument that might lead to physical constraints on the parameter space in place of fine-tuning [20].

We will not apply the constraint $f \leq 50$ in the rest of this section because we also want to display the asymptotic behavior of solutions at very large values of $m_{1/2}$ and $m_0$, but will do so in Sec. IX where we study the implications of this work for SUSY searches at accelerators. We will see that, for some choices of $m_t^{\text{pole}}$, $\tan\beta$, and $A_0$, both $m_0$ and $m_{1/2}$ are bounded from above by purely physical criteria, and no fine-tuning constraint is needed.

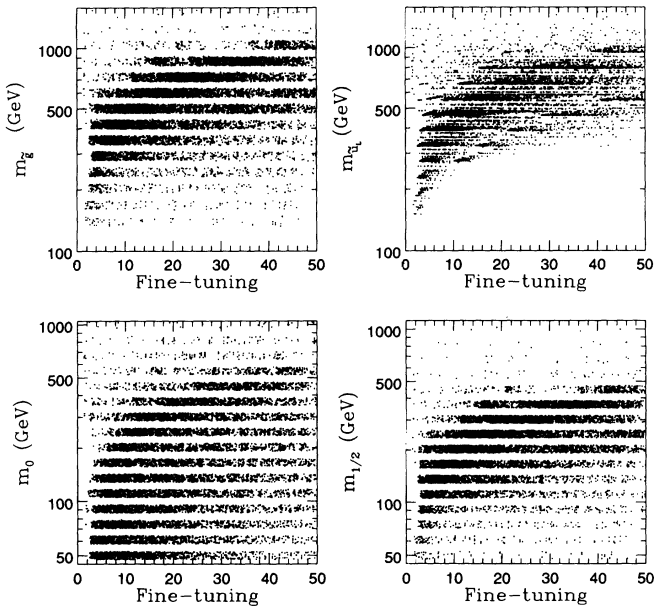


FIG. 13. Scatter plot of (a) $m_{\tilde{g}}$, (b) $m_{\tilde{u}_L}$, (c) $m_0$, and (d) $m_{1/2}$ vs fine-tuning for solutions consistent with all applied constraints. Notice that the cut $f \leq 50$ typically gives sparticle masses $m_{\tilde{q}}, m_{\tilde{g}} \lesssim 1\,\text{TeV}$ but in some cases (all of which have large $\tan\beta$) they can be significantly heavier.

## B. Constrained minimal parameters space (COMPASS)

### 1. General properties

We now focus on the region of the parameter space consistent with all the constraints listed above. This region certainly meets our expectations for where SUSY might be realized because the gauge couplings unify there, correct EWSB takes place, and the experimental and cosmological constraints are satisfied. In this constrained region of parameters (COMPASS) we now analyze the various relations that result between the SUSY spectra and the implications for SUSY searches. Next, we will study what additional restrictions are implied by imposing the dark matter constraint.

Several typical examples of solutions resulting from our analysis are presented in more detail in Figs. 7–9 and in Tables IV–VI. In the graphs we show the typical ranges of several interesting parameters. In the tables we display the lowest and largest values of various masses selected after scanning all the choices of parameters compatible with COMPASS. (The ranges selected by DM, presented in the last two columns, will be discussed shortly.) We see that the allowed mass ranges are rather broad and typically allow for masses as light as, or not much heavier than present experimental limits.

On the other hand, we see that, without constraining $m_{1/2}$ and $m_0$ from above by the fine-tuning constraint, all the masses can (for some $m_t^{\text{pole}}$ and $\tan\beta$) become very large, with the squark, gluino, and heavy Higgs bosons ($H$, $A$, and $H^\pm$) typically being the heaviest and the sleptons, charginos, and neutralinos being significantly lighter, except for $m_0$ large and $m_{1/2} = O(m_Z)$ where $m_{\tilde{l}} \approx m_{\tilde{q}} \gg m_{\tilde{g}}$. Very large values of $m_0 \gg m_{1/2}$ and large values of $m_{1/2} \gg m_0$ are typically disallowed by $\Omega_\chi h_0^2 < 1$, charged LSP, color breaking (tachyonic $\tilde{t}_1$), and no EWSB. But for many choices of parameters, one can only exclude both large $m_{1/2}$ and $m_0$ by imposing the fine-tuning constraint. Thus we see that without further constraints or criteria, COMPASS still allows for a wide range of SUSY masses, though these masses are correlated in very specific ways.

A particularly important quantity in the MSSM is the Higgs boson and/or Higgsino mass parameter $\mu$. In contrast with $m_{1/2}$, $m_0$, and $A_0$, $\mu$ does not break SUSY and therefore *a priori* it could be much larger than $m_Z$. Similarly, while supergravity suggests a value of order $m_Z$ for $m_0$ and $m_{1/2}$, it generically does not say anything about the origin of $\mu_0 = \mu(M_X)$. On the other hand, phenomenologically, it would be very surprising if one of the defining parameters of the MSSM were much larger than others. In our analysis $\mu$ is determined by the other input parameters and the adopted constraints. We find $|\mu|$ broadly in the range of values spanned by either $m_{1/2}$ or $m_0$. Two typical patterns can be identified. In the cases when the constraint from EWSB does not exclude the upper left-hand part of the $(m_{1/2}, m_0)$ plane, we find $|\mu| \sim m_{1/2}$ for $m_{1/2} \gg m_0$ and $|\mu| \sim m_0$ for $m_0 \gg m_{1/2}$. Otherwise, $|\mu| \sim m_{1/2}$ for small $m_0$ but slowly decreases as $m_0$ grows. Overall, the values of

TABLE IV. The lower and upper limits for the case $m_t^{\rm pole} = 145\,{\rm GeV}$, $\tan\beta = 1.5$, $A_0/m_0 = 0$, and $\mathrm{sgn}\,\mu_0 = -1$ (Fig. 7) for all the solutions in COMPASS (with no fine-tuning cut satisfying $f \leq 50$ imposed), and for the subset of solutions selected by either the MDM or CDM constraint. Because of the finite-size grid in our numerical sampling the limits presented here could be somewhat relaxed and should be treated only as indicative.

| Mass limits | COMPASS | | CDM | | MDM | |
|---|---|---|---|---|---|---|
| (GeV) | Lower | Upper | Lower | Upper | Lower | Upper |
| $h$ | 61 | 79 | 62 | 73 | 61 | 71 |
| $A$ | 635 | 1934 | 691 | 1340 | 658 | 1115 |
| $\widetilde{e}_L$ | 183 | 595 | 241 | 403 | 208 | 332 |
| $\widetilde{e}_R$ | 111 | 408 | 190 | 267 | 141 | 207 |
| $\widetilde{\tau}_1$ | 110 | 407 | 190 | 267 | 140 | 207 |
| $\widetilde{\tau}_2$ | 183 | 595 | 241 | 403 | 208 | 332 |
| $\widetilde{\nu}_L$ | 176 | 592 | 236 | 400 | 202 | 328 |
| $\widetilde{u}_L$ | 550 | 1621 | 571 | 1129 | 559 | 943 |
| $\widetilde{u}_R$ | 530 | 1549 | 552 | 1082 | 539 | 905 |
| $\widetilde{t}_1$ | 342 | 1199 | 354 | 810 | 347 | 660 |
| $\widetilde{t}_2$ | 607 | 1546 | 620 | 1112 | 612 | 948 |
| $\chi_1^0$ =LSP | 97 | 356 | 97 | 233 | 97 | 189 |
| $\chi_2^0$ | 182 | 669 | 183 | 440 | 182 | 356 |
| $\chi_1^\pm$ | 180 | 668 | 182 | 440 | 180 | 355 |
| $\widetilde{g}$ | 596 | 1780 | 597 | 1234 | 598 | 1028 |

$\mu$ resulting from the analysis are closely related to $m_{1/2}$ and $m_0$ and only for such values of $\mu$ does the CMSSM appear to be self-consistent.

One important consequence is that the lightest neutralino $\chi$ is in most cases gauginolike (more specifically, $b$-ino-like) [20]. (Figures 7-9 and Tables IV-VI show typical neutralino mass ranges and compositions; see also Fig. 32.) This is quite a remarkable theoretical prediction of the CMSSM in light of the fact that a $b$-ino-like neutralino has been selected theoretically as the unique attractive candidate for (neutralino) dark matter [84,91]. Notice also that, while $\chi$ is typically at least 80% (and in most cases 90%) $b$-ino, it is never a *pure* $b$-ino state. Various analytic approximations for $\Omega_\chi h_0^2$ and related bounds derived for a pure $b$-ino may thus be misleading [96].

It is worth noting that the LSP has typically a dominant $b$-ino component because $|\mu|$ almost always comes out somewhat larger than $M_2 \simeq 0.8 m_{1/2}$ (compare Fig. 31). The composition and scaling properties of the neutralinos and charginos in the plane $(\mu, M_2)$ have been well understood [91,92,96]. In particular, for $|\mu| \gtrsim M_2$ the lightest neutralino is mostly gauginolike (in fact, $b$-ino-like; see, e.g., Fig. 1 and the discussion of gaugino purity in Ref. [91]). For gaugino like LSP's the masses

TABLE V. The same as in Table IV but for $m_t^{\rm pole} = 145\,{\rm GeV}$, $\tan\beta = 5$, $A_0/m_0 = -1$, and $\mathrm{sgn}\,\mu_0 = -1$ (Fig. 8).

| Mass limits | COMPASS | | CDM | | MDM | |
|---|---|---|---|---|---|---|
| (GeV) | Lower | Upper | Lower | Upper | Lower | Upper |
| $h$ | 91 | 113 | 96 | 112 | 94 | 108 |
| $A$ | 209 | 1773 | 346 | 1402 | 314 | 1115 |
| $\widetilde{e}_L$ | 118 | 1208 | 202 | 1047 | 175 | 1022 |
| $\widetilde{e}_R$ | 84 | 1070 | 162 | 1015 | 127 | 1007 |
| $\widetilde{\tau}_1$ | 81 | 1067 | 160 | 1012 | 125 | 1004 |
| $\widetilde{\tau}_2$ | 120 | 1206 | 203 | 1046 | 176 | 1021 |
| $\widetilde{\nu}_L$ | 89 | 1205 | 187 | 1044 | 157 | 1019 |
| $\widetilde{u}_L$ | 326 | 2175 | 480 | 1965 | 417 | 1368 |
| $\widetilde{u}_R$ | 318 | 2095 | 465 | 1877 | 407 | 1310 |
| $\widetilde{t}_1$ | 196 | 1615 | 310 | 1552 | 250 | 1064 |
| $\widetilde{t}_2$ | 408 | 2011 | 538 | 1877 | 481 | 1333 |
| $\chi_1^0$ =LSP | 29 | 437 | 76 | 435 | 59 | 286 |
| $\chi_2^0$ | 63 | 801 | 122 | 789 | 106 | 521 |
| $\chi_1^\pm$ | 51 | 800 | 112 | 788 | 101 | 520 |
| $\widetilde{g}$ | 294 | 2153 | 502 | 2151 | 419 | 1491 |

TABLE VI. The same as in Table IV but now for $m_t^{\rm pole} = 170\,{\rm GeV}$, $\tan\beta = 20$, $A_0/m_0 = 0$, and $\mathrm{sgn}\,\mu_0 = -1$ (Fig. 9).

| Mass limits | COMPASS | | CDM | | MDM | |
|---|---|---|---|---|---|---|
| (GeV) | Lower | Upper | Lower | Upper | Lower | Upper |
| $h$ | 113 | 131 | 116 | 125 | 114 | 119 |
| $A$ | 532 | 1502 | 564 | 1020 | 532 | 828 |
| $\widetilde{e}_L$ | 244 | 1069 | 244 | 1011 | 244 | 832 |
| $\widetilde{e}_R$ | 167 | 1023 | 167 | 1004 | 167 | 824 |
| $\widetilde{\tau}_1$ | 144 | 980 | 144 | 960 | 144 | 788 |
| $\widetilde{\tau}_2$ | 250 | 1051 | 250 | 991 | 250 | 816 |
| $\widetilde{\nu}_L$ | 230 | 1066 | 230 | 1008 | 230 | 828 |
| $\widetilde{u}_L$ | 641 | 1681 | 677 | 1156 | 641 | 931 |
| $\widetilde{u}_R$ | 631 | 1611 | 654 | 1110 | 631 | 924 |
| $\widetilde{t}_1$ | 441 | 1302 | 501 | 883 | 464 | 607 |
| $\widetilde{t}_2$ | 584 | 1579 | 687 | 1117 | 605 | 814 |
| $\chi_1^0$ =LSP | 28 | 353 | 34 | 232 | 34 | 152 |
| $\chi_2^0$ | 51 | 657 | 62 | 432 | 62 | 281 |
| $\chi_1^\pm$ | 50 | 657 | 61 | 432 | 61 | 281 |
| $\widetilde{g}$ | 207 | 1812 | 249 | 1257 | 249 | 874 |

roughly satisfy the relations

$$m_\chi \simeq M_1 \simeq 0.5 M_2, \tag{32}$$

$$m_{\chi_2^0} \simeq m_{\chi_1^\pm} \simeq 2 m_\chi, \tag{33}$$

$$m_{\chi_{3,4}^0} \simeq m_{\chi_2^\pm} \simeq |\mu|. \tag{34}$$

(These approximations improve as $|\mu| \gg M_2$.) It is important to note that in this approach, these relations are characteristic to most solutions in COMPASS, and do not come from GUT-dependent constraints, such as proton decay.

In some regions of the $(m_{1/2}, m_0)$ plane we do find LSP's with significant Higgsino components. This happens for both $m_{1/2}$ and $m_0$ small ($\lesssim 100\,{\rm GeV}$), the region typically excluded by experiment. It also happens in relatively small regions close to where EWSB cannot be achieved. There $|\mu|$ is smaller than $m_{1/2}$. In a few other cases we also find Higgsino-like LSP's for larger $m_{1/2}$ and $m_0$. This happens for small $m_t^{\rm pole}$, $\tan\beta$ well above one, and very large $A_0$ (e.g., for $m_t^{\rm pole} = 120\,{\rm GeV}$, $3 \lesssim \tan\beta \lesssim 20$, $A_0/m_0 = 3$, $\mathrm{sgn}\,\mu_0 = \pm 1$) in a relatively limited region of large $m_{1/2} \approx m_0 \gtrsim 400\,{\rm GeV}$ disfavored by fine-tuning (compare Fig. 12). Higgsino-like LSP's have been shown, however, to provide very little relic abundance [84]. For $m_\chi > m_Z, m_W, m_t$ the $\chi$ pair annihilation into those respective final states ($ZZ$, $WW$, $t\bar{t}$) is very strong [96]. Both below and above those thresholds, there are additional coannihilation [86] processes of the LSP with $\chi_1^\pm$ and $\chi_2^0$, which in this case are almost mass degenerate with the LSP. Coannihilation reduces $\Omega_\chi h_0^2$ below any interesting level [24,97]. Higgsino-like LSP's thus do not solve the DM problem. Except for those relatively rare cases we find an LSP of at least 80% $b$-ino purity.

It is also interesting to explore what values of $\mu$ at the GUT scale ($\mu_0$) result from the analysis. We choose to display it in terms of the ratio $|\mu_0|/m_0$. A very simple relation emerges: $|\mu_0|/m_0$ decreases from a few in the large $m_{1/2}$ and small $m_0$ region down to one or less in the opposite extreme. If, for some choices of parameters, the ratio falls down to zero, no proper EWSB occurs.

One other parameter of the model is $B$, which does not run very much between its GUT value $B_0$ and $B(m_Z)$ (see Table VIII). A typical tendency is for $B/m_0$ to grow with $m_{1/2}$ and decrease with $m_0$. We also show in Fig. 14 a scatter plot of $B_0$ vs $A_0$ for $m_t^{\rm pole} = 145\,{\rm GeV}$ for all the solutions belonging to COMPASS. The value of $B_0$ that

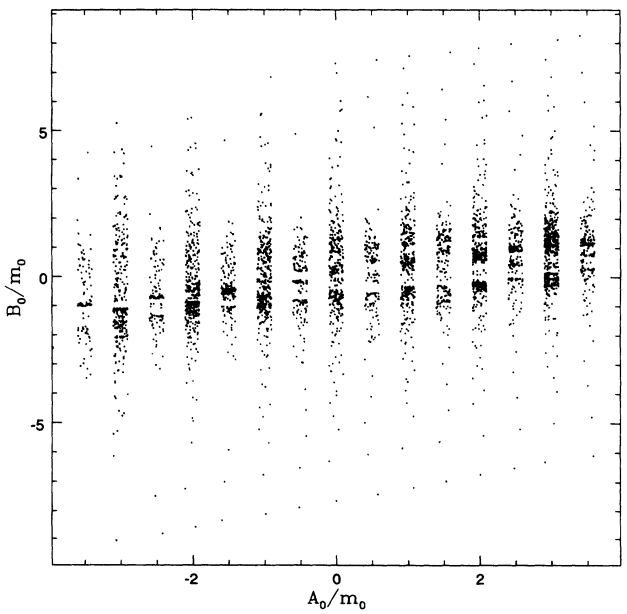


FIG. 14. Scatter plot of $B_0/m_0$ vs $A_0/m_0$ for all allowed solutions (COMPASS) with $m_t^{\rm pole} = 145\,{\rm GeV}$. The quantized appearance is due to numerical sampling and is not significant.

we obtain as an output of our procedure rarely yields the relation $B_0 = A_0 - m_0$ that is often imposed by other analyses.

In this section we have focused mostly on the case $m_t^{\rm pole} = 145\,{\rm GeV}$. Varying $m_t^{\rm pole}$ leads to significant modifications but the general features remain, as can be seen by comparing Figs. 7–9. We find for $m_t^{\rm pole} = 170\,{\rm GeV}$ that the constraint coming from imposing proper EWSB becomes much weaker. Similarly, the regions where the lightest neutralino is not the LSP become pushed toward even larger $m_{1/2}$. For a given point in the $(m_{1/2}, m_0)$ plane $\alpha_s(m_Z)$ grows with $m_t^{\rm pole}$ mostly due to the $\sin^2\theta_W$ dependence on $m_t$ [Eq. (26)], as discussed in Sec. VI B.

#### 2. *Regions favored by the dark matter constraint*

We now point out the subregion of COMPASS which is favored by the hypothesis that the LSP is the dominant component of either cold or mixed dark matter. As we discussed in Sec. VII D 4, there is now abundant evidence for the existence of DM in the Universe. The neutralino has become one of the most attractive candidates for DM. In the pure CDM scenario one expects the LSP relic abundance to be in the range given approximately by (29), while in the currently more favored mixed (CDM+HDM) scenario it should roughly satisfy the range (30).

Applying either (29) or (30) to the parameter space under consideration results in selecting only relatively narrow bands in the plane $(m_{1/2}, m_0)$ whose shape and location vary with other parameters but typically correspond to both $m_{1/2}$ and $m_0$ in the range of a few hundred GeV. (See Figs. 7–9.) Of course, they fall into the region constrained by the age of the Universe ($\Omega_\chi h_0^2 < 1$).

More importantly, requiring enough DM [i.e., taking lower limits in either (29) or (30)] typically leads to *lower* limits on both $m_{1/2}$ and $m_0$ and, as a result, also on the SUSY mass spectra which are higher than in COMPASS alone. It is interesting that the mass ranges consistent with either (29) or (30) are typically less accessible at LEP II and Fermilab. This can be seen by comparing the lower limits allowed by COMPASS with those selected by the CDM or MDM scenarios in Tables IV–VI. (See also Table VIII and the discussion in Sec. IX I.) For example, in the case presented in Fig. 8 and Table V applying the DM constraints causes the chargino $\chi_1^\pm$ and the sleptons to be completely inaccessible to LEP II and the gluino to be above the reach of Fermilab. It also makes it harder to discover $h$ and other particles. On the other hand, the DM constraint severely lowers the upper ranges of masses for all the particles making them much more likely to be accessible at future accelerators such as the NLC or LHC. Prospects of searches for various particles will be discussed in more detail in Sec. IX, and in particular the detectability of the lightest Higgs boson as a function of LEP II beam energy will be analyzed in Sec. IX B 2. Here we only note that, with large enough $\sqrt{s}$, $h$ has a very good chance of being discovered at LEP II.

While one might argue that the constraints (29) or (30) do not carry the same weight as some other constraints listed above, they do reflect our current cosmological expectations and serve as a strong guide to those regions of the parameter space in which SUSY solves the DM problem.

### C. Effect of the full effective Higgs potential

The results from our analysis have also served to reinforce the need for using the full one-loop effective potential in the minimization procedure [51]. We already argued in Sec. II that the one-loop contributions to $V_{\rm Higgs}$ were important in order to stabilize the scale dependence of the potential, but one can also see the net effect of using the full one-loop $V_{\rm Higgs}$ in our model-building results. As well, one can see the smaller role played by the nonleading contributions to $V_{\rm Higgs}$, that is, contributions not coming from the $t - \tilde{t}$ splitting [22,26,53,54]. In Fig. 15 we have shown two plots of the $(m_{1/2}, m_0)$ plane for the choice of input parameters as in Figure 8. Fig. 15(a) shows the region of parameter space allowed after we have excluded the regions in which EWSB did not occur (labeled $E$), where the LSP was charged or colored (labeled $L$), and where the neutralino relic abundance would "overclose" the Universe (labeled $A$), for the renormalization group-improved tree level potential only. On the other hand, Fig. 15(b) shows the parameter space available for the same choices of parameters, but now with the renormalization group-improved one-loop effective potential with leading terms only. Notice that the regions in which EWSB did not occur have enlarged, taking over some of the regions which were excluded before on the basis of their LSP being electrically charged. However, the strong bound placed on the parameter space by DM constraints has considerably weakened, leaving the region in which $m_0 \simeq m_{1/2} \to$ large available, pending a fine-tuning cut. We note also that the effect of including the one-loop contributions to $V_{\rm Higgs}$ is negligible in the region $m_{1/2} \ll m_0$ favored by the proton decay constraint [19,30] in the minimal SU(5) GUT.

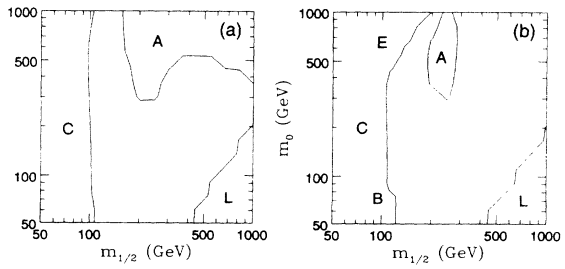


FIG. 15. Plots of the $(m_{1/2}, m_0)$ parameter space showing regions excluded by lack of EWSB (labeled E), LSP not being the neutralino (L), and the age of the Universe (A), for (a) no one-loop contributions to $V_{\rm Higgs}$ and (b) leading one-loop contributions to $V_{\rm Higgs}$. See text for discussion of full one-loop contributions to $V_{\rm Higgs}$. For these plots we have taken $m_t^{\rm pole} = 145\,{\rm GeV}$, $\tan\beta = 5$, $A_0/m_0 = -1$ and ${\rm sgn}\,\mu_0 = -1$ [compare Fig. 8(a)].

Finally, including all (leading and nonleading) terms does not modify the situation sizably as can be seen by comparing Figs. 15(b) and 8(a). The qualitative difference is extremely small, which we found to be a general result.

## IX. APPLICATIONS

### A. Overview

The analysis described in previous sections has led us to a restricted parameter space for $m_t^{\rm pole}$, $\tan\beta$, $m_{1/2}$, $m_0$, $A_0$, and $\mathrm{sgn}\,\mu_0 = \pm 1$ in the CMSSM which we call COMPASS (see Sec. VIII B). Most previous studies of SUSY predictions have preferred to fix some of these parameters by assumptions and vary one or two, either with or without constraints. This is useful and interesting and can lead to instructive predictions, but there is always doubt about their generality.

We have taken the alternative approach of studying the fully constrained parameter space described in Sec. VIII. We know that any point in COMPASS is already guaranteed to have gauge coupling unification, a Higgs mechanism, all phenomenological constraints satisfied, etc. We can then ask a variety of questions about the regularities of the resulting solutions, whether they have predictions of interest, and so forth. For example, we can ask: what fraction of solutions gives a spectrum of sparticles that can be detected at LEP II and Fermilab (or any other present or future facility), and in what channels do we most expect to find sparticles? What do the solutions predict for $\mathrm{BR}(b \to s\gamma)$, $\Gamma(Z \to b\bar{b})$? What is $\Omega_\chi h_0^2$ for the solutions? When new experimental or theoretical information is available it can be easily added to constrain the parameters further. In the following we describe a number of such results. More specifically, in this section we examine the solutions that pass all the theoretical, experimental, and cosmological constraints listed in Secs. VII–VIII, i.e., solutions in COMPASS. We impose two additional cuts. We keep only those solutions which require no large fine-tuning of parameters. We take $f \leq 50$ which roughly corresponds to the heaviest squark, gluino, and Higgs boson masses falling below 1 TeV, except for very large $\tan\beta$ where $m_{\tilde{g}}$ and $m_{\tilde{q}}$ can be larger (see Sec. VIII A 8). We also impose the lower bound $B(b \to s\gamma) > 1.5 \times 10^{-4}$ [70] (see Sec. VII B). The solutions in this restricted set will be called "acceptable." Most of the results presented in this section have been derived with $m_t^{\rm pole} = 145\,\mathrm{GeV}$, but in some cases we consider other values of $m_t^{\rm pole}$.

Recall that our constraints do not require a detailed knowledge of the physics at the high scale. Our parameter space is intended to be the most general one which is independent of multifarious GUT scenarios. It is for this reason that we do not impose a constraint on the lifetime of the proton. The proton decay constraints have been included first by Arnowitt and Nath [19], and also by Lopez *et al.* [30] mainly in an SU(5) GUT. They find a longer proton lifetime for smaller $\tan\beta$ and smaller $m_{1/2}$, so this region of the parameter space is enhanced for them. We will study the implications of adding assumptions about unification and a GUT group in the near future.

We have also assumed a common scalar mass $m_0$ and a common gaugino mass $m_{1/2}$, both of which can be relaxed, which we will consider in the near future. Keeping these comments in mind, we now discuss some CMSSM (constrained MSSM) results.

### B. Higgs physics

#### 1. What is $m_h$ due to?

In a supersymmetric theory with electroweak symmetry breaking the Higgs boson mass is calculable, and it is very interesting to ask what parameters in the theory play a role in determining the value of $m_h$. The tree-level mass matrix for the two CP-even scalar bosons is

$$M^2 = \begin{pmatrix} -B\mu\tan\beta + \frac{1}{2}(g_1^2+g_2^2)v^2\cos^2\beta & B\mu - \frac{1}{2}(g_1^2+g_2^2)v^2\sin\beta\cos\beta \\ B\mu - \frac{1}{2}(g_1^2+g_2^2)v^2\sin\beta\cos\beta & -B\mu\cot\beta + \frac{1}{2}(g_1^2+g_2^2)v^2\sin^2\beta \end{pmatrix}, \tag{35}$$

where $m_Z^2 = \frac{1}{2}(g_1^2+g_2^2)v^2$ and $v^2 = v_d^2 + v_u^2$. If $B\mu = 0$ or if $v^2 = 0$ then this matrix has a zero eigenvalue. Thus in supersymmetry one cannot think of $m_h$ as coming only from the Higgs self-interaction. Any interpretation is complicated since $B\mu$, $\tan\beta$, and $v^2$ are all involved. Furthermore, the one-loop effective potential can yield $m_h$ significantly above the tree-level result [63].

Haber [98] has emphasized that there is a lower limit on $m_h$; even if the tree-level value is zero the one-loop potential generates a mass. He finds a lower value above 60 GeV, but that assumes 1 TeV squark masses. We agree that there is a lower limit, but it is sensitive to squark masses, as shown in Fig. 16 where we plot the *lower limit* of $m_h$ versus $\sqrt{m_{\tilde{t}_1} m_{\tilde{t}_2}}$ which contributes the largest radiative correction to $m_h$. The lower limit basically arises because of the way the EW breaking comes about in SUSY. Equation (15) leads to a lower limit on $B\mu(= m_3^2)$ and thus a lower limit on $m_h$.

Effectively, $m_h$ arises from three sources: the product of SUSY parameters $B\mu$, the value of the VEV's (whose sum in quadrature is fixed numerically by $m_Z$), and the one-loop radiative corrections. To demonstrate how these sources of Higgs boson mass interplay, we show in Figs. 17 and 18 plots of $m_h$ vs $\tan\beta$ and $m_h$ vs $\sqrt{|B\mu|}$, where $m_h$ is the full radiatively corrected Higgs boson mass. The upper limit on $m_h$ is due to the usual argument that in

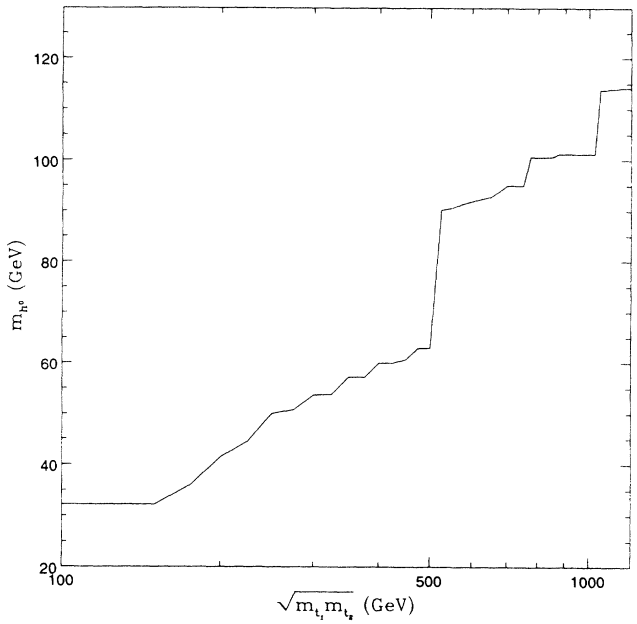


FIG. 16. Lowest $m_h$ versus $\sqrt{m_{\tilde{t}_1} m_{\tilde{t}_2}}$ for all acceptable solutions with $m_t^{\rm pole} = 145\,{\rm GeV}$. We allow $m_h < 60\,{\rm GeV}$ for the purposes of this graph only.

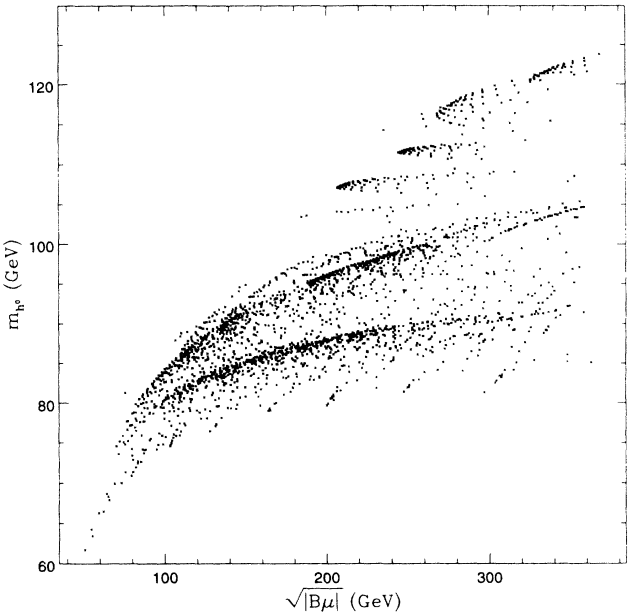


FIG. 18. Scatter plot of $m_h$ vs $\sqrt{|B\mu|}$ for all acceptable solutions with $m_t^{\rm pole} = 145\,{\rm GeV}$ and $\tan\beta$=5. Note that $\sqrt{|B\mu|}$ is usually larger than $m_Z$.

SUSY the Higgs self-coupling is fixed by the gauge couplings with an additional contribution from the radiative corrections [99].

One can see a strong correlation between $\tan\beta$ and the allowed $m_h$. This is expected since the tree-level upper bound for $m_h$ goes like $|\cos 2\beta|$. In fact, we find from our solutions that, for $m_t^{\rm pole} = 145\,{\rm GeV}$, $\tan\beta < 5$ if $m_h < 85\,{\rm GeV}$. Therefore, if LEP II finds the Higgs boson then $\tan\beta$ is constrained to be less than 5 for all our surviving solutions. Solutions with $\tan\beta \geq 5$ and $m_h < 85\,{\rm GeV}$ are excluded mainly by one of three effects: (1) the chargino or sneutrino mass is too low; (2) the LSP is not the neutralino; or (3) electroweak symmetry breaking does not occur. Figure 19 shows the distribution of $m_h$ for all acceptable models with $m_t^{\rm pole} = 145\,{\rm GeV}$.

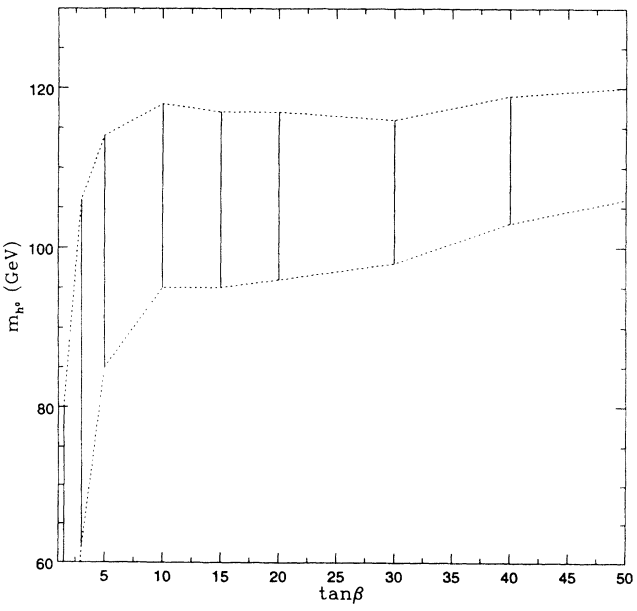


FIG. 17. Plot of $m_h$ vs $\tan\beta$ for all acceptable solutions with $m_t^{\rm pole} = 145\,{\rm GeV}$. The solid vertical bands express the range in $m_h$ for a given $\tan\beta$. The dotted lines show the clear envelope of $m_h$ vs $\tan\beta$ that we obtain in the CMSSM. Note that if $m_h \lesssim 85\,{\rm GeV}$ then $\tan\beta \lesssim 5$. The discretization of $\tan\beta$ is merely from numerical sampling and is not physically significant.

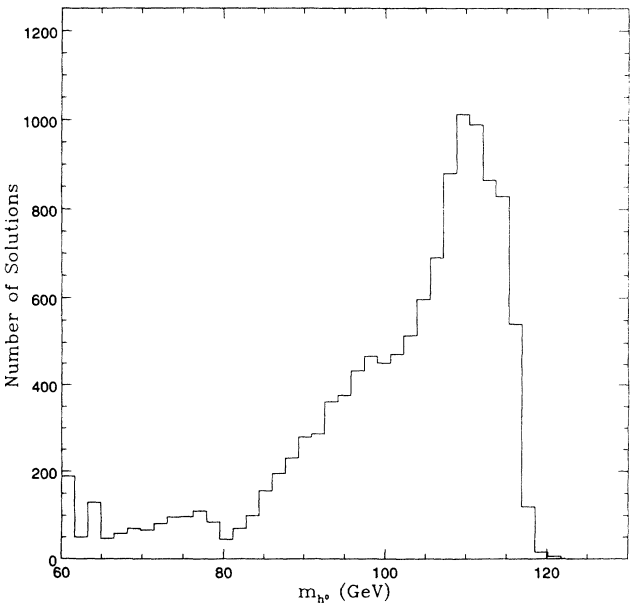


FIG. 19. Histogram of $m_h$ for all acceptable solutions with $m_t^{\rm pole} = 145\,{\rm GeV}$.

### 2. *Detection of the Higgs boson*

Interestingly, we find essentially no solutions for which the $h + A$ mode is detectable at $\sqrt{s} \lesssim 210\,\text{GeV}$ (fewer than 0.1% of the solutions), since $m_A$ is too large for all CMSSM.

Almost all solutions have $\sin^2(\beta - \alpha) > 0.98$, so the $Zh$ cross section [which is proportional to $\sin^2(\beta - \alpha)$] is not suppressed [31]. Thus the experimental limit on the SM Higgs boson effectively applies to the $h$ of the MSSM in all acceptable solutions. The current LEP bound is $m_h \gtrsim 62\,\text{GeV}$ [66]. That $\sin^2(\beta - \alpha) \approx 1$ and that $m_A$ is not small enough for the $h + A$ channel to be accessible at LEP are related.

A similar result holds for the $t\bar{t}h$ coupling. It has a factor $\cos\alpha/\sin\beta$ which is within a few percent of one over essentially the entire set of solutions, so that methods to detect $h$ by radiation off a top quark will work essentially as well for the SUSY $h$ as for the SM Higgs boson.

In Fig. 20 we show the percent of solutions with $m_t^{\text{pole}} = 145\,\text{GeV}$ for which $h$ is detectable at a given $\sqrt{s}$. One can see that about 30% of the solutions are detectable when LEP energy increases to 178 GeV, increasing to about 75% if $\sqrt{s}$ is increased up to 210 GeV; for the MSSM 100% is reached at $\sqrt{s} \simeq 220\,\text{GeV}$. This limit is well known since in the MSSM the upper limit on $m_h$ is about 125 GeV for $m_t^{\text{pole}} \lesssim 150\,\text{GeV}$.

A number of groups [100] have examined the detectability of at least one SUSY Higgs boson at LEP or Superconducting Super Collider (SSC) and/or LHC. They concluded that much of the complete parameter space could be covered, but not all. Results were often presented on a $\tan\beta$ vs $m_A$ plot. In Fig. 21 we show where our constrained solutions appear on such a plot. We also mark the approximate region within which the detection of at least one SUSY Higgs boson was found unlikely [100]. Amusingly, about 2/3 of the solutions that do fall in the region are detectable at LEP II or Fermilab in some other channel.

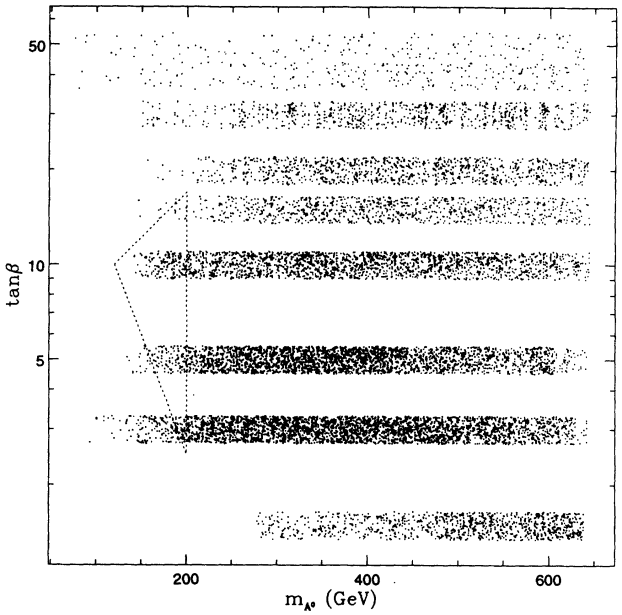


FIG. 21. Scatter plot of $\tan\beta$ vs $m_A$ for all acceptable solutions with $m_t^{\text{pole}}$=145 GeV. The band structure is due to numerical sampling and is not physically significant. The dotted triangular region is the approximate region in which it is difficult to detect at least one Higgs boson [100].

We also present in Fig. 22 a scatter plot of $m_h$ vs $m_A$ for all acceptable solutions for $m_t^{\text{pole}} = 145\,\text{GeV}$. The distinct branches seen in the graphs correspond to different choices of $\tan\beta$. One can see how $m_h$ grows with $m_A$

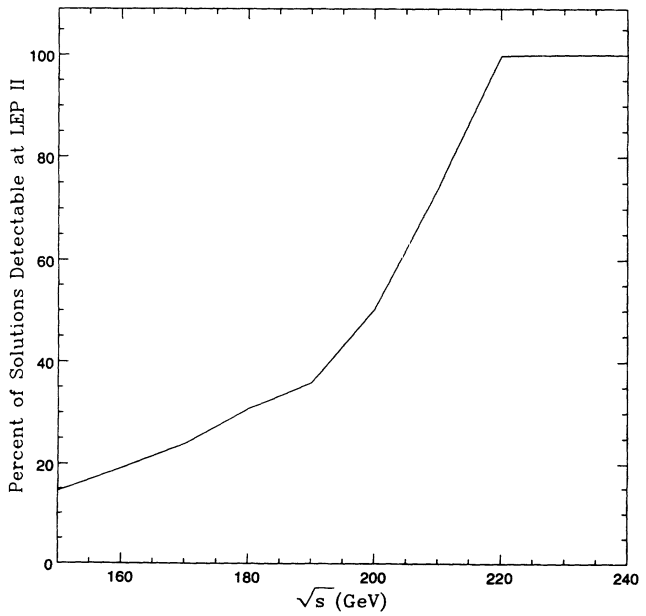


FIG. 20. Percentage of all the acceptable solutions for $m_t^{\text{pole}} = 145\,\text{GeV}$ with $h$ being detectable at LEP II versus center-of-mass energy (GeV).

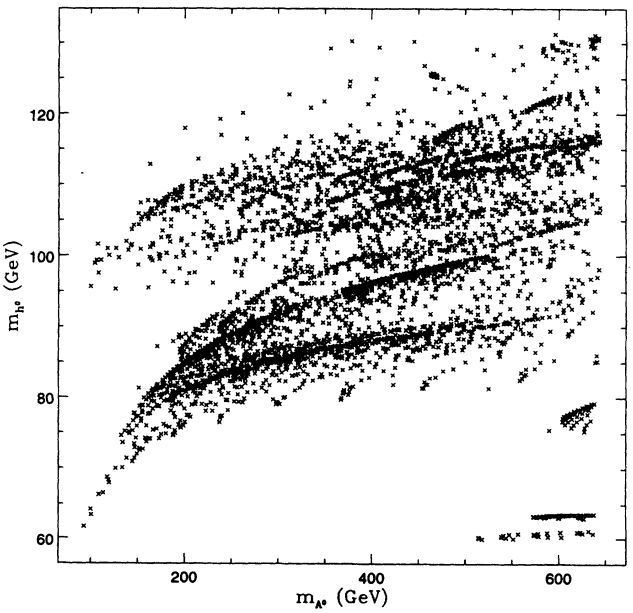


FIG. 22. Scatter plot of $m_h$ vs $m_A$ for all acceptable solutions with $m_t^{\text{pole}}$=145 GeV. The various bands correspond to different choices of $\tan\beta$. The gap in the lower portion of the plot is due to solutions with $1.5 < \tan\beta < 3$ which were missed due to our finite grid.

and $\tan\beta$. The dependence is smeared to some extent by varying all the other parameters of the model.

### C. What is the origin of $m_t$?

We have remarked on several aspects of the role of $m_t$ in other sections. Here we discuss briefly the questions of what contributes to the mass of $m_t$. Of course, the main question is why $m_t \gg m_b$ and how that is answered in supersymmetry. More explicitly, once we are below the scale where EW breaking has occurred, one can write, at a scale Q,

$$m_t(Q) = h_t(Q)v(Q)\tan\beta(Q)/\sqrt{1+\tan^2\beta(Q)}, \quad (36)$$

for the top quark running mass, and likewise for the bottom,

$$m_b(Q) = h_b(Q)v(Q)/\sqrt{1+\tan^2\beta(Q)}. \quad (37)$$

If the SU(2) symmetry were not broken here, we might expect $m_t$ to be only a little larger than $m_b$. To understand the effects that can enter, we can take the ratio at $m_t$,

$$\frac{m_t(Q=m_t)}{m_b(Q=m_t)} = \frac{h_t(m_t)}{h_b(m_t)}\tan\beta \quad (38)$$

and we can define

$$r \equiv \frac{h_t(m_t)/h_b(m_t)}{h_{t0}/h_{b0}}, \quad (39)$$

where $h_{t,b0} \equiv h_{t,b}(M_X)$. Then finally

$$\frac{m_t(m_t)}{m_b(m_t)} = r\frac{h_{t0}}{h_{b0}}\tan\beta. \quad (40)$$

Thus the large ratio $m_t(m_t)/m_b(m_t) \approx 50$ could be due to any of three factors: $\tan\beta$, the ratio of the Yukawa couplings at the high scale, and/or the RGE running of the Yukawa couplings, as expressed by the value of $r$.

The RGE's of the top and bottom Yukawa couplings are

$$\frac{dh_t}{dt} = \frac{h_t}{8\pi^2}\left(-\frac{8}{3}g_3^2 - \frac{3}{2}g_2^2 - \frac{13}{30}g_1^2 + 3h_t^2 + \frac{1}{2}h_b^2\right), \quad (41)$$

$$\frac{dh_b}{dt} = \frac{h_b}{8\pi^2}\left(-\frac{8}{3}g_3^2 - \frac{3}{2}g_2^2 - \frac{7}{30}g_1^2 + 3h_b^2 + \frac{1}{2}h_t^2 + \frac{1}{2}h_\tau^2\right). \quad (42)$$

Since the $g_1^2$ and $h_\tau^2$ contributions are numerically very small, we see that if $h_b \approx h_t$ at the high scale, they will run down together, in which case the large value of $m_t$ is generated predominantly by large $v_u$, and necessarily $\tan\beta \simeq m_t/m_b$ is large. For $h_t$ larger than $h_b$ at the high scale, $m_t$ increases relative to $m_b$ from the running, and the physical $m_t$ is reached with a smaller $\tan\beta$. To illustrate these effects we show in Fig. 23 a scatter plot of $h_{t0}/h_{b0}$ vs $\tan\beta$ for the constrained solutions, all with $m_t^{\rm pole} = 145\,\text{GeV}$. We see that $(h_{t0}/h_{b0})\tan\beta \simeq 60$ is a good approximation to the results except for very large and small $\tan\beta$, so that the large value of $m_t$ cannot be interpreted as coming from the running; it must be input, either as a large GUT-scale ratio $h_{t0}/h_{b0}$ or as a large $\tan\beta$. In particular, if $h$ is discovered at LEP178, then the large $m_t$ must be due to the top Yukawa couplings at the GUT scale (compare Fig. 17).

### D. $B(b \to s\gamma)$

The recently reported upper bound $B(b \to s\gamma) < 5.4 \times 10^{-4}$ (see Sec. VII B) has spurred an increased interest in predictions for $b \to s\gamma$ in SUSY. Barbieri and Giudice [73] have reminded us that in the limit of unbroken supersymmetry the MSSM prediction (including the standard model part) is zero due to a theorem of Ferrara and Remiddi [101], and they have shown that SUSY solutions will give reasonable values for this rate. Garisto and Ng [76], and others, have also done a general SUSY analysis of the implications of $B(b \to s\gamma)$.

In Fig. 24 we show a histogram of $B(b \to s\gamma)$ for all the solutions. We have checked that the solutions in the peak come from all over the parameter space and in no sense

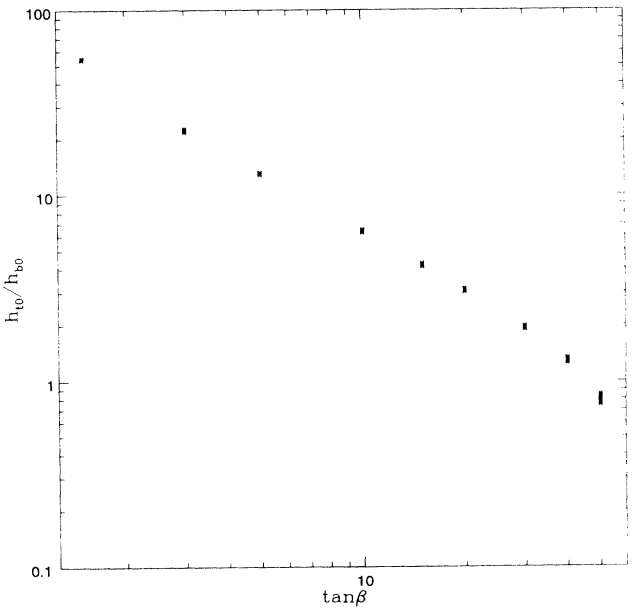


FIG. 23. The ratio of the top Yukawa to the bottom Yukawa couplings at the GUT scale vs $\tan\beta$ for all acceptable solutions with $m_t^{\rm pole} = 145\,\text{GeV}$. We see that $\left(\frac{h_{t0}}{h_{b0}}\right)\tan\beta \simeq 60$ is not a bad description, so the running cannot help much to account for the large size of the $m_t/m_b$ ratio; it must be imposed either via $\left(\frac{h_{t0}}{h_{b0}}\right)$ or via $\tan\beta$. If $\tan\beta$ is not large, as we might expect, then a large $\left(\frac{h_{t0}}{h_{b0}}\right)$ is required as input.

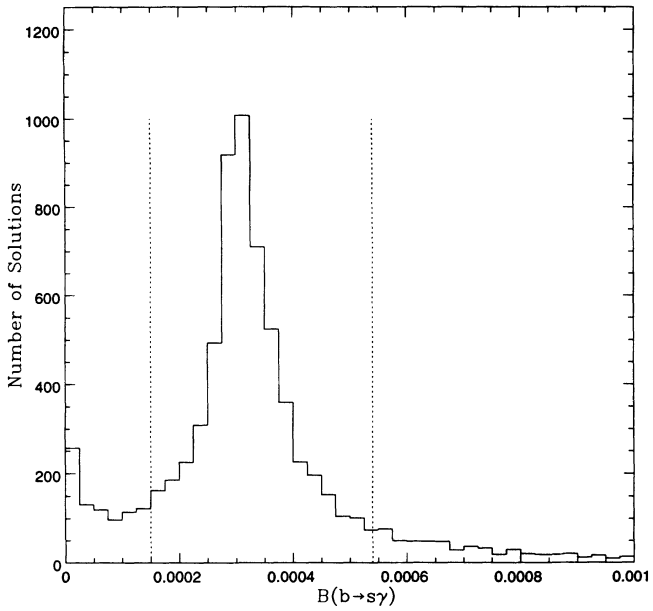


FIG. 24. Histogram of $B(b \to s\gamma)$ for all otherwise acceptable solutions with $m_t^{\rm pole} = 145\,{\rm GeV}$. The dotted lines indicate the upper and lower bounds on $B(b \to s\gamma)$ imposed as discussed in the text. The SM prediction is $3.1 \times 10^{-4}$ corresponding to the formulas of Ref. [73]. More recent QCD correction estimates [77] lead to a SM $B(b \to s\gamma) \simeq 4.3 \times 10^{-4}$.

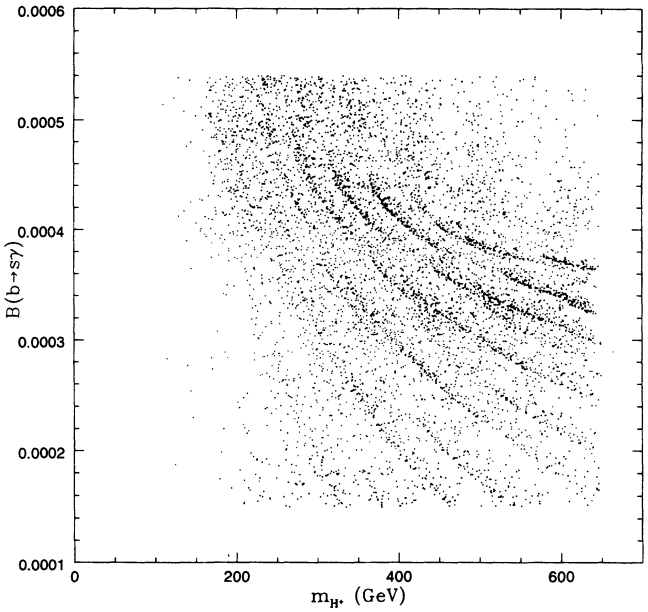


FIG. 25. Scatter plot of $B(b \to s\gamma)$ vs $m_{H^\pm}$ for all acceptable solutions with $m_t^{\rm pole} = 145\,{\rm GeV}$. The faint banding visible in the figure is from numerical sampling and is not physically significant.

represents a decoupling region. For a typical solution the magnitudes of the $W$-$t$ loop, the $H^\pm$-$t$ loop, and the $\chi^\pm$-$\tilde{t}$ loop contributions are all about the same, with the $W$-$t$ and $H^\pm$-$t$ loops having the same sign and the $\chi^\pm$-$\tilde{t}$ loop having the opposite sign. We see that the CMSSM naturally produces solutions in the right range. These results are predictions in the sense that here we impose no constraint on the model space from $b \to s\gamma$ data. [For other uses of the model space we cut at the upper and lower limits indicated in the figure, so that our model space does include the $B(b \to s\gamma)$ constraint in general, except for the present discussion.]

Some authors [74] have in the past claimed that this decay strongly constrains charged Higgs boson masses. To show that there is no strong constraint in the CMSSM, we show in Fig. 25 a plot of $B(b \to s\gamma)$ vs $m_{H^+}$ for the solutions in the region between the upper and lower limits. That is, every $m_{H^+}$ in Fig. 25 gives a $B(b \to s\gamma)$ consistent with experiment.

Finally, it is interesting to look at $B(b \to s\gamma)$ vs $\tan\beta$ in Fig. 26. Smaller $\tan\beta$ values concentrate somewhat in the allowed region, though acceptable solutions occur at any $\tan\beta$. In the large $\tan\beta$ region the chargino contribution can be quite large and negative [75,76].

### E. Detection of SUSY at LEP II and Fermilab

There are a number of possible ways to detect supersymmetric partners at Fermilab or LEP II. We estimate that about 32% of all CMSSM acceptable solutions (see Sec. IX A) have either a superpartner or the light Higgs boson detectable at LEP with $\sqrt{s} = 178\,{\rm GeV}$ and 500 ${\rm pb}^{-1}$, or at Fermilab (with, say, 500 ${\rm pb}^{-1}$ integrated luminosity), or both ($h$ will only be detectable at LEP II, not Fermilab). We include in this sample all solutions with $m_t^{\rm pole} = 145\,{\rm GeV}$, $m_0 \leq 1\,{\rm TeV}$, $m_{1/2} \leq 1\,{\rm TeV}$, and $f \leq 50$; that is conservative, giving $\tilde{q}$ and $\tilde{g}$ masses over 2 TeV for the largest $m_0$, $m_{1/2}$. The solutions with large $m_0$, $m_{1/2}$ are generally not accessible at Fermilab or LEP II, but they also do not increase the number of

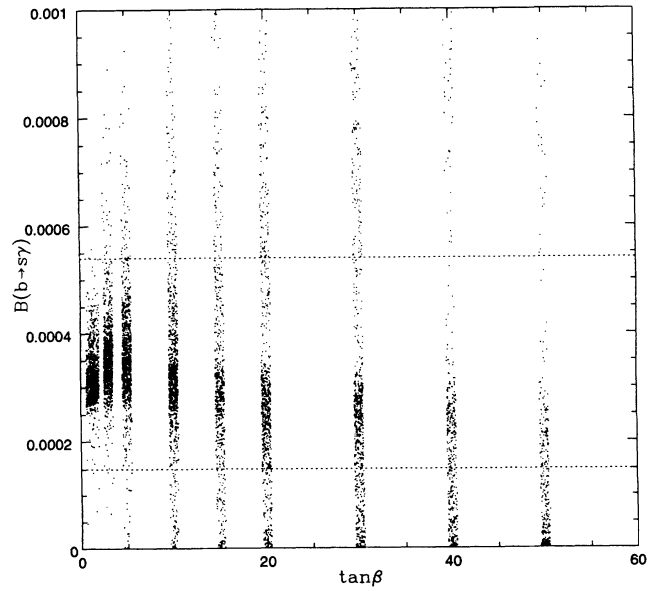


FIG. 26. $B(b \to s\gamma)$ vs $\tan\beta$ for all acceptable solutions with $m_t^{\rm pole} = 145\,{\rm GeV}$. In order to demonstrate the density of points, $\tan\beta$ is slightly smeared around its numerically sampled value.

acceptable solutions rapidly enough to dilute the 32% result even if larger $m_0$, $m_{1/2}$ were to be included. The results do not vary rapidly with $m_t$. These numbers are for solutions with $\Omega_\chi h_0^2 < 1$.

At LEP II 24% of the acceptable solutions allow detection via one-sided events, $e^+e^- \to \chi_2^0\chi_1^0$, where $\chi_1^0 \equiv \chi$, followed by $\chi_2^0 \to l^+l^-\chi_1^0$. And 18% will have pair production of the lightest chargino, and 8.6% detection of $h$. There is overlap, of course, and 30% of all solutions are detectable at LEP II. Selectrons are detectable in 3.6%, a light stop 0.7%, and $h + A$ in 0.06% of the solutions.

An interesting way, perhaps the only way at LEP, to determine if $h$ is a SUSY Higgs boson is to measure the cross section for $e^+e^- \to h +$ nothing [102]. In the standard model this entire cross section should be from $e^+e^- \to h(\to b\bar{b}) + Z(\to \nu\bar{\nu})$ and will be very accurately known. In SUSY there is also a contribution from $e^+e^- \to \chi_2^0(\to h + \chi_1^0) + \chi_1^0$; unfortunately this contribution is larger than 10% of the SM cross section in only 0.6% of the solutions at LEP 178 but would be the "proof" of SUSY in these cases; at larger $\sqrt{s}$ the fraction of solutions where this effect could be observed increases rapidly.

As an illustration, we show in Fig. 27 what fractions of the $(m_0, m_{1/2})$ plane would be constrained by SUSY searches at LEP II if $m_t^{\rm pole} = 145\,\text{GeV}$. The kinematic criteria that we use to determine the detectability at LEP178 are $m_{\chi_1^\pm} < 85\,\text{GeV}$, $m_{\tilde{f}} < 85\,\text{GeV}$ (for any sfermion), $m_{\chi_1^0} + m_{\chi_2^0} < 170\,\text{GeV}$, $m_h + m_A < 170\,\text{GeV}$, and $m_h + m_Z < 170\,\text{GeV}$. We also require that any event-signature lepton have energy above 5 GeV or any quark have energy above 10 GeV. The regions marked by crosses (empty boxes) will always (never) be accessible to LEP II for any combination of input parameters. Filled boxes mark the regions accessible for some combinations of parameters. In window (a) we show the combination of possible SUSY searches at LEP II by applying the criteria listed above. In window (b) we show the same for the chargino $\chi_1^\pm$ alone, and in window (c) for the lightest Higgs boson assuming $m_h < 80\,\text{GeV}$. ($h$ is a very SM-like Higgs boson.) Finally, window (d) shows how much larger a region would be explored by searching for $h$ up to 110 GeV. Remember that very large values of $m_{1/2}$ are disfavored by the fine-tuning constraint (compare, e.g., Fig. 13).

At Fermilab gluino detection will occur in 11% of all solutions, squark detection in 5%, detection of $\chi_1^0\chi_1^\pm$ in 25%, $\chi_1^\pm\chi_1^\mp$ in 14%, $\chi_2^0\chi_1^0$ in 24%, $\chi_2^0\chi_1^\pm$ in 12%, $\tilde{t}_1 + \bar{\tilde{t}}_1$ in 4%. These combine to make 26% of all solutions being detectable at Fermilab. The Fermilab-LEP overlap is large, so combining them only increases the percentage of solutions detectable at Fermilab or LEP II to the above-mentioned 32%.

The kinematic criteria that we use to determine the detectability at Fermilab are $m_{H^\pm} < m_t^{\rm pole} - 5\,\text{GeV}$, $m_{\tilde{g}} < 300\,\text{GeV}$, $m_{\chi_1^\pm} < 85\,\text{GeV}$, $m_{\tilde{q}} < 300\,\text{GeV}$, and $m_{\chi_1^0} + m_{\chi_2^0} < 170\,\text{GeV}$. We also require that any event-signature lepton or quark have energy above 15 GeV. Some of the percentages listed above for the detectability of different channels will decrease, particularly at Fermilab, when detection efficiencies and cuts to reduce background are considered. But with sufficient luminosity and sufficiently good detectors the above numbers should be approached. We are presently undertaking full simulations of signals and backgrounds to determine reliable signatures and strategies. There have been previous studies of Fermilab and LEP II detectability in some depth [103]. Our only advance so far over some of these is that their

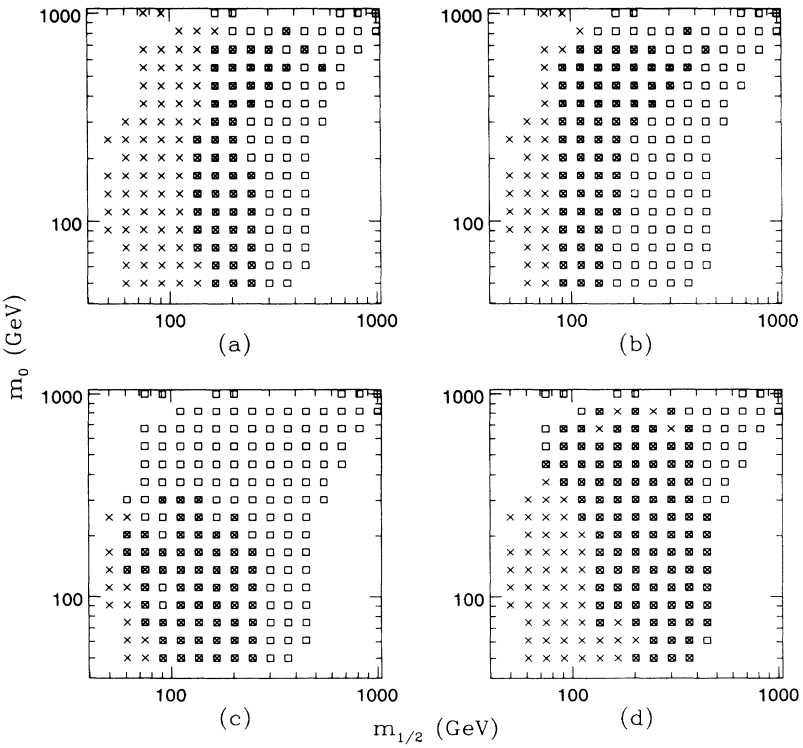


FIG. 27. Regions of the $(m_0, m_{1/2})$ plane to be explored by SUSY searches at LEP II if $m_t^{\rm pole} = 145\,\text{GeV}$. Crosses (empty boxes) mark the regions that will always (never) be accessible to LEP II for any combination of input parameters. Solid boxes mark the regions accessible for some combinations of parameters. Empty regions are excluded by our set of constraints. In window (a) we show the combination of possible (direct) SUSY searches at LEP II as described in the text. In window (b) we show the LEP II search potential for the chargino $\chi_1^\pm$ alone, and in windows (c) and (d) for the lightest Higgs boson assuming ability to find $h$ with masses $m_h < 80\,\text{GeV}$ and 110 GeV, respectively. ($h$ is a very SM-like Higgs boson.) Very large values of $m_{1/2}$ are disfavored by the fine-tuning constraint.

conclusions are based on a parameter space some parts of which are excluded because the various constraints are not satisfied.

We note that at Fermilab, for gluinos lighter than 300 GeV, 80% of solutions have squarks heavier than gluinos, so that the appropriate way to simulate $\tilde{g}$ detection is to take $m_{\tilde{q}} > m_{\tilde{g}}$ in the first approximation.

We have also investigated our CMSSM parameter space to see how the top quark search at Fermilab could be affected by supersymmetry. We find that for $m_t^{\rm pole} = 170$ GeV approximately 3% of all acceptable solutions kinematically allow one or more of the following: $t \to bH^{\pm}$ decay, $t \to \tilde{t}_1\chi_1^0$ decay, or $\tilde{g} \to \tilde{t}_1 t$ with $\tilde{g} < 250$ GeV. (For smaller $m_t^{\rm pole}$ this fraction is reduced.) Any one of these kinematic possibilities can significantly alter the kinematic analysis and/or the effective rates (after cuts) of top quark production. Once the top physics at Fermilab settles into place if none of these is observed then the parameter space is reduced a few percent.

Some reduction in detectable solutions would occur if the $\chi_1^{\pm} - \chi_1^0$ mass difference were so small that the resulting lepton or jet from $\chi_1^{\pm}$ decay were too soft to detect. Figure 28 shows a plot of $m_{\chi_1^{\pm}} - m_{\chi_1^0}$ vs $m_{\chi_1^{\pm}}$ from which we see that most solutions have no problem here; and Figure 29 shows the energy of the lepton or jet from $\chi_1^{\pm}$ decay.

We will report a study on how effective higher energy linear colliders will be at studying SUSY for the constrained model space later. For now we note that NLC with $\sqrt{s} = 350$ GeV will be able to detect $h$ and at least one superpartner for about 75% of the constrained solutions; this number grows to about 97% as $\sqrt{s}$ grows to 500 GeV.

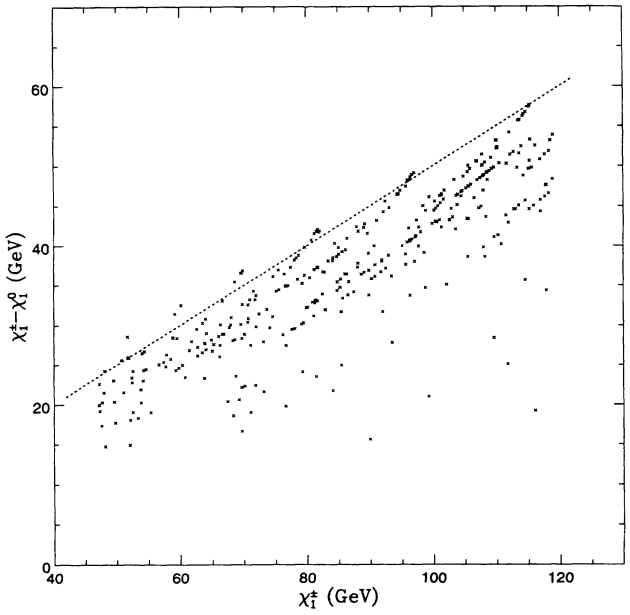


FIG. 28. $m_{\chi_1^{\pm}} - m_{\chi_1^0}$ vs $m_{\chi_1^{\pm}}$ for all acceptable solutions with $m_t^{\rm pole} = 145$ GeV and $m_{\chi_1^{\pm}} < 120$ GeV. The line represents $m_{\chi_1^{\pm}} = 2m_{\chi_1^0}$ which is approximately true for a gauginolike LSP. While the line is an approximate description of the results it is not accurate enough for detailed use.

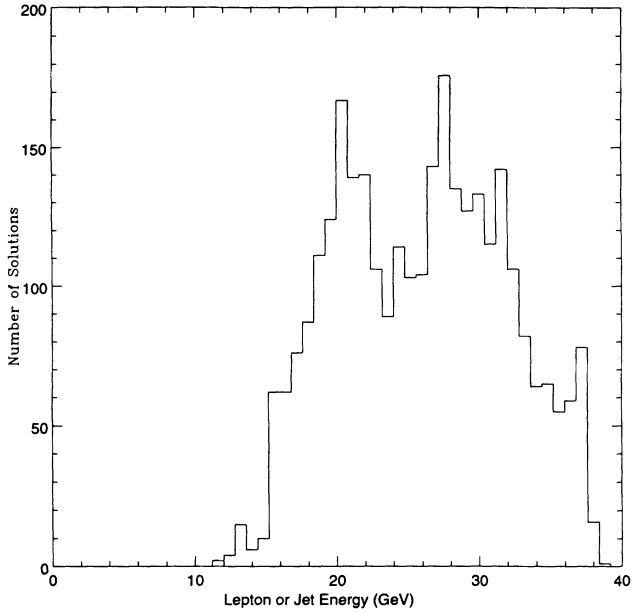


FIG. 29. Histogram of lepton or jet energy from $\chi_1^{\pm}$ decay for acceptable solutions with $m_{\chi_1^{\pm}} < 120$ GeV.

If $h$ is not detected at LEP II once $\sqrt{s} \approx 210$ GeV, most but far from all solutions will be excluded, particularly if $m_t^{\rm pole} \approx 145$ GeV. Figure 19 shows a histogram of $m_h$ values and one can see that most solutions are below 110 GeV. In solutions with a Higgs sector extended beyond that of the minimal one there is still an upper limit on $m_h$, but it can be as large as about 146 GeV [104].

Overall, we conclude that, while not finding superpartners at LEP II and Fermilab does eliminate nearly a third of the parameter space, it will still leave many possibilities open.

### F. What if Fermilab and LEP II do not detect a sparticle?

If superpartners are not detected at LEP II or Fermilab then much of the low $(m_0, m_{1/2})$ parameter space can be excluded. Bounds on $m_{1/2}$ are determined mainly by the bounds on the gluino. The gluino mass is related to $m_{1/2}$ by

$$m_{1/2} = \xi_{\tilde{g}} m_{\tilde{g}}. \tag{43}$$

We find the lower limit of $\xi_{\tilde{g}} = \alpha_X/\alpha_s(m_{\tilde{g}})$ to be [compare text below Eq. (22)]

$$\xi_{\tilde{g}} > 0.36. \tag{44}$$

So if $m_{\tilde{g}}$ is determined from experiment at Fermilab to be greater than 300 GeV then

$$m_{1/2} > (0.36)(300\,\text{GeV}) = 107\,\text{GeV}. \tag{45}$$

Bounds can also be placed on $m_{1/2}$ by direct searches on the lightest chargino. By taking the square $(MM^T)$ of the chargino mass matrix we find that

$$m^2_{\chi_1^{\pm}} < \xi_{\chi_1^{\pm}} m^2_{1/2} + 2m^2_W \cos^2\beta, \tag{46}$$

where

$$\xi_{\chi_1^\pm} \equiv \frac{M_2^2}{m_{1/2}^2} < \frac{16}{25}. \tag{47}$$

So if $m_{\chi_1^\pm} > M_W$ then the $\tan\beta$–dependent bound for $m_{1/2}$ is

$$m_{1/2} > m_W \tfrac{5}{4}\sqrt{1-2\cos^2\beta} \tag{48}$$

For high $\tan\beta$ this bound ($\sim 100\,\mathrm{GeV}$) would become comparable to the resulting bound on $m_{1/2}$ from the gluino search. In any case, bounds on $m_{1/2}$ are obtained straightforwardly from direct sparticle searches.

It is more difficult to put bounds on $m_0$. Although the squarks and sleptons gain mass from $m_0$ they also have contributions from the gaugino masses [compare Eq. (23)]. Therefore bounds on $m_0$ from direct searches of squarks and sleptons must be presented as a function of $m_{1/2}$. Letting $\tilde{f}$ represent any squark or slepton and $\hat{m}_{\tilde{f}}$ the lower mass bound of $\tilde{f}$ we can write the inequality relation that constrains the $(m_0, m_{1/2})$ plane:

$$m_0^2 + b_{\tilde{f}_{L,R}} m_{1/2}^2 > \hat{m}_{\tilde{f}}^2 - m_f^2 \mp m_Z^2 \cos 2\beta \times \left[T_3^{f_{L,R}} - Q_{f_{L,R}} \sin^2\theta_W\right]. \tag{49}$$

For example, for $\tilde{f} = \widetilde{e_L}$,

$$\tfrac{9}{2}0 < b_{\widetilde{e_L}} < \tfrac{1}{2}. \tag{50}$$

The upper and lower bounds on $b_{\widetilde{e_L}}$ are good to within 5% accuracy. As can be clearly seen from Eq. (49) the slepton bound translates to an ellipse (first quadrant) in the $(m_0, m_{1/2})$ plane where all $(m_0, m_{1/2})$ inside the ellipse are excluded.

### G. What if Fermilab or LEP II does find a sparticle?

If Fermilab or LEP II discover one or more sparticles we would like to extract from this the GUT-scale Lagrangian. That is, we would like to extract the supersymmetric input parameters $m_0$, $m_{1/2}$, $A_0$, $\tan\beta$, and $\mathrm{sgn}\,\mu_0$ from all the observables that are sensitive to them (we assume that we know $m_t$). In this section we briefly discuss how this should be done. It turns out that this is more difficult than it first appears; analytic methods are of limited applicability.

The equations used in the last section to put bounds on $m_0$ and $m_{1/2}$ given bounds on the gluino and sfermions can also be used to pin down $m_0$ and $m_{1/2}$. In general, each fixed value of an observable, whether it be a mass or a cross section or an asymmetry or anything else, generates a hypersurface in input parameter space ($m_0$, $m_{1/2}$, $\tan\beta$, $A_0$, $\mathrm{sgn}\,\mu_0$). (The gluino mass, for example, would predominantly determine $m_{1/2}$ up to additional uncertainties discussed below.) The effective dimensionality of this surface is determined by how many input parameters significantly affect the value of the observable. Determining this hypersurface is very difficult because of all the nonlinearities in relating low-energy parameters to the input parameters through self-consistent solutions of many RGE's. In the last section and in Refs. [105] there are some simple equations that allow us to estimate functional relations between input parameters and sparticle masses. Even though these simple relations are often a good approximation to the full analysis we must keep in mind that every observable necessarily depends on all input parameters, though with varying importance. For example, a precise determination of $m_{1/2}$ from $m_{\tilde{g}}$ is limited because $\alpha_s(m_{\tilde{g}})$ depends in general on all sparticle thresholds (at one loop):

$$m_{\tilde{g}} = \frac{\alpha_s(m_{\tilde{g}})}{\alpha_X} m_{1/2} = f(m_0, m_{1/2}, A_0, \tan\beta, \mathrm{sgn}\,\mu_0). \tag{51}$$

Likewise, determination of the precise gaugino contributions to sfermion masses requires detailed knowledge of the sparticle thresholds which introduce all input parameters into the final determination of the sfermion masses. Methods based on analytic expressions are clearly limited. They may suffice to provide rough estimates of input parameters, especially soon after the discovery of a given particle, when the experimental bounds will be still large, but they cannot be improved to accommodate a complex analysis based on several well-measured observables.

Our approach to the problem of determining input parameters from low-energy observables does allow for such improvements. We explore wide ranges of the input parameter space and let the computer do the work. We have really already employed this technique to generate the COMPASS of the CMSSM. We have cut hypersurfaces in input parameter space with Higgs and sparticle mass bounds, $\mathrm{BR}(b \to s\gamma)$ limits, $\Omega_\chi h_0^2$ bounds, fine-tuning limit, $\alpha_s(m_Z)$, etc. However, highly precise measurements of observables especially sensitive to supersymmetric loop corrections, or direct measurements of sparticle production, will pin down the input parameters which determine those low-energy observables.

We present in Table VII an example of how several experimental measurements can shrink the input parameters space to a "point" which would in turn allow us to predict all other observables (other sparticle masses, cross sections, etc.). The first row in Table VII lists the range allowed for each input parameter given detection of just the lightest Higgs boson ($m_h$ determined from experiment to be, say, $m_h = 80 \pm 5\,\mathrm{GeV}$). The value of $\mu$ is evaluated at $m_Z$ and its sign is the one of $\mathrm{sgn}\,\mu_0$. We see that just knowing the mass of the lightest Higgs boson alone clearly does not significantly constrain any of the input parameters. The next row in Table VII lists the range allowed for each input parameter given detection of just the lightest chargino ($\chi_1^\pm$ determined by experiment to be, say, $m_{\chi_1^\pm} = 70 \pm 5\,\mathrm{GeV}$). Here again knowledge of just one mass, the lightest chargino, does not significantly constrain input parameter space. In the next three rows we list the range of input parameters given detection of just $m_{\tilde{t}_1}$ ($m_{\tilde{t}_1} = 110 \pm 10\,\mathrm{GeV}$), just $\tilde{g}$ ($m_{\tilde{g}} = 210 \pm 10\,\mathrm{GeV}$), and just $\tilde{e}_L$ ($m_{\tilde{e}_L} = 95 \pm 5\,\mathrm{GeV}$).

TABLE VII. Table demonstrating how input parameter space ($m_0$, $m_{1/2}$, $A_0$, $\tan\beta$, and $\mathrm{sgn}\,\mu_0$) is constrained by detection of particles. The initial ranges of input parameters are listed in Sec. VIII A. For this example we assume detection of these particles to mean $m_h = 80 \pm 5\,\mathrm{GeV}$, $m_{\chi_1^\pm} = 70 \pm 5\,\mathrm{GeV}$, $m_{\tilde{t}_1} = 110 \pm 10\,\mathrm{GeV}$, $m_{\tilde{g}} = 210 \pm 10\,\mathrm{GeV}$, and $m_{\tilde{e}_L} = 95 \pm 5\,\mathrm{GeV}$. If more than one particle type is listed in the "Detected particle(s)" column then the range for each of the input parameters is found from knowledge of *all listed* particle masses. Keep in mind that the ranges of parameters listed in the table are values obtained on our numerical sampling grid and therefore have errors associated with them corresponding to the grid spacing. For example, when we quote $m_{1/2} = 74\,\mathrm{GeV}$ we really mean that we find no acceptable solutions with $m_{1/2} \leq 61\,\mathrm{GeV}$ (the next lowest $m_{1/2}$ value on our grid) and no acceptable solutions with $m_{1/2} \geq 91\,\mathrm{GeV}$ (the next highest $m_{1/2}$ on our grid). If our grid were very fine grained, then we could quote ranges that would more accurately reflect how well the parameters were determined, and that reflect the experimental errors better.

| Detected particle(s) | $m_0$ | $m_{1/2}$ | $A_0/m_0$ | $\tan\beta$ | $\mu$ |
|---|---|---|---|---|---|
| $h$ | $\leq 671$ | $\leq 549$ | Unbounded | Unbounded | -472 – 253 |
| $\chi_1^\pm$ | Unbounded | 74 – 450 | Unbounded | $\leq 40$ | -477 – 332 |
| $\tilde{t}_1$ | $\leq 549$ | 61 – 202 | Unbounded | $\leq 20$ | -428 – 420 |
| $\tilde{g}$ | Unbounded | 74 | Unbounded | $\geq 3$ | -460 – 205 |
| $\tilde{e}_L$ | $\leq 74$ | 61 – 111 | Unbounded | $\leq 5$ | -237 – 172 |
| $h$, $\chi_1^\pm$ | $\leq 368$ | 74 – 136 | Unbounded | $\leq 3$ | -414 – 169 |
| $h$, $\chi_1^\pm$, $\tilde{t}_1$ | $\leq 302$ | 74 – 111 | -3.0 – -1.0 | $\leq 3$ | -414 – 140 |
| $h$, $\chi_1^\pm$, $\tilde{t}_1$, $\tilde{g}$ | $\leq 136$ | 74 | -3.0 – -1.5 | 3 | 120 – 140 |
| $h$, $\chi_1^\pm$, $\tilde{t}_1$, $\tilde{g}$, $\tilde{e}_L$ | 61 | 74 | -2.5 – -2.0 | 3 | 120 – 130 |

The next row assumes detection of $h$ *and* $\chi_1^\pm$. Notice how the combination of these two masses restricts $m_0$, $m_{1/2}$, and $\tan\beta$ far beyond what knowledge of each mass can do individually.

As we progress down the rows of the table with each subsequent row assuming more and more detected particles, the input parameters become more and more constrained until $m_0$, $m_{1/2}$, $\tan\beta$, and $\mathrm{sgn}\,\mu_0$ are determined precisely at the level of our numerical sampling. Only $A_0$ remains stubbornly undetermined though it is better constrained. This is a general rule about $A_0$: few observables are very sensitive to it. Observables which depend on third generation sparticle left-right mixing are most sensitive to $A_0$.

As this example shows, by generating many self-consistent solutions and "filling up" input parameter space with them, we have the means by which to use all observables simultaneously to constrain input parameter space. This approach of generating solutions with the most precision possible, calculating observables without untrustworthy simplifying assumptions, and then simultaneously comparing all the generated solutions with all the calculated observables is a powerful way to analyze and constrain minimal supersymmetry. It is this approach that will quickly enable us to add better measurements of observables and any new observables to the CMSSM, including possible announcements of sparticle detection. With our method we can go directly from data to the parameters of the effective Lagrangian at the unification scale.

### H. The $\Gamma(Z \to b\bar{b})$ partial width

Precision measurements at LEP II currently show a slight deviation from the standard model value for the extracted value of $\Gamma_{b\bar{b}}/\Gamma_{\mathrm{had}}$. The current LEP average [46] is

$$R_b = \frac{\Gamma_{b\bar{b}}}{\Gamma_{\mathrm{had}}} = 0.2200 \pm 0.0027. \tag{52}$$

Several groups [106] have studied the loop corrections to this partial width in the standard model. The SM prediction for $R_b$ is heavily dependent upon the value of $m_t$, but [46] the predicted value is $1.5\sigma$ lower than the measured value for $m_t^{\mathrm{pole}} = 145\,\mathrm{GeV}$ and it gets even lower for higher $m_t^{\mathrm{pole}}$.

The supersymmetric contributions to this decay width have been calculated in Refs. [107,108]. We use the equations of Ref. [108] to calculate the supersymmetric contributions to $R_b$ within the CMSSM. We perform scalar integral reductions and numerical calculations from Ref. [109].

In Fig. 30 we plot the histogram of all acceptable solutions with $m_t^{\mathrm{pole}} = 145\,\mathrm{GeV}$ and $0.16 < \Omega_\chi h_0^2 < 0.33$. Notice that within the CMSSM the supersymmetric contributions tend to increase $R_b$. This increase in $R_b$ is mainly due to light $\tilde{t}_i$ and $\chi_i^\pm$. Interestingly, if we require the calculated $R_b$ to be within $1\sigma$ of the measured value, then approximately 75% of the resulting solutions will be detectable at LEP II and 83% of the solutions will be detectable at Fermilab. The channel which is by far most detectable at LEP II for these solutions is $\chi_1^\pm\chi_1^\mp$ production. At Fermilab many possible channels for detection of sparticles are allowed: $\tilde{g}$, $\chi_1^\pm\chi_1^\mp$, $\chi_1^\pm\chi_1^0$, $\chi_1^\pm\chi_2^0$, and $\chi_1^0\chi_2^0$.

### I. Neutralino LSP as dark matter

As we have already seen in Sec. VIII, the relic abundance $\Omega_\chi h_0^2$ of the lightest neutralino is an important

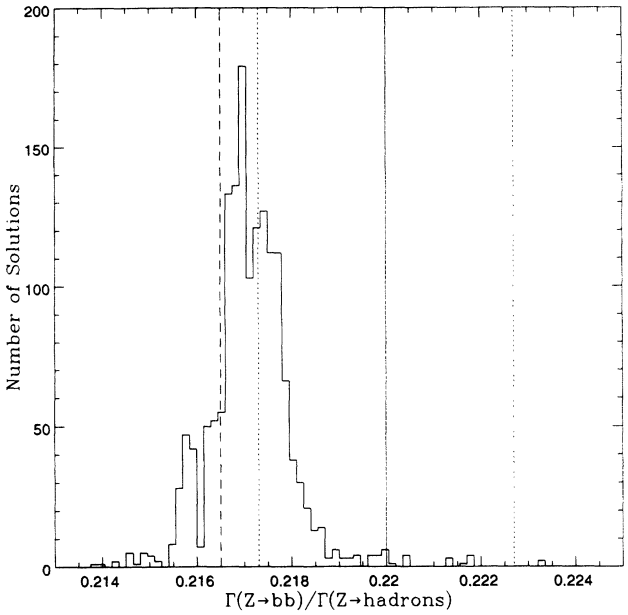


FIG. 30. Histogram of $R_b = \Gamma_{b\bar{b}}/\Gamma_{\rm had}$ for all acceptable solutions with $m_t^{\rm pole} = 145\,{\rm GeV}$ and $0.16 < \Omega_\chi h_0^2 < 0.33$. The central solid line is the measured value of $R_b$ and the outside dotted lines are the one standard deviation errors on the measurement. The dashed line is the standard model calculated value of $R_b$ given $m_t^{\rm pole} = 145\,{\rm GeV}$.

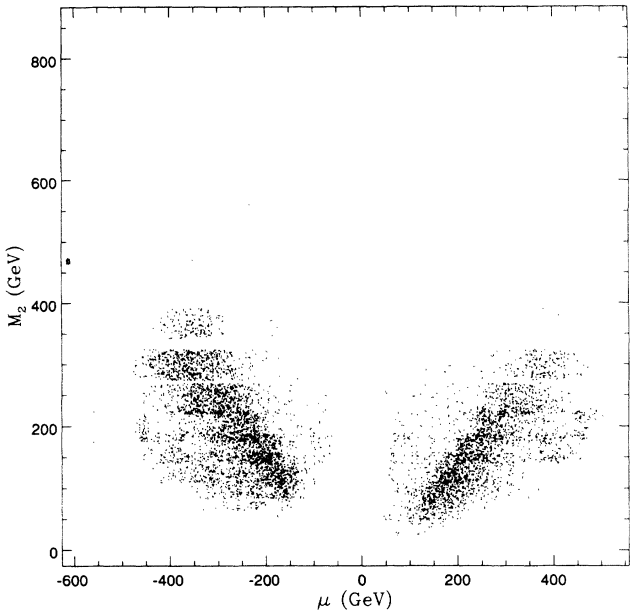


FIG. 31. Scatter plot in the plane $(\mu, M_2)$ for the acceptable solutions with $m_t^{\rm pole} = 145\,{\rm GeV}$. Notice a large concentration of points below the diagonals $M_2 = |\mu|$ which shows that the LSP is gauginolike in most of the solutions.

quantity which plays a significant role in constraining the parameter space of the CMSSM. If the Universe is at least 10 billion years old then $\Omega_\chi h_0^2 < 1$ (and the Universe's age of 15 billion years or more gives $\Omega_\chi h_0^2 \lesssim 0.25$), see Sec. VII D 3. We have also seen in Sec. VIII B that over significant regions of the model parameter space the LSP provides enough dark matter in either the CDM [$0.25 \lesssim \Omega_\chi h_0^2 \lesssim 0.5$, see (29)] or currently more favored MDM [$0.16 \lesssim \Omega_\chi h_0^2 \lesssim 0.33$, see (30)] scenarios (see Sec. VII D 4). This is a remarkable property of the CMSSM given the fact that, unlike in the case of many phenomenological quantities, calculating $\Omega_\chi h_0^2$ involves elements of the physics of the early Universe and *a priori* the resulting predictions for the LSP relic abundance could be completely incompatible with the expectation of low-energy SUSY.

In this section we provide some more insights into the cosmological properties of the neutralino LSP. First, for the restricted set of "acceptable solutions," as described in Sec. IX A, and for $m_t^{\rm pole} = 145\,{\rm GeV}$ we show in Fig. 31 a scatter plot in the plane $(\mu, M_2)$. Notice a large concentration of solutions below the diagonals $M_2 = |\mu|$ corresponding to the LSP being mostly gauginolike [see also the discussion above and below Eq. (32)]. This property is even more explicitly pronounced in Fig. 32 where we show for $m_t^{\rm pole} = 145\,{\rm GeV}$ and $\tan\beta = 10$ a scatter plot of the LSP wave function ($Z_{11}^2$ for the $b$-ino, etc.) with an additional constraint $0.16 < \Omega_\chi h_0^2 < 0.33$ (MDM) imposed. Notice that the LSP is mainly a $b$-ino, as expected [91]. This has been already illustrated for a few specific cases in Figs. 7–9. A very similar plot can be made for any value of $\tan\beta$ and changes little for the CDM scenario. Without the MDM (or CDM) constraint imposed, we find in Fig. 32 also some points with somewhat smaller $b$-ino purity, with the largest concentration however still remaining at large $Z_{11}^2$.

We also examine the predictions for the LSP relic density resulting from our restricted set of acceptable solutions defined in Sec. IX A, corresponding roughly to our

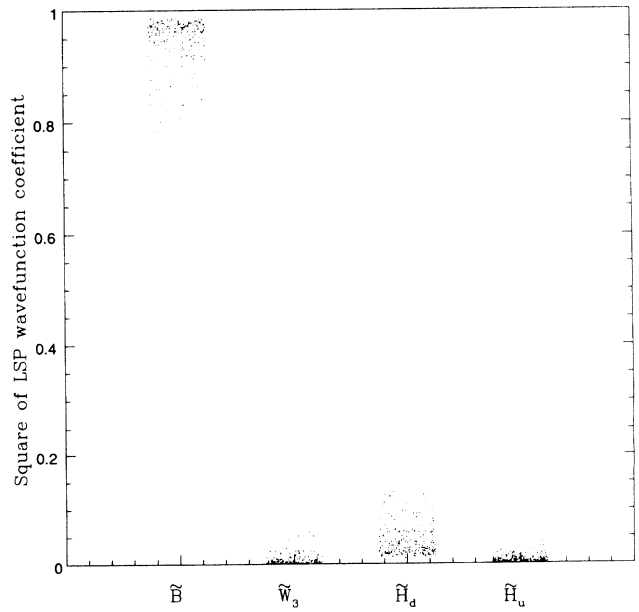


FIG. 32. Scatter plot of the LSP wave function for the acceptable solutions for which $0.16 < \Omega_\chi h_0^2 < 0.33$ (MDM scenario), and for $m_t^{\rm pole} = 145\,{\rm GeV}$ and $\tan\beta = 10$. Each solution contributes scatter plot points corresponding to its $\widetilde{B}$, $\widetilde{W}$, $\widetilde{H}_d$, and $\widetilde{H}_u$ components. Note that the LSP is mainly $\widetilde{B}$ in all these solutions.

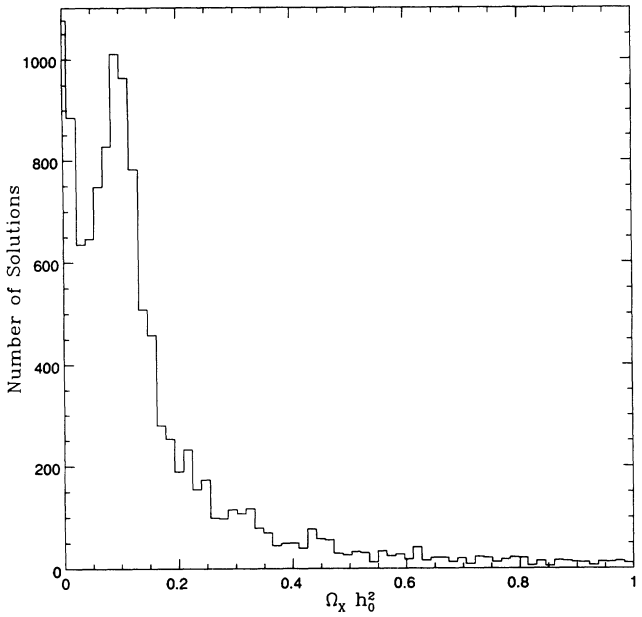


FIG. 33. Histogram of $\Omega_\chi h_0^2$ for all acceptable solutions (with an initial selecting cut $\Omega_\chi h_0^2 < 1$ imposed) for $m_t^{\rm pole} = 145\,{\rm GeV}$. Notice a strong peak around $\Omega_\chi h_0^2 \approx 0.1$ showing that in the CMSSM the MDM scenario is somewhat more favored relative to the CDM one.

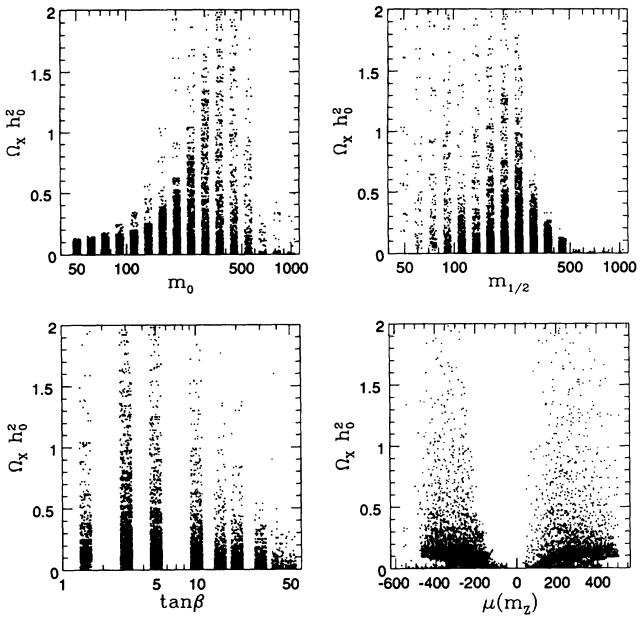


FIG. 34. $\Omega_\chi h_0^2$ vs (a) $m_0$, (b) $m_{1/2}$, (c) $\tan\beta$, and (d) $\mu$, for otherwise acceptable solutions with $m_t^{\rm pole} = 145\,{\rm GeV}$. The bound $\Omega_\chi h_0^2 < 1$ comes from the age of the Universe of 10 billion years or more. The ranges $0.16 \lesssim \Omega_\chi h_0^2 \lesssim 0.33$ and $0.25 \lesssim \Omega_\chi h_0^2 \lesssim 0.5$ are favored by the MDM and CDM scenarios, respectively. The banding in $m_0$, $m_{1/2}$, and $\tan\beta$ is from numerical sampling and is not physically significant.

expectations for low-energy SUSY. In Fig. 33 we plot a histogram of $\Omega_\chi h_0^2$ for all otherwise acceptable solutions with $m_t^{\rm pole} = 145\,{\rm GeV}$. Notice that there is a strong peak at $\Omega_\chi h_0^2 \approx 0.1$ suggesting that in the CMSSM the MDM scenario is somewhat more favored relative to the CDM one. Within the framework of CMSSM we can view this result one of two ways, either as a prediction for $\Omega_\chi$ (given $h_0$) for solutions which satisfy all other criteria, or that cold dark matter puts a severe constraint on the CMSSM if we demand that the LSP contributes most of the (cold) dark matter needed in the either the MDM or CDM scenarios. Both viewpoints are quite constraining: the first viewpoint for LSP (cold) dark matter and the second for the parameter space of the CMSSM.

Finally, in Fig. 34 we plot $\Omega_\chi h_0^2$ vs $m_{1/2}$, $m_0$, $\tan\beta$, and $\mu$. (In these graphs we lift the constraint $\Omega_\chi h_0^2 < 1$.) Notice that the ranges of $\Omega_\chi h_0^2$ favored by both MDM and CDM generally select both $m_{1/2}$, $m_0$, and $|\mu|$ (which is an output parameter in our analysis) in a broad region of a few hundred GeV. For small $m_{1/2}, m_0 \lesssim 100\,{\rm GeV}$ the relic density is too small because some sleptons are rather light there (roughly less than 100 GeV) which enhances the $t$-channel pair-annihilation $\chi\chi \to f\bar{f}$ [91]. Also notice that large $\tan\beta$ produces more solutions with low $\Omega_\chi h_0^2$ than do the solutions with low $\tan\beta$ which is due to a very strong enhancement in the LSP pair-annihilation cross section caused by the exchanged pseudoscalar $A$ [56]. (The coupling $A\chi\chi$ scales like $\tan\beta$.)

### J. The SUSY spectrum

By varying our input parameters over wide ranges of values we can consider what ranges of sparticle and Higgs boson masses one should expect from the CMSSM. In Fig. 35 we present a scatter plot of mass vs particle type for all the acceptable solutions in CMSSM with $m_t^{\rm pole} = 145\,{\rm GeV}$. Little changes significantly with varying $m_t^{\rm pole}$. In the next section we will further prejudice

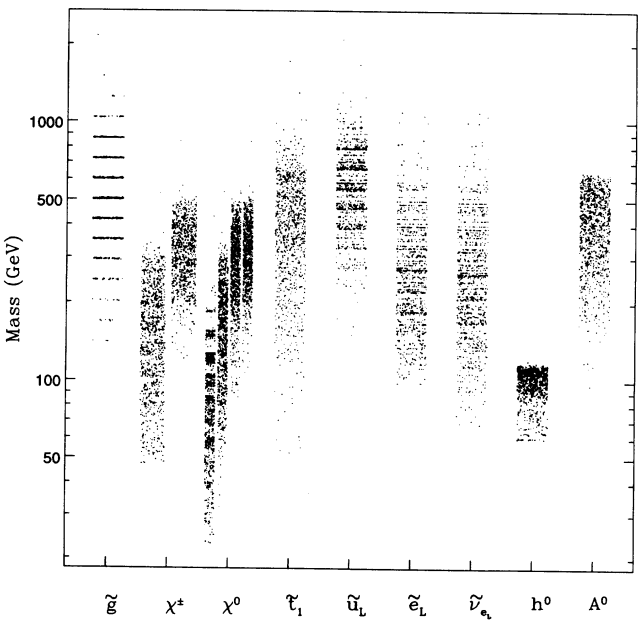


FIG. 35. Scatter plot of mass vs particle type for all acceptable solutions in our data set with $m_t^{\rm pole} = 145\,{\rm GeV}$ and $f \leq 50$. The horizontal bands are due to numerical sampling and are not of significance.

our parameter space in order to find sample solutions that are preferred theoretically.

### K. Physics prejudice enhancement of part of model space?

In this section we apply some experimental and theoretical prejudices to the acceptable solutions. For example, solutions with $B(b \to s\gamma) \approx 5.4 \times 10^{-4}$ are less favored than solutions with $B(b \to s\gamma) \approx 3.5 \times 10^{-4}$. Furthermore, theoretically we prefer solutions with lower fine-tuning. These are just two examples. Other prejudices that we can apply on the solutions are $m_b(M_X)/m_\tau(M_X) \simeq 1$, the LSP providing the right amount of cold dark matter, and $\alpha_s(m_Z)$ close to its experimental central value. As can be gleaned from previous sections, some of these prejudices work against others in some respects.

We have attempted to select a subset of all the solutions which are most likely to satisfy all (or most) of the above prejudices. We do that by effectively "squeezing" the solutions: select a preferred value for each constraint above and reducing the errors (or allowed region) by a factor of 2. In analyzing this squeezed set we find that the fraction of solutions which are detectable at LEP II and Fermilab goes down by about a factor of 2. That is, only about 18% of this set of solutions is detectable at Fermilab or LEP II, whereas in the full set the fraction is 32%. We therefore find that *the set of solutions which best satisfies our current experimental and theoretical prejudices are characteristically more difficult to detect than the full set of solutions allowed by current experiment.* Table VIII presents three examples of such solutions. Solutions 1 and 3 are not detectable at LEP II or Fermilab, but Solution 2 is in the chargino, $h$ (LEP II) and gluino (Fermilab) channels. We view this section as an initial attempt to add weighted physics criteria in order to select a part of the model space to use for other considerations such as phenomenological predictions or theoretical studies.

## X. SUMMARY AND COMMENTS

Encouraged by gauge coupling (grand) unification as implied by LEP we have made an attempt to frame SUSY by reconsidering minimal supersymmetry in the light of GUT's. We have parametrized the whole multitude of low-energy SUSY masses and couplings in terms of just five free parameters (and the sign of $\mu$), including the mass of the top quark $m_t$ which will soon be known. We have demanded gauge coupling unification and proper electroweak symmetry breaking. In further reducing the allowed parameter space we have included all the relevant experimental and cosmological constraints that can

TABLE VIII. Three representative solutions—one with rather light sparticles and the other two with intermediate to heavy sparticles. All masses are given in GeV. Some neutralino and chargino masses are quoted as negative. This is merely an indication of the phase of the mass eigenstates (expressed as $\eta_i$ by some authors); we include it in case people wish to use these numbers in calculations, but only magnitudes should be considered as experimentally relevant. $\widetilde{t}_{1,2}$ are physical eigenstates, while $\widetilde{t}_{L,R}$ correspond to the top squark mass-matrix entries. Same for the stau and the sbottom.

| Model parameters | Solution 1 | Solution 2 | Solution 3 |
|---|---|---|---|
| $\tan\beta$, $m_t^{\rm pole}$ | 10, 145 | 1.5, 145 | 5, 170 |
| $m_0$, $m_{1/2}$, $A_0/m_0$ | 247, 302, -2.5 | 91, 111, 2.5 | 111, 247, 2.5 |
| $B_0/m_0$, $B(m_Z)$ | -0.67, -0.03 | 2.84, 2.20 | 0.02, -0.46 |
| $\mu_0$, $\mu(m_Z)$, $\alpha_s(m_Z)$ | 394, 450, 0.124 | -214, -218, 0.127 | 303, 304, 0.129 |
| $\alpha_X$, $M_X/10^{16}$ GeV | 0.041, 1.64 | 0.042, 2.21 | 0.041, 2.04 |
| $h$, $H$, $A$, $H^\pm$ | 116, 346, 345, 354 | 62, 317, 305, 315 | 113, 326, 324, 333 |
| $\widetilde{e}_L$, $\widetilde{\mu}_L$, $\widetilde{\tau}_L$ | 328, 328, 324 | 124, 124, 124 | 211, 211, 211 |
| $\widetilde{e}_R$, $\widetilde{\mu}_R$, $\widetilde{\tau}_R$ | 276, 276, 268 | 104, 104, 104 | 152, 152, 152 |
| $\widetilde{\nu}_{e_L}$, $\widetilde{\nu}_{\mu_L}$, $\widetilde{\nu}_{\tau_L}$ | 318, 318, 318 | 114, 114, 114 | 197, 197, 197 |
| $\widetilde{u}_L$, $\widetilde{c}_L$, $\widetilde{t}_L$ | 700, 700, 634 | 283, 283, 299 | 570, 570, 555 |
| $\widetilde{u}_R$, $\widetilde{c}_R$, $\widetilde{t}_R$ | 677, 677, 620 | 276, 276, 271 | 551, 551, 492 |
| $\widetilde{d}_L$, $\widetilde{s}_L$, $\widetilde{b}_L$ | 705, 705, 622 | 288, 288, 266 | 575, 575, 534 |
| $\widetilde{d}_R$, $\widetilde{s}_R$, $\widetilde{b}_R$ | 676, 676, 667 | 276, 276, 276 | 550, 550, 549 |
| $\widetilde{\tau}_1$, $\widetilde{\tau}_2$ | 266, 326 | 104, 124 | 151, 212 |
| $\widetilde{t}_1$, $\widetilde{t}_2$ | 419, 705 | 177, 363 | 445, 594 |
| $\widetilde{b}_1$, $\widetilde{b}_2$ | 620, 670 | 264, 278 | 533, 550 |
| $\chi_1^\pm$, $\chi_2^\pm$ | 239, -468 | 53, 257 | 192, -329 |
| $\chi_1^0$ =LSP, $\chi_2^0$, $\chi_3^0$, $\chi_4^0$ | 126, 239, -457, 464 | 27, 65, -220, 263 | 102, 191, -316, 324 |
| $M_1$, $M_2$, $M_3 = \widetilde{g}$ | 126, 245, 718 | 45, 90, 292 | 102, 200, 610 |
| $B(b \to s\gamma)$ | $3.52 \times 10^{-4}$ | $2.97 \times 10^{-4}$ | $4.76 \times 10^{-4}$ |
| $m_b(M_X)/m_\tau(M_X)$ | 0.794 | 0.750 | 0.794 |
| $\Omega_\chi h_0^2$ | 0.27 | 0.24 | 0.22 |
| $\widetilde{B}$ and gaugino purities | 0.99, 0.99 | 0.67, 0.87 | 0.98, 0.98 |

be imposed without choosing a specific GUT gauge group at the unification scale. We have not found the present experimental bounds on SUSY particle masses to be particularly constraining; in fact they are only beginning to limit the lower range of the SUSY masses. In contrast, rather robust cosmological constraints such as requiring that the Universe be at least 10 billion years old and that the LSP not be electrically charged, rule out large fractions of the SUSY parameter space. Furthermore, much more specific conclusions about the resulting SUSY mass spectra and properties can be drawn if one expects the neutralino LSP to be the dominant dark matter component (in either cold- or mixed-DM scenarios) in the flat Universe.

A number of groups have already reported studies along the same lines we follow. Our work is more comprehensive and complete in that more of the theoretical and phenomenological constraints are included than in any previous work, and precision to the few percent level is required wherever appropriate in a fully consistent manner. We also include more applications than have been considered previously.

It is only by combining all the constraints and exploring wide ranges of parameters that one is able to establish where SUSY might be realized. Remarkably, we find that SUSY is preferably realized in the range of Higgs boson, sfermion, and gaugino masses of several hundred GeV and below, with larger values sometimes allowed by our constraints but disfavored by too much fine-tuning. At this point one still cannot favor any range of $m_t$, unless one insists on the $m_b$-$m_\tau$ unification which in most cases (but not always) implies a very heavy top quark. Similarly, all values of $\tan\beta$ between one and about 50–60 (perturbative upper bound) are still allowed, although the resulting phenomenology often differs considerably in the small and large $\tan\beta$ regime. On the other hand, significant constraints can be placed on the $(m_{1/2}, m_0)$ plane. The region $m_{1/2} \gg m_0$ is invariably excluded by requiring either electroweak symmetry breaking or neutral LSP, while $m_0 \gg m_{1/2}$ is typically ruled out by either EWSB or a lower bound on the age of the Universe. References [19,30] have argued that the region $m_0 \gg m_{1/2} \approx m_Z$ (and small $\tan\beta \lesssim 8$) appears to be favored by bounds on the proton decay in the simplest SUSY SU(5) model, but we prefer not to rely on an SU(5) GUT, so this region is not favored for us.

We have made a first survey of phenomenological implications for future SUSY searches in high-energy experiments. We find reasonable chances for eventually finding a chargino at LEP II and the gluino or gauginos at the Tevatron. The light Higgs boson $h$ has a very good chance of being discovered at LEP II but most likely only if its beam energy is pushed close to or beyond 200 GeV. On the other hand, the chances are very slim with the currently approved $\sqrt{s} = 178\,\text{GeV}$. The LHC will produce large quantities of all superpartners.

Several predictions follow from our analysis which could have served to falsify the CMSSM before the sweeping supercollider searches for the squarks, Higgs bosons, and the gluino are done.

We derive a general *upper* bound on $\alpha_s(m_Z) < 0.133$. For larger $m_t$, and for some regions of $\tan\beta$ when $m_t$ is smaller, there is a lower bound $\alpha_s(m_Z) \gtrsim 0.117$. In the regions where the bound is not implied by the physics constraints, it is implied instead by the addition of a fine-tuning constraint. GUT-scale threshold corrections may be sizable and modify these limits by several percent. (In this paper we have ignored all GUT-scale corrections because we have not yet studied specific unification gauge groups and their Higgs boson structures, although we do assume $\sin^2\theta_W(M_X) = 3/8$.)

Within our parameter space the light Higgs boson mass is very SM-like and $m_h \lesssim 120\,\text{GeV}$ for $m_t^{\text{pole}} = 145\,\text{GeV}$ and $m_h \lesssim 130\,\text{GeV}$ for $m_t^{\text{pole}} = 170\,\text{GeV}$, with somewhat lower values usually favored. We also find that $m_h > 85\,\text{GeV}$ for $\tan\beta > 5$. If $h$ had been discovered below about 30 GeV, our entire parameter space would have been excluded.

The charged Higgs boson is always significantly heavier than $m_W$ and its discovery should not be expected at LEP II and most likely even at the NLC500. Other heavy Higgs bosons ($H$ and $A$) are almost degenerate in mass with $H^\pm$. If $H^\pm$ is discovered below about 110 GeV, our entire parameter space is excluded.

If $B(Z \to b\bar{b}) < 0.214$ and $m_t^{\text{pole}} \lesssim 150\,\text{GeV}$, all solutions are excluded. Similar bounds exist for larger $m_t^{\text{pole}}$.

The LSP is almost invariably of the gaugino-type (more precisely $b$-ino-type), as advocated early in Ref. [91]. If the cold dark matter is not of this type, almost all solutions from this study are excluded. If at least one sfermion (other than the top squark or sneutrino) had always been lighter than about 80 GeV, there would have been too little neutralino DM [110]. Furthermore, had the sneutrino been the LSP, the CMSSM would not have predicted enough DM.

Several clear patterns and relations among the masses of the Higgs and SUSY particles arise which can be tested in future accelerators.

We have also addressed several related issues recently discussed in the literature. We agree with [3,5,8,10] about the need to use two-loop RGE's and to include multiple thresholds in considering the running of the gauge couplings. One-loop RGE's and simplified one-step approaches can each lead to errors in $\alpha_s(m_Z)$ of some 10% (while the experimental error is at the 5% level). We emphasize that it is inappropriate to use the so-called effective SUSY-breaking scale $M_{\text{SUSY}}^{\text{eff}}$ in deriving the GUT mass scale $M_X$ and gauge coupling $\alpha_X$. In particular, the value of $M_X$ derived this way can be twice that coming from the full two-loop calculation. We have noted that GUT-scale corrections of 10–15 % to the relation $m_b(M_X) = m_\tau(M_X)$ may have a significant impact on the resulting mass of the bottom quark $m_b(m_b)$ and may allow for this relation to hold for wide ranges of both $m_t^{\text{pole}}$ and $\tan\beta$. We also find it very important to use the one-loop effective Higgs boson potential particularly in the range of large masses ($\gtrsim 1\,\text{TeV}$) where it can lead to qualitatively different conclusions than had we simply used the tree-level potential.

Remarkably, we find that for larger $m_t^{\text{pole}}$ it is possible to place upper bounds on all superpartner masses of

$\sim$1 TeV, without imposing any fine-tuning criterion. For smaller $m_t^{\rm pole}$ this is still true for some regions of $\tan\beta$ near one, but not for all.

Ultimately the goal is to go from experimental data to a determination of the effective Lagrangian of the supersymmetric and (perhaps) unified theory at a scale of $\sim 10^{16}$ GeV. We have shown by example that an effective and perhaps optimal way to do this as data becomes available is to systematically reduce the allowed parameter space numerically. Once the high-scale Lagrangian is known, perhaps the patterns among its parameters will lead toward an understanding of how SUSY is broken and what the underlying theory is.

Minimal supersymmetry is a very attractive theoretical framework which makes several falsifiable phenomenological and cosmological predictions while at the same time encompassing all the remarkable experimental successes of the standard model. The most natural ranges for supersymmetric particle masses typically lie above the reach of currently operating accelerators (LEP, Fermilab) but may be accessible to the upgraded LEP and Fermilab, and should be successfully explored by the next generation of colliders.

## ACKNOWLEDGMENTS

This work was supported in part by the U.S. Department of Energy. We have benefited from conversations with R. Arnowitt, M. Einhorn, H. Haber, S. Kelley, B. Lynn, M. Peskin, N. Polonsky, P. Ramond, R. Roberts, J. F. Zhou and many others.

[1] P. Langacker, in *Particles, Strings and Cosmology—90,* Proceedings of the First International Symposium, Boston, Massachusetts, 1990, edited by P. Nath and S. Reucroft (World Scientific, Singapore, 1990); P. Langacker and M.-X. Luo, Phys. Rev. D **44**, 817 (1991).

[2] For reviews, see, e.g., H.-P. Nilles, Phys. Rep. **110**, 1 (1984); H. E. Haber and G. L. Kane, *ibid.* **117**, 75 (1985); L. E. Ibáñez and G. G. Ross, in *Perspectives in Higgs Physics*, edited by G. L. Kane (World Scientific, Singapore, 1993).

[3] J. Ellis, S. Kelley, and D. V. Nanopoulos, Phys. Lett. B **260**, 131 (1991).

[4] U. Amaldi, W. de Boer, and H. Fürstenau, Phys. Lett. B **260**, 447 (1991).

[5] F. Anselmo, L. Cifarelli, A. Peterman, and A. Zichichi, Nuovo Cimento **104A**, 1817 (1991); **105A**, 581 (1992).

[6] See, e.g., J. Ellis, G. L. Fogli, and E. Lisi, Phys. Lett. B **285**, 238 (1992).

[7] T. Rizzo, Phys. Rev. D **45**, 3903 (1992); U. Amaldi, W. de Boer, P. Frampton, H. Fürstenau, and J.T. Liu, Phys. Lett. B **281**, 374 (1992); L. Lavoura and L. Wolfenstein, Phys. Rev. D **48**, 264 (1993).

[8] R. G. Roberts and G. G Ross, Nucl. Phys. **B377**, 571 (1992).

[9] R. Barbieri and L. J. Hall, Phys. Rev. Lett. **68**, 752 (1992); L. J. Hall and U. Sarid, *ibid.* **70**, 2673 (1993).

[10] P. Langacker and N. Polonsky, Phys. Rev. D **47**, 4028 (1993).

[11] K. Hagiwara and Y. Yamada, Phys. Rev. Lett. **70**, 709 (1993).

[12] V. Barger, M. S. Berger, and P. Ohmann, Phys. Rev. D **47**, 1093 (1993).

[13] A. Faraggi, B. Grinstein, and S. Meshkov, Phys. Rev. D **47**, 5018 (1993); A. Faraggi and B. Grinstein, Report No. SSCL-496, August 1993 (unpublished); B. Lynn, Report No. SSCL-506, September 1993 (unpublished).

[14] H. Arason, D. J. Castaño, B. Keszthelyi, S. Mikaelian, E. J. Piard, P. Ramond, and B. D. Wright, Phys. Rev. D **46**, 3945 (1992).

[15] H. Arason, D. J. Castaño, B. Keszthelyi, S. Mikaelian, E. J. Piard, P. Ramond, and B. D. Wright, Phys. Rev. D **47**, 232 (1993). See also A. Giveon, L. J. Hall, and U. Sarid, Phys. Lett. B **271**, 138 (1991); P. H. Frampton, J. T. Liu, and M. Yamaguchi, *ibid.* **277**, 130 (1992).

[16] V. Barger, M.S. Berger, P. Ohmann, and R.J.N. Phillips, Phys. Lett. B **314**, 351 (1993).

[17] M. Carena, S. Pokorski, and C. Wagner, Nucl. Phys. **B406**, 59 (1993).

[18] P. Langacker and N. Polonsky, Phys. Rev. D **49**, 1454 (1994).

[19] R. Arnowitt and P. Nath, Phys. Lett. B **287**, 89 (1992); Phys. Rev. Lett. **69**, 725 (1992); Phys. Lett. B **299**, 58 (1993); Northeastern University Report No. NUB-TH-3048-92 (unpublished).

[20] R. G. Roberts and L. Roszkowski, Phys. Lett. B **309**, 329 (1993).

[21] S. Kelley, J. L. Lopez, D. V. Nanopoulos, H. Pois, and K. Yuan, Phys. Lett. B **273**, 423 (1991).

[22] S. Kelley, J. L. Lopez, D. V. Nanopoulos, H. Pois, and K. Yuan, Nucl. Phys. **B398**, 3 (1993).

[23] J. L. Lopez, D. V. Nanopoulos, and A. Zichichi, Phys. Lett. B **291**, 255 (1992).

[24] M. Drees and M. Nojiri, Phys. Rev. D **47**, 376 (1993).

[25] W. de Boer, R. Ehret, and D. I. Kazakov, presented at the XVI International Symposium on Lepton-Photon Interactions, Ithaca, New York, 1993 (unpublished).

[26] D. J. Castaño, E. J. Piard, and P. Ramond, University of Florida Report No. UFIFT-HEP-93-18, August 1993 (unpublished).

[27] V. Barger, M. S. Berger, and P. Ohmann, Phys. Rev. D **49**, 4908 (1994).

[28] P. Nath and R. Arnowitt, Phys. Rev. Lett. **70**, 3696 (1993).

[29] P. Nath and R. Arnowitt, Phys. Lett. B **289**, 368 (1992).

[30] J. Lopez, D. V. Nanopoulos, and H. Pois, Phys. Rev. D **47**, 2468 (1993).

[31] J. L. Lopez, D. V. Nanopoulos, H. Pois, X. Wang, and A. Zichichi, Phys. Lett. B **306**, 73 (1993).

[32] L. E. Ibáñez and G. G. Ross, Phys. Lett. **110B**, 215 (1982); K. Inoue, A. Kakuto, H. Komatsu, and S. Takeshita, Prog. Theor. Phys. **68**, 927 (1982); L. Alvarez-Gaumé, J. Polchinsky, and M. Wise, Nucl. Phys. **B221**, 495 (1983); J. Ellis, D. V. Nanopoulos, and K. Tamvakis, Phys. Lett. **121B**, 123 (1983).

[33] H. E. Haber, G. L. Kane, and M. Quirós, Phys. Lett. **160B**, 297 (1985); Nucl. Phys. **B273**, 333 (1986);

R. Arnowitt (private communication).
[34] L. Girardello and M. T. Grisaru, Nucl. Phys. **B184**, 65 (1982).
[35] V. Kaplunovsky and J. Louis, Phys. Lett. B **306**, 269 (1993); A. Brignole, L. E. Ibáñez, and C. Muñoz, Madrid Report No. FTUAM-26/93, August 1993 (unpublished); A. Lleyda and C. Muñoz, Phys. Lett. B **317**, 82 (1993); C. Muñoz (private communication).
[36] L. J. Hall, R. Rattazzi, and U. Sarid, Report No. LBL-33997, June 1993 (unpublished).
[37] J. Hisano, H. Murayama, and T. Yanagida, Nucl. Phys. **B402**, 46 (1993); K. Babu and S. M. Barr, Phys. Rev. D **48**, 5354 (1993).
[38] L. E. Ibáñez, D. Lüst, and G. G. Ross, Phys. Lett. B **272**, 251 (1991).
[39] S. P. Martin, Phys. Rev. D **46**, 2769 (1992).
[40] J. Ellis, S. Kelley, and D. V. Nanopoulos, Nucl. Phys. **B373**, 55 (1992); Phys. Lett. B **287**, 95 (1992).
[41] J. Hisano, H. Murayama, and T. Yanagida, Phys. Rev. Lett. **69**, 1014 (1992).
[42] H. E. Haber and R. Hempfling, Phys. Rev. D **48**, 4280 (1993).
[43] D. R. T. Jones, Phys. Rev. D **25**, 581 (1982); M. B. Einhorn and D. R. T. Jones, Nucl. Phys. **B196**, 475 (1982); J. E. Björkman and D. R. T. Jones, *ibid.* **B259**, 533 (1985). The relevant RGE's are summarized in Ref. [12].
[44] M. E. Machacek and M. T. Vaughn, Nucl. Phys. **B222**, 83 (1983); **B236**, 221 (1984); **B249**, 70 (1985). The relevant RGE's are summarized in Ref. [12].
[45] I. Antoniadis, J. Ellis, S. Kelley, and D. V. Nanopoulos, Phys. Lett. B **272**, 31 (1991); U. Amaldi, W. de Boer, P. H. Frampton, H. Fürstenau, and J. T. Liu, *ibid.* **281**, 374 (1992).
[46] The LEP Collaborations ALEPH, DELPHI, L3, OPAL, and The LEP Electroweak Working Group, Report No. CERN/PPE/93-157, August 1993 (unpublished).
[47] N. Gray, D. J. Broadhurst, W. Grafe, and K. Schilcher, Z. Phys. C **48**, 673 (1990). See also Ref. [14].
[48] V. Barger, M. S. Berger, and P. Ohmann, presented at the SUSY93 Workshop, Boston, Massachusetts, 1993 (unpublished).
[49] S. Titard and F. J. Ynduráin, this issue, Phys. Rev. D **49**, 6007 (1994).
[50] G. Kramer and B. Lampe, Z. Phys. A **339**, 189 (1991). See also S. J. Brodsky and H. J. Lu, SLAC Report No. SLAC-PUB-6389, November 1993 (unpublished).
[51] G. Gamberini, G. Ridolfi, and F. Zwirner, Nucl. Phys. **B331**, 331 (1990).
[52] M. Sher, Phys. Rep. **179**, 723 (1989).
[53] R. Arnowitt and P. Nath, Phys. Rev. D **46**, 3981 (1992).
[54] B. de Carlos and A. Casas, Phys. Lett. B **309**, 320 (1993).
[55] L. E. Ibáñez and C. López, Nucl. Phys. **B233**, 511 (1984); L. E. Ibáñez, C. López, and C. Muñoz, *ibid.* **B256**, 218 (1985).
[56] J. Ellis and L. Roszkowski, Phys. Lett. B **283**, 252 (1992).
[57] See, e.g., M. Dine, A. Kagan, and S. Samuel, Phys. Lett. B **243**, 250 (1990).
[58] Y. Nir and N. Seiberg, Phys. Lett. B **309**, 337 (1993).
[59] G. F. Giudice and E. Roulet, Phys. Lett. B **315**, 107 (1993).
[60] BES Collaboration, J. Z. Bai *et al.*, Phys. Rev. Lett. **69**, 3021 (1992).
[61] D. V. Nanopoulos and D. A. Ross, Nucl. Phys. **B157**, 273 (1979); O. V. Tarasov, A. A. Vladimirov, and A.Yu. Zharkov, Phys. Lett. **93B**, 429 (1980); R. Tarrach, Nucl. Phys. **B183**, 384 (1981); D. R. T. Jones, Phys. Rev. D **25**, 581 (1982); S. G. Gorishny, A. L. Kataev, and S. A. Larin, Sov. J. Nucl. Phys. **40**, 329 (1984). The relevant RGE's are summarized in Ref. [14].
[62] J. Ellis and F. Zwirner, Nucl. Phys. **B338**, 317 (1990).
[63] Y. Okada, M. Yamaguchi, and T. Yanagida, Prog. Theor. Phys. **85**, 1 (1991); Phys. Lett. B **262**, 54 (1991); H. E. Haber and R. Hempfling, Phys. Rev. Lett. **66**, 1815 (1991); J. Ellis, G. Ridolfi, and F. Zwirner, Phys. Lett. B **257**, 83 (1991); **262**, 477 (1991); R. Barbieri, M. Frigeni, and F. Caravaglio, *ibid.* **258**, 395 (1991).
[64] See, e.g., K. Riles, presented at the Workshop on Physics at Current Accelerators and the Supercollider, Argonne, Illinois 1993 (unpublished).
[65] DELPHI Note 92-172 PHYS (1992); we thank K. Riles for pointing out to us the new top squark bound by DELPHI and A. Lopez-Fernando and R. Keranen (DELPHI) for explaining to us the salient points of the analysis.
[66] ALEPH Collaboration, D. Buskulic *et al.*, Phys. Lett. B **313**, 312 (1993).
[67] CDF Collaboration, F. Abe *et al.*, Phys. Rev. Lett. **69**, 3439 (1992).
[68] H. Baer, X. Tata, and J. Woodside, Phys. Rev. D **44**, 207 (1991).
[69] L. Roszkowski, Phys. Lett. B **252**, 471 (1990).
[70] CLEO Collaboration, E. Thorndike *et al.*, CLEO Report No. CLEO 93-06 (unpublished); Phys. Rev. Lett. **71**, 674 (1993).
[71] C. Bernard, P. Hsieh, and A. Soni, Washington University Report No. HEP/93-35, July 1993 (unpublished).
[72] S. Bertolini, F. Borzumati, A. Masiero, and G. Ridolfi, Nucl. Phys. **B353**, 591 (1991).
[73] R. Barbieri and G. Giudice, Phys. Lett. B **309**, 86 (1993).
[74] J. L. Hewett, Phys. Rev. Lett. **70**, 1045 (1993); V. Barger, M. S. Berger, and R. J. N. Phillips, *ibid.* **70**, 1368 (1993); M. A. Diaz, Phys. Lett. B **304**, 278 (1993). See also M. A. Diaz, Vanderbilt Report No. VAND-TH-93-11 (unpublished).
[75] N. Oshima, Nucl. Phys. **B404**, 20 (1993).
[76] R. Garisto and J. N. Ng, Phys. Lett. B **315**, 372 (1993).
[77] K. Adel and Y.-P. Yao, Phys. Rev. D **49**, 4945 (1994). See also M. Ciuchini, E. Franco, G. Martinelli, L. Reina, and L. Silvestrini, Phys. Lett. B **316**, 127 (1993).
[78] See, e.g., J. P. Derendinger and C. A. Savoy, Nucl. Phys. **B237**, 307 (1984).
[79] J. Gunion, H. E. Haber, and M. Sher, Nucl. Phys. **B306**, 1 (1988).
[80] E. Kolb and M. Turner, *The Early Universe* (Addison-Wesley, New York, 1989).
[81] R. Cahn and S. Glashow, Science **213**, 607 (1981); D. J. Hegyi and K. Olive, Phys. Lett. **126B**, 28 (1983); A. De Rújula, S. Glashow, and U. Sarid, Nucl. Phys. **B333**, 173 (1990); E. Nardi and E. Roulet, Phys. Lett. B **245**, 105 (1990); A. Gould, B. Draine, R. Romani, and S. Nussinov, *ibid.* **238**, 337 (1990); S. Dimopoulos, D. Eichler, R. Esmailzadeh, and G. Starkman, Phys. Rev. D **41**, 2388 (1990).
[82] M. Drees, G. Jungman, M. Kamionkowski, and M. No-

jiri, Madison Report No. MAD-PH-766, June 1993 (unpublished).
[83] M. Srednicki, R. Watkins, and K. A. Olive, Nucl. Phys. **B310**, 693 (1988).
[84] L. Roszkowski, in *Properties of SUSY Particles*, Proceedings of the XXIII Workshop, 1992, edited by L. Cifarelli and V. Khoze (World Scientific, Singapore, 1993). Erice, Italy.
[85] G. L. Kane and I. Kani, Nucl. Phys. **B277**, 525 (1986).
[86] K. Griest and D. Seckel, Phys. Rev. D **43**, 3191 (1991).
[87] G. Gelmini and P. Gondolo, Nucl. Phys. **B360**, 145 (1991).
[88] K. Olive, D. N. Schramm, G. Steigman, and T. Walker, Phys. Lett. B **236**, 454 (1990); T. Walker, G. Steigman, D. N. Schramm, H.-S. Kang, and K. Olive, Astrophys. J. **53**, 51 (1991).
[89] C. Alcock *et al.*, Nature (London) (to be published); E. Aubourg *et al.*, *ibid*; A. Udalski *et al.*, Acta Astron. **43**, 289 (1993).
[90] K. Griest (private communication).
[91] L. Roszkowski, Phys. Lett. B **262**, 59 (1991).
[92] J. Ellis, J. S. Hagelin, D. V. Nanopoulos, K. A. Olive, and M. Srednicki, Nucl. Phys. **B238**, 453 (1984).
[93] R. K. Schaefer and Q. Shafi, Nature (London) **359**, 199 (1992); M. Davis, F. Summers, and D. Schegel, *ibid.* **359**, 393 (1992); A. N. Taylor and M. Rowan-Robinson, *ibid.* **359**, 396 (1992); A. Klypin, J. Holtzman, J. Primack, and E. Regős, Astrophys. J. **416**, 1 (1993).
[94] L. E. Ibáñez, Phys. Lett. **137B**, 160 (1984); J. S. Hagelin, G. L. Kane, and S. Raby, Nucl. Phys. **B241**, 638 (1984).
[95] R. Barbieri and G. F. Giudice, Nucl. Phys. **B306**, 63 (1988).
[96] K. A. Olive and M. Srednicki, Phys. Lett. B **230**, 78 (1989).
[97] S. Mizuta and M. Yamaguchi, Phys. Lett. B **298**, 120 (1993).
[98] H. E. Haber, U.C. Santa Cruz Report No. SCIPP-93-22 (unpublished); M. A. Diaz and H. E. Haber, Phys. Rev. D **46**, 3086 (1992).
[99] See, e.g., H. E. Haber, in *Perspectives in Higgs Physics*, edited by G. L. Kane (World Scientific, Singapore, 1993).
[100] Z. Kunszt and F. Zwirner, Nucl. Phys. **B385**, 3 (1992); V. Barger, M. S. Berger, A. Stange, and R. J. N. Phillips, Phys. Rev. D **45**, 4128 (1992); J. F. Gunion and L. H. Orr, *ibid.* **46**, 2052 (1992); H. Baer, M. Bisset, D. Dicus, C. Kao, and X. Tata, *ibid.* **47**, 1062 (1993).
[101] S. Ferrara and E. Remiddi. Phys. Lett. **53B**, 347 (1974).
[102] H. E. Haber, G. L. Kane, I. Kani, and M. Quirós, Nucl. Phys. **B283**, 111 (1987).
[103] H. Baer, C. Kao, and X. Tata, Phys. Rev. D **48**, 5175 (1993); H. Baer, J. Sender, and X. Tata, Hawaii Report No. UH-511-773-93 (unpublished); H. Baer, A. Bartl, D. Karatas, W. Majerotto, and X. Tata, Int. J. Mod. Phys. A **4**, 4111 (1989); A. Bartl, H. Fraas, and W. Majerotto, Z. Phys. C **30**, 441 (1986); H. Baer, X. Tata, and J. Woodside, Phys. Rev. D **45**, 142 (1992); X. Tata and D. Dicus, *ibid.* **35**, 2110 (1987).
[104] G. L. Kane, C. Kolda, and J. D. Wells, Phys. Rev. Lett. **70**, 2686 (1993). See also J. R. Espinosa and M. Quirós, Phys. Lett. B **302**, 51 (1993).
[105] A. Faraggi, J. S. Hagelin, S. Kelley, and D. V. Nanopoulos, Phys. Rev. D **45**, 3272 (1992); M. Olechowski and S. Pokorski, Nucl. Phys. **B404**, 590 (1993); S. P. Martin and P. Ramond, Phys. Rev. D **48**, 5365 (1993); S. Orito, in *Proceedings of the Workshop on Physics and Experiments with Linear $e^+e^-$ Colliders*, Waikaloa, Hawaii, 1993, edited by F. Harris (World Scientific, Singapore, 1993); JLC Group, KEK Report 92-16 (December 1992).
[106] A. Akhundov, D. Bardin, and T. Riemann, Nucl. Phys. **B276**, 1 (1986); J. Bernabeu, A. Pich, and A. Santamaria, Phys. Lett. B **200**, 569 (1988); W. Beenaker and W. Hollik, Z. Phys. C **40**, 141 (1988).
[107] A. Djouadi, G. Girardi, C. Verzegnassi, W. Hollik, and F. M. Renard. Nucl. Phys. **B349**, 48 (1991).
[108] M. Boulware and D. Finnell, Phys. Rev. D **44**, 2054 (1991).
[109] R. G. Stuart, Comput. Phys. Commun. **48**, 367 (1988); B. A. Kniehl and R. G. Stuart, Comput. Phys. Commun. **72**, 175 (1992).
[110] L. Roszkowski, Phys. Lett. B **278**, 147 (1992).

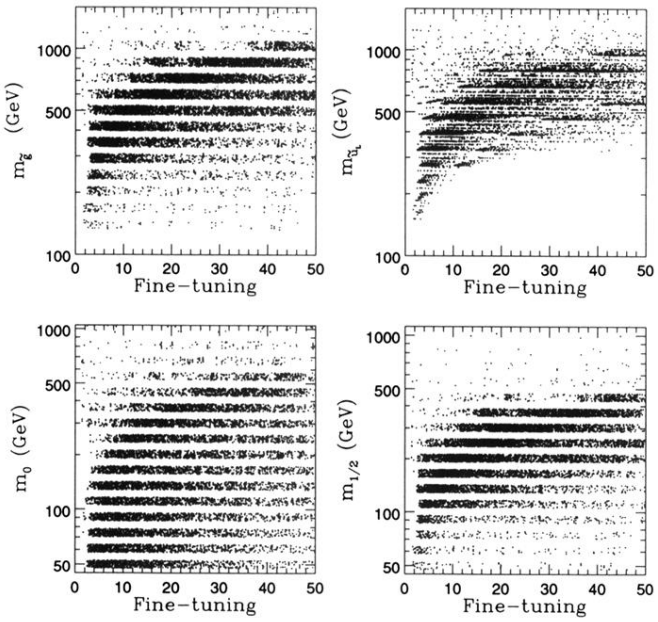


FIG. 13. Scatter plot of (a) $m_{\tilde{g}}$, (b) $m_{\tilde{u}_L}$, (c) $m_0$, and (d) $m_{1/2}$ vs fine-tuning for solutions consistent with all applied constraints. Notice that the cut $f \leq 50$ typically gives sparticle masses $m_{\tilde{q}}, m_{\tilde{g}} \lesssim 1\,\text{TeV}$ but in some cases (all of which have large $\tan\beta$) they can be significantly heavier.

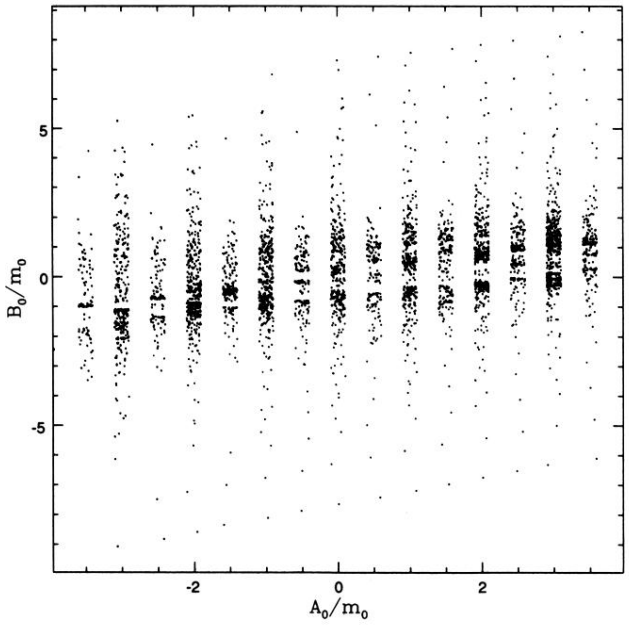


FIG. 14. Scatter plot of $B_0/m_0$ vs $A_0/m_0$ for all allowed solutions (COMPASS) with $m_t^{\rm pole} = 145\,{\rm GeV}$. The quantized appearance is due to numerical sampling and is not significant.

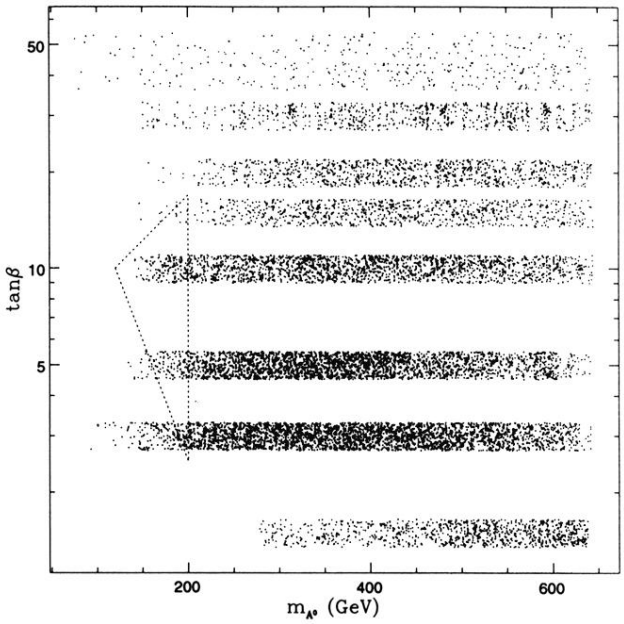


FIG. 21. Scatter plot of $\tan\beta$ vs $m_A$ for all acceptable solutions with $m_t^{\rm pole}$=145 GeV. The band structure is due to numerical sampling and is not physically significant. The dotted triangular region is the approximate region in which it is difficult to detect at least one Higgs boson [100].

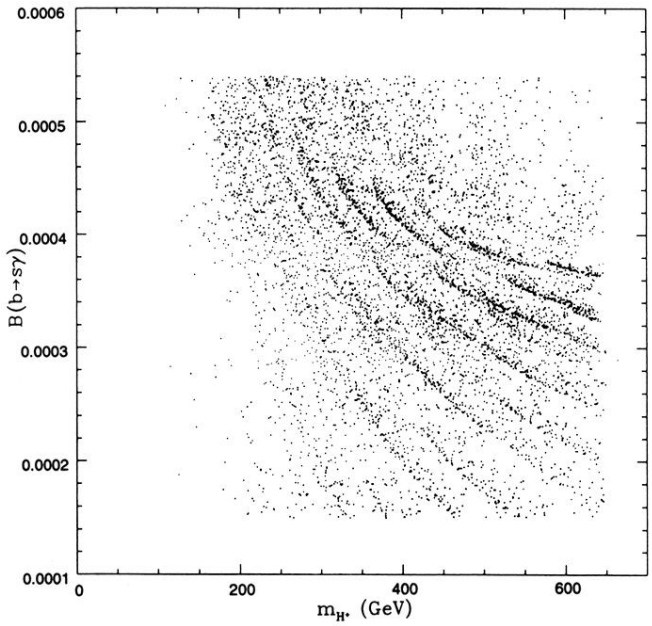


FIG. 25. Scatter plot of $B(b \to s\gamma)$ vs $m_{H^\pm}$ for all acceptable solutions with $m_t^{\rm pole} = 145\,{\rm GeV}$. The faint banding visible in the figure is from numerical sampling and is not physically significant.

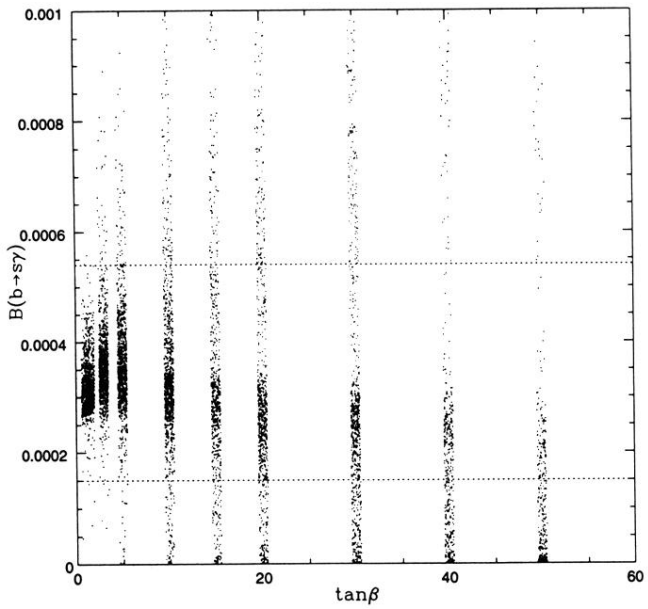


FIG. 26. $B(b \to s\gamma)$ vs $\tan\beta$ for all acceptable solutions with $m_t^{\rm pole} = 145\,{\rm GeV}$. In order to demonstrate the density of points, $\tan\beta$ is slightly smeared around its numerically sampled value.

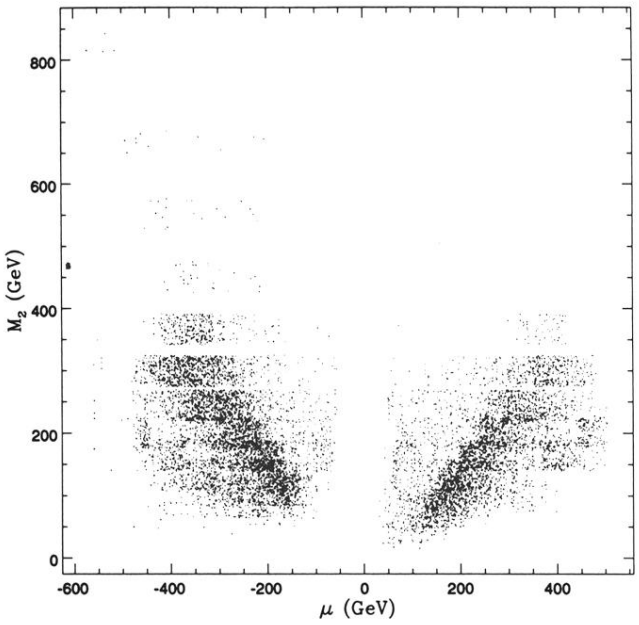


FIG. 31. Scatter plot in the plane $(\mu, M_2)$ for the acceptable solutions with $m_t^{\rm pole} = 145\,{\rm GeV}$. Notice a large concentration of points below the diagonals $M_2 = |\mu|$ which shows that the LSP is gauginolike in most of the solutions.

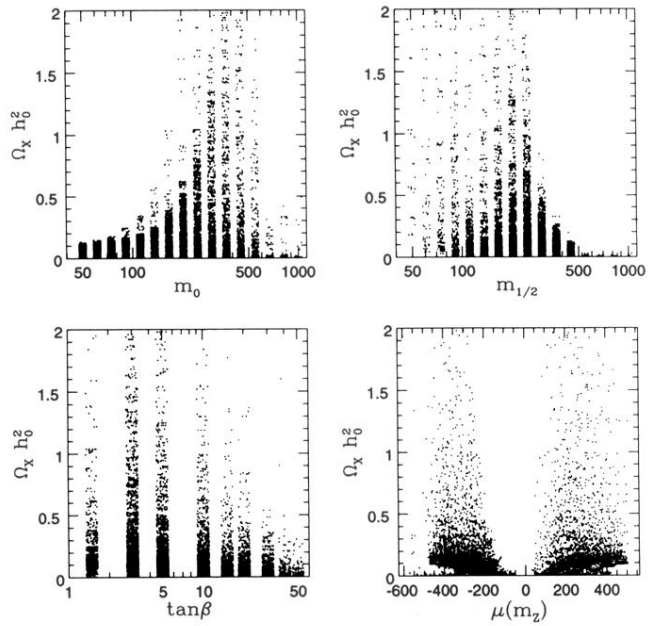


FIG. 34. $\Omega_\chi h_0^2$ vs (a) $m_0$, (b) $m_{1/2}$, (c) $\tan\beta$, and (d) $\mu$, for otherwise acceptable solutions with $m_t^{\rm pole} = 145\,{\rm GeV}$. The bound $\Omega_\chi h_0^2 < 1$ comes from the age of the Universe of 10 billion years or more. The ranges $0.16 \lesssim \Omega_\chi h_0^2 \lesssim 0.33$ and $0.25 \lesssim \Omega_\chi h_0^2 \lesssim 0.5$ are favored by the MDM and CDM scenarios, respectively. The banding in $m_0$, $m_{1/2}$, and $\tan\beta$ is from numerical sampling and is not physically significant.

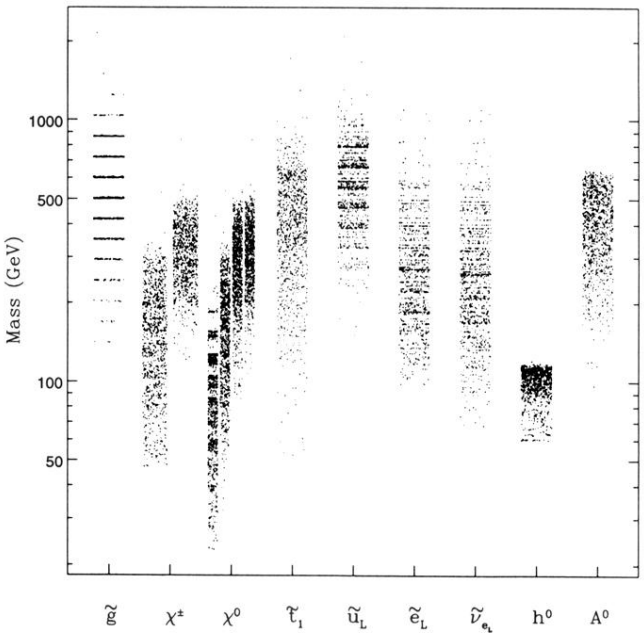


FIG. 35. Scatter plot of mass vs particle type for all acceptable solutions in our data set with $m_t^{\rm pole} = 145\,{\rm GeV}$ and $f \leq 50$. The horizontal bands are due to numerical sampling and are not of significance.